

# TUMSAT-OACIS Repository - Tokyo

University of Marine Science and Technology

(東京海洋大学)

Novel tempering technology for Tuna *Thunnus obesus* and its model food development

メタデータ	言語: eng 出版者: 公開日: 2021-12-14 キーワード (Ja): キーワード (En): 作成者: 陳, 怡璇, Chen, Yixuan メールアドレス: 所属:
URL	<a href="https://oacis.repo.nii.ac.jp/records/2275">https://oacis.repo.nii.ac.jp/records/2275</a>

**Master's Thesis**

**NOVEL TEMPERING TECHNOLOGY FOR TUNA  
*Thunnus obesus* AND ITS MODEL FOOD  
DEVELOPMENT**

**September 2021**

**Graduate School of Marine Science and Technology  
Tokyo University of Marine Science and Technology  
Master Course of Food Science and Technology**

**CHEN YIXUAN**



**Master's Thesis**

**NOVEL TEMPERING TECHNOLOGY FOR TUNA  
*Thunnus obesus* AND ITS MODEL FOOD  
DEVELOPMENT**

**September 2021**

**Graduate School of Marine Science and Technology  
Tokyo University of Marine Science and Technology  
Master Course of Food Science and Technology**

**CHEN YIXUAN**

# Content

<b>Chapter 1 Introduction</b> .....	1
<b>1.1 Background and objective</b> .....	1
<b>1.2 Literature review</b> .....	2
1.2.1 Thawing Technology .....	2
1.2.2 Application of novel thawing technologies of aquatic products .....	5
1.2.3 Model food .....	6
1.2.4 Model food in food processing .....	6
1.2.5 Numerical simulation.....	7
1.2.6 Numerical simulation in food processing .....	8
<b>1.3 Structure of this dissertation</b> .....	9
References.....	12
<b>Chapter 2 Model food development for tuna (<i>Thunnus obesus</i>) in radio frequency and microwave tempering using grass carp mince</b> .....	15
<b>2.1 Introduction</b> .....	15
<b>2.2 Materials and methods</b> .....	16
2.2.1 Materials preparation.....	16
2.2.2 Composition determination.....	17
2.2.3 Dielectric properties measurement.....	17
2.2.4 Penetration depth.....	18
2.2.5 Thermal properties .....	18
2.2.6 Tempering experiment and temperature measurements.....	19
2.2.7 Statistical analysis .....	21
<b>2.3 Results and discussion</b> .....	21
2.3.1 Composition determination.....	21
2.3.2 Effect of additives on dielectric properties .....	22
2.3.3 Effect of additives on thermal properties.....	33
2.3.4 Temperature distributions.....	35
<b>2.4 Conclusions</b> .....	43
References.....	45
<b>Chapter 3 Numerical simulation of RF tempering tuna process with different electrodes and sample shapes</b> .....	48
<b>3.1 Introduction</b> .....	48
<b>3.2 Materials and methods</b> .....	48
3.2.1 Materials preparation.....	48
3.2.2 Radio frequency tempering of tuna.....	49
<b>3.3 Computer simulation</b> .....	49
3.3.1 Computer simulation of the tempering tuna process.....	49
3.3.2 Modeling .....	50
3.3.3 Different electrode shapes .....	52
3.3.4 Different sample shapes.....	53

3.3.5 Temperature Uniformity Index (TUI).....	53
3.4 Results and discussion .....	54
3.4.1 Simulated and experimental results of tuna tempering process .....	54
3.4.2 Electric field intensity distribution with different shapes of electrode plates.....	55
3.4.3 Temperature rise curve under different electrode plates.....	57
3.4.4 Temperature distribution under different electrode plates .....	59
3.4.5 Tempering uniformity evaluation under different electrode plates.....	61
3.5 Conclusion .....	62
References.....	63
<b>Chapter 4 Ohmic tempering of minced tuna and its model food made with Allaska pollock surimi</b>	
– Evaluation of electrical conductivities.....	64
4.1 Introduction.....	64
4.2 Material and methods.....	66
4.2.1 Material preparation .....	66
4.2.2 Temperature monitoring .....	67
4.2.3 Measurement of EC .....	68
4.2.4 Experimental tempering using an OH system.....	69
4.2.5 Statistical analysis .....	69
4.3 Results and discussion .....	70
4.3.1 EC values of minced tuna and model foods blocks .....	70
4.3.2 Experimental voltage gradient control during OT .....	75
4.4 Conclusions.....	83
References.....	85
<b>Chapter 5 Numerical simulation of ohmic tempering process of tuna.....</b>	<b>88</b>
5.1 Introduction.....	88
5.2 Materials and methods .....	89
5.2.1 Materials preparation.....	89
5.2.2 Instruments and equipment .....	89
5.2.3 Ohmic tempering of tuna .....	89
5.3 Computer simulation .....	89
5.3.1 Computer simulation of the tempering tuna process.....	89
5.3.2 Modeling .....	90
5.3.3 Applying optimum voltage control .....	92
5.3.4 Temperature Uniformity Index (TUI).....	93
5.4 Results and discussion .....	93
5.4.1 Temperature history of OT under constant voltage.....	93
5.4.2 Temperature history after OT under constant voltage .....	94
5.4.3 Computer simulation of OT under segmented voltage.....	96
5.5 Conclusions.....	98
References.....	100
<b>Chapter 6 General conclusions .....</b>	<b>101</b>
<b>Acknowledgement.....</b>	<b>103</b>

## Chapter 1 Introduction

### 1.1 Background and objective

Tuna is a highly migratory fish. Tuna meat is rich in nutrition, rich in high-quality protein and unsaturated fatty acids DHA (docosahexaenoic acid) and EPA (eicosapentaenoic acid) and contains a variety of vitamins and minerals. Tuna fishery is an important part of marine economy with high economic value, wide distribution and abundant resource reserves. Commercial tuna mainly includes seven species, which are yellowfin tuna, skipjack tuna, bigeye tuna, albacore tuna, Atlantic bluefin tuna, Pacific bluefin tuna, and southern bluefin tuna. Fig. 1-1 showed the top 10 tuna fishing nations and regions, 2018.

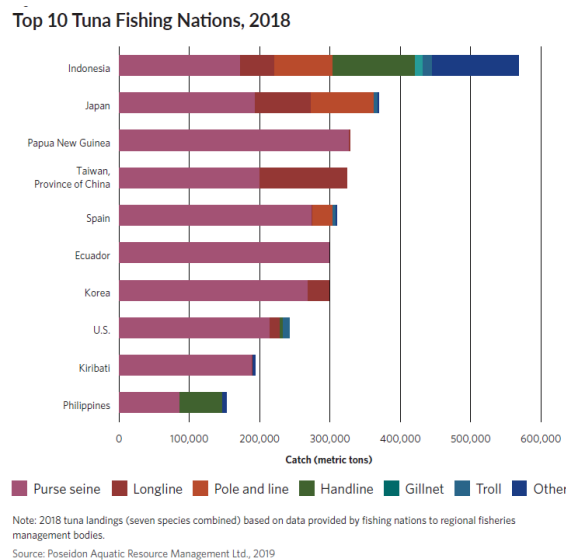


Fig. 1-1 Top 10 Tuna fishing nations, 2018

As novel thawing technologies, radio frequency (RF) thawing technology and ohmic thawing technology have many advantages. However, the capital cost of the equipment and the lack of systematic research in experimental development are still the biggest obstacles to their application in industrial production. For the application of novel thawing or heating technology, especially in the development of thawing and heating process for high-value aquatic products (e.g., tuna), low-cost model food is usually introduced as a substitute for high-value aquatic products for process exploration and repeated experiments, so as to reduce the cost. In this study, low-cost aquatic products are used as model materials because the proportion of moisture and

protein is similar to that of tuna. And these materials are easy to obtain and prepare, and the dielectric properties, electrical conductivity and thermal properties are easy to adjust. At the same time, the process of RF and ohmic tempering tuna was numerically simulated, and the model was verified by experiments. In addition, the effects of electrode shape and material shape on the temperature distribution of RF tempering process and the effect of segmented voltage on the uniformity of ohmic tempering (OT) process were investigated.

## **1.2 Literature review**

### **1.2.1 Thawing Technology**

In industrial process, frozen products are usually tempered to  $-5\text{ }^{\circ}\text{C}$  to  $-1\text{ }^{\circ}\text{C}$  for easy cutting or completely thawed for subsequential application. Tempering usually raises the temperature of samples to just below their freezing point ( $-5\text{ }^{\circ}\text{C}$  to  $-1\text{ }^{\circ}\text{C}$ ) while thawing usually raises the temperature of them above  $0\text{ }^{\circ}\text{C}$  (James, 1999; Seyhun, Ramaswamy, Zhu, Sumnu, & Sahin, 2012). According to its mechanism, thawing methods can be divided into external thawing and internal thawing: external thawing refers to the external heat sources and thawing through medium heat transfer; internal thawing refers to the generation heat from inside the food. The traditional thawing method is generally external thawing, such as air thawing, water thawing and so on. The novel thawing method uses the internal thawing mechanism, mainly through sound waves, pressure, electromagnetic waves and so on to achieve the purpose of rapid thawing, such as ultrasonic thawing, ultra-high pressure thawing, ohmic thawing, microwave thawing, RF thawing, high voltage electrostatic field thawing, far infrared thawing and so on. These thawing methods do not depend on the temperature of external heat source and has high energy conversion rate. However, due to the difference of penetration ability, sample size, shape, and composition, it is easy to produce uneven heating, resulting in the destruction of the quality of aquatic products.

#### **1.2.1.1 Traditional thawing technologies**

Traditional thawing techniques are generally external thawing methods, such as air thawing and water thawing.

Air thawing is the thawing of aquatic products by convective heat transfer using air as the thawing medium, with a general air temperature of 14 ~ 15 °C and relative humidity of 95 % ~ 98 %. Air thawing includes static air thawing and flowing air thawing. Usually, the thawing rate can be adjusted by controlling air temperature, humidity, flow rate and so on.

Water thawing uses water as thawing medium, and the general temperature of water is 10 °C. Aquatic products are thawed by means of heat conduction and heat convection. The heat transfer performance of water is better than that of air, so the thawing time is significantly shorter than that of air thawing. Water thawing includes hydrostatic water thawing and running water thawing.

Traditional thawing is widely used due to low cost and convenient operation, but it usually takes a long time and has a large temperature difference between the surface and the interior of the frozen products. Air thawing has serious water evaporation and is prone to juice loss, dry consumption, surface discoloration, etc. And water thawing is easy to make the meat gray color, serious loss of soluble substances, and susceptible to microbial contamination, so it is more suitable for thawing of aquatic products with packaging. The drawbacks of traditional thawing technology have been paid attention to, and the development of novel thawing technology is imperative. The disadvantages of traditional thawing technology have been paid attention to, and the development of new thawing technology is extremely necessary.

#### **1.2.1.2 Novel thawing technologies**

The novel thawing technologies are generally internal thawing methods, including ultrasonic thawing, high voltage electrostatic field thawing, microwave thawing, RF thawing, ohmic thawing and so on.

Ultrasonic thawing: ultrasonic thawing is a thermal effect caused by intense high-frequency oscillation after the medium absorbs ultrasonic energy. The absorption of ultrasonic energy in the frozen area of aquatic products is higher than that in the unfrozen area, and the ultrasonic wave generates more heat when it penetrates two different media (Cai et al., 2018; Kentish & Feng, 2014). Therefore, the absorption

position of ultrasonic energy is near the freezing point at the junction of the freezing and thawing zone (Kentish & Feng, 2014).

High-voltage electrostatic field thawing: high-voltage electrostatic field thawing uses a high-voltage electrostatic field and the resulting corona wind to produce heating and non-heating effects on frozen products. The principle is to place the frozen product in a high-voltage electrostatic field. It uses high-voltage electrostatic micro-energy to break the hydrogen bonds of water molecules in the ice crystal structure and break the dynamic balance of polymerization and depolymerization of water molecules, which make the ice crystal transition to the smaller ice crystal and then transition to the state of liquid water (He, Jia, Tatsumi, & Liu, 2016). While the ion wind formed by charged particles accelerate the heat conduction and increase the thawing rate. At the same time, the ozone generated by the ionization of air by high-voltage electrostatic field has a certain inhibitory effect on the growth and reproduction of microorganisms, and the ozone on the surface of frozen products can also isolate a certain amount of oxygen, which can slow down the oxidation of protein and fat and improve the color of meat (He, Liu, Nirasawa, Zheng, & Liu, 2013).

Microwave thawing: microwave thawing uses ion dipole polarization and dipole rotation in frozen products to generate heat, especially water molecules, resulting in intermolecular rotation, vibration and friction. Studies have shown that, compared with the traditional thawing methods, microwave thawing can significantly improve the thawing rate (Baygar & Alparslan, 2015; Ku, Jeong, Park, Jeon, Kim, & Kim, 2014).

Radio frequency thawing: RF thawing uses alternating electromagnetic field to stimulate ion couple polarization, ion oscillation, polarity rotation and friction to generate heat (Alfaifi, et al., 2014; Farag, Duggan, Morgan, Cronin, & Lyng, 2009). The shape, volume, surface area, composition, dielectric properties, thermophysical properties, surrounding media of the sample and RF system affect the electromagnetic field distribution and the heating process (Koray Palazoglu & Miran, 2017; Llave, Terada, Fukuoka, & Sakai, 2014).

Ohmic thawing: ohmic thawing takes frozen products as resistance, which

converts electric energy into thermal energy through the change of impedance and dielectric loss. Ohmic thawing can shorten the thawing time, which is two to three times faster than that of the traditional heat conduction method. Compared with the traditional water thawing, it can improve the uniformity of meat internal thawing, reduce the drip loss rate, and maintain the quality of frozen products (Bozkurt & Icier, 2012; Icier, Izzetoglu, Bozkurt, & Ober, 2010). The efficiency is high, and the energy conversion rate is up to 90%. With the increase of ohmic thawing potential gradient, the thawing rate can be significantly increased, which has advantages over traditional thawing (Duygu & Umit, 2015; Liu, Llave, Jin, Zheng, Fukuoka, & Sakai, 2017; Richa, et al., 2017).

### **1.2.2 Application of novel thawing technologies of aquatic products**

Many emerging novel technologies for tempering and thawing frozen products have been reported in the literature (Luyun Cai, Cao, Regenstein, & Cao, 2019), such as microwave heating, RF heating (Li, et al., 2018; Llave, et al., 2014), ohmic heating (OH) (Icier, et al., 2010; Liu, et al., 2017), high-voltage electrical field heating (Mousakhani-Ganjeh, Hamdami, & Soltanizadeh, 2015), ultra-high pressure (Zhu, Su, He, Ramaswamy, Le Bail, & Yu, 2014), and ultrasound (Gambuteanu & Alexe, 2015).

Farag, et al. (2009) used RF system (27.12 MHz, 400 W) to thaw 4 kg of frozen meat blocks and showed that the temperature reached  $-4.9^{\circ}\text{C}$  at 400 W for 11 min. The result showed that RF thawing technology could shorten the thawing time to one-thirtieth of the conventional method, with a more uniform temperature distribution and lower energy consumption. Koray Palazoglu, et al. (2017) studied RF thawing (27.12 MHz, 2 kW) of frozen shrimp blocks and found that it took 7-11 min to thaw 1.75 kg of shrimp blocks from  $-22^{\circ}\text{C}$  to  $-5$  to  $-3^{\circ}$  without serious inhomogeneities, but the temperature at the corners was slightly higher than the center. L. Liu, et al. (2017) studies the thawing process of different parts of tuna under ohmic thawing technology and found that low moisture increased the electrical conductivity and accelerated the ohmic thawing rate, while high fat decreased the electrical conductivity and reduced the thawing rate.

### **1.2.3 Model food**

For the application of novel thawing or tempering technologies, the optimal process parameters need to be obtained through a large number of repeated experiments, which will greatly increase the cost, especially high-value aquatic products. Therefore, it is significant to develop model foods with low-cost, convenient preparation, uniform composition, similar dielectric properties, electrical conductivity and thermal properties to the target materials for process development.

### **1.2.4 Model food in food processing**

In previous studies, some model foods have been developed for simulating various food materials mostly in thawing, tempering and sterilization processes. Llave, Mori, Kambayashi, Fukuoka, and Sakai (2016) confirmed the efficacy of using tylose paste as a model food of lean tuna muscle during MW thawing and heating in the temperature range -30 to +60 °C. The internal and surface temperature profiles of tylose paste with 0.5% NaCl matched those of lean tuna muscle after 90 s MW heating at 2450 MHz. Cong, Liu, Tang, and Xue (2012) developed a model food with whey protein 5%, whey protein isolate 3%, gellan gum 1%, D-ribose 0.5% and water 90.5% matching the properties of the sea cucumbers in a 915 MHz single-mode MW sterilization process from 20 to 120 °C. Auksornsri, Bornhorst, Tang, Tang, and Songsermpong (2018) developed a model food based on rice flour gel (30 g/100 g rice flour, 13.5 g/100 g tapioca starch, 0.1 g/100 g xanthan gum, and 0.5 g/100 g D-ribose) to simulate medium-moisture foods (0.2–0.6 g water/g) during MW assisted thermal sterilization. Icier and Ilicali (2005) investigated the OH of tylose samples with different salt concentrations and minced beef samples with different fat contents at the temperature range of 30 to 60 °C using different voltage gradients 10–50 V/cm. They found that tylose samples with 0.5% and 0.67% of salt content showed similar EC values and OH rates than the minced beef samples having higher and lower fat contents.

Some common additives could regulate the dielectric properties of model foods. For example, salt was commonly added to increase the dielectric loss factor, and sucrose was used to reduce the dielectric constant. Zhang, et al. (2015) found that 0.3 g/mL

sucrose addition decreased the dielectric constant and increased the gel strength of gellan gel by decreasing the free water content. However, gellan gel with 0.5 g/mL sucrose addition was softer with the deformable gel network, and vegetable oil was used to reduce dielectric constant (Hu, Toyoda, & Ihara, 2008; Ryyanen, 1995). According to Luan, et al. (2015), the dielectric constant of bentonite pastes was significant reduced by adding vegetable oil at 915 and 2450 MHz. These recent studies revealed that tylose, whey protein, and gellan powder with appropriate additions could be used to simulate various food materials being used as dummy loads.

### **1.2.5 Numerical simulation**

The numerical simulation methods include Finite Element Method (FEM), Discrete Element Method (DEM) and Boundary Element Method (BEM). In this study, the finite element method is used, which is a mathematical approximation to simulate the real physical system (geometry and load conditions). By using simple and interactive elements, a finite number of unknowns can be used to get infinitely close to the unknowns of the real system. Through the finite element method, coupling different physical models and inputting parameters such as material parameters and boundary conditions, the thawing process of aquatic products can be simulated, observed, and analyzed. In the RF and ohmic thawing and tempering process, the three-dimensional temperature field and electromagnetic field which cannot be observed with the naked eye, can be analyzed by the simulation results, which is beneficial to the fine analysis of the thawing and tempering process.

The numerical simulation method is used to accurately simulate the tempering process of materials in the electromagnetic field coupling heat transfer based on the dielectric properties, electrical conductivity (EC) and thermophysical parameters of materials. In the process of thawing and tempering, the material undergoes phase transition, and the moisture, density, specific heat capacity, thermal conductivity and dielectric properties of the material will change with the temperature, so the relevant parameters need to be set and the model created. For the latent heat in the thawing process, apparent specific heat method, enthalpy method and quasi-enthalpy method

are usually used (Pham, 2006). In addition, the initial and boundary conditions also affect the reliability of numerical simulation. Figure 1-2 shows the diagram flow the steps of traditional numerical simulation.

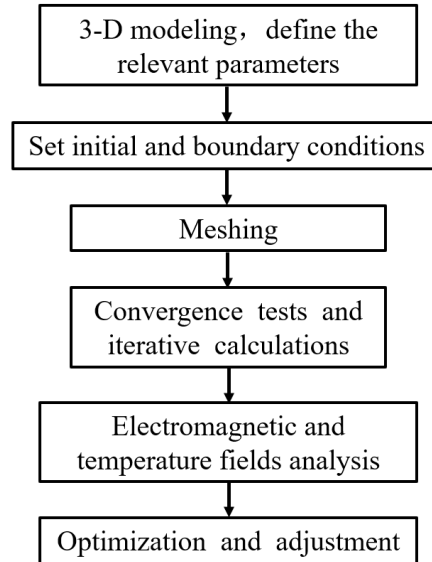


Fig. 1-2 Strategies mathematical simulation calculation

### 1.2.6 Numerical simulation in food processing

In recent years, numerical simulation has become an effective tool to study the electric field distribution and temperature field distribution under the novel technology for the problem of uniformity during the thawing and tempering of aquatic products. Llave, Liu, Fukuoka, and Sakai (2015) used FEMAP and PHOTO software to establish a three-dimensional finite element model of RF thawing under the condition of air natural convection, and simulated the RF thawing process of tuna at 13.56 MHz RF from  $-60^{\circ}\text{C}$  to  $-3^{\circ}\text{C}$ . The transient temperature distribution and electromagnetic field intensity distribution during thawing process were predicted. It was found that when the size of the upper plate was the same as that of the sample, the temperature distribution of the sample was the most uniform, and when the central temperature reached  $-3^{\circ}\text{C}$ , the temperature difference was just  $9.6^{\circ}\text{C}$ . Guo, Llave, Jin, Fukuoka, and Sakai (2017) simulated the 20 kHz high frequency ohmic heating process of non-uniform two-component materials under different filling modes. The simulation results were consistent with the temperature distribution measured by experiments, and the relative root mean square error is 2.59%. It was found that different components and

different arrangement and filling methods led to non-uniform conductivity distribution, non-uniform electric field intensity distribution and non-uniform current density distribution in the cavity, thus increasing the non-uniformity of temperature distribution. S. Liu, Ogiwara, Fukuoka, and Sakai (2014) simulated the heating of household microwave ovens by finite element method and found that the edges and corners of materials were easy to be heated, and cold points were easy to appear in the center and bottom. By exploring different rotation angles of the rotary table, the composition and geometry of the material, it was proved that the rotary table could effectively alleviate the uneven heating phenomenon.

### **1.3 Structure of this dissertation**

Developing model foods is important in the application of novel thawing or tempering technologies with the aim of reducing experimental cost in repeated experiments. In this study, both RF and OT processes were experimentally conducted and simulated for the thawing/tempering of frozen tuna. In addition, the development of two tuna model foods was conducted to facilitate the computer simulation works.

This dissertation included five chapters. The first of the study use low-cost fish as raw materials to develop model foods that can replace tuna for RF tempering temperature curve and temperature distribution analysis and perform finite element numerical simulation and optimization analysis of RF tempering tuna. The latter are to the use of low-cost surimi as raw materials to develop model food that can replace tuna for OT temperature curve and temperature distribution analysis and perform finite element numerical simulation and optimization analysis of OT tempering tuna. The detail contents were shown as below:

In chapter 1, the background and objectives of this research were described.

In chapter 2, low-cost model foods were necessary for developing radio frequency (RF) and microwave (MW) thawing and tempering process for tuna to reduce experimental cost. In this study, grass carp mince with vegetable oil (1.0-8.0% wt), methylcellulose (MC, 1.0-8.0% wt) and NaCl (0.25-4.0% wt) were investigated for

their effect on dielectric properties and tempering temperature distribution to simulate tuna. The dielectric properties of the model foods and tuna were both measured over 1-2500 MHz and -40 to +40 °C. The temperature distributions of tuna and the developed model foods after RF (27.12 MHz) and microwave (2450 MHz) tempering from -55 °C were both determined for comparison.

In chapter 3, the use of computer simulation of tuna RF tempering process can effectively reduce the experimental workload, reduce the research and development cost, control the variables and optimize the design. The electromagnetic field-heat conduction model was established by using finite element analysis to numerically simulate the tuna RF tempering process, and the experimental temperature field and the simulated temperature field were compared and analyzed. The effects of different electrode plate shapes (plane electrode; electrode with needle type surface; electrode with pyramid type surface) and different material shapes (rectangular, cylindrical) on the RF tempering process were also compared.

In chapter 4, inexpensive and practical model foods are necessary for developing ohmic tempering (OT) of tuna to reduce experimental cost. In this study, the effect of salt addition (0%, 0.25%, 0.5%, 1.0%, and 2.0%) in pollock surimi within the temperature range of -40 °C to 10 °C and frequency range of 50 Hz to 20 kHz, and adjusting voltage were evaluated to develop a model food for OT of minced tuna by comparing their electrical conductivity (EC) values and temperature distribution. The EC values of the model food increased with the increasing salt content, temperature, and frequency. Adjusting the voltage during OT in three steps (400 V, -35 °C ~ -20 °C; 200 V, -20 °C ~ -10 °C; 100 V, -10 °C ~ -4 °C), improved the uniformity of the temperature distribution of the samples.

In chapter 5, the use of computer simulation of tuna ohmic thawing to establish a manipulable, observable, and analytical model allows for more precise and specific control of variables. The electromagnetic field-heat conduction model was used to numerically simulate the tuna OT process using finite element analysis. The uniformity of the tempering process was enhanced for the heating non-uniformity problem that

occurs in the experiment. By finding the abrupt change in thawing rate and segmenting the ohmic thawing voltage by applying 400 V from 0 to 676 s and reducing the voltage to 200 V at 676 s, a more uniform temperature distribution was studied.

Finally, in chapter 6 the general conclusions of this thesis are shown.

## References

- Alfaifi, B., Tang, J., Jiao, Y., Wang, S., Rasco, B., Jiao, S., & Sablani, S. (2014). Radio frequency disinfestation treatments for dried fruit: Model development and validation. *Journal of Food Engineering*, *120*, 268-276.
- Auksornsri, T., Bornhorst, E. R., Tang, J., Tang, Z., & Songsermpong, S. (2018). Developing model food systems with rice based products for microwave assisted thermal sterilization. *Lwt*, *96*, 551-559.
- Baygar, T., & Alparslan, Y. (2015). Effects of multiple freezing (-18 +/- 2 degrees C) and microwave thawing cycles on the quality changes of sea bass (*Dicentrarchus labrax*). *J Food Sci Technol*, *52*(6), 3458-3465.
- Bozkurt, H., & Icier, F. (2012). Ohmic thawing of frozen beef cuts. *Journal of Food Process Engineering*, *35*(1), 16-36.
- Cai, L., Cao, M., Cao, A., Regenstein, J., Li, J., & Guan, R. (2018). Ultrasound or microwave vacuum thawing of red seabream (*Pagrus major*) fillets. *Ultrason Sonochem*, *47*, 122-132.
- Cai, L., Cao, M., Regenstein, J., & Cao, A. (2019). Recent advances in food thawing technologies. *Comprehensive Reviews in Food Science and Food Safety*, *18*(4), 953-970.
- Cong, H., Liu, F., Tang, Z., & Xue, C. (2012). Dielectric properties of sea cucumbers (*Stichopus japonicus*) and model foods at 915MHz. *Journal of Food Engineering*, *109*(3), 635-639.
- Duygu, B., & ümit, G. (2015). Application of Ohmic Heating System in Meat Thawing. *Procedia - Social and Behavioral Sciences*, *195*, 2822-2828.
- Farag, K. W., Duggan, E., Morgan, D. J., Cronin, D. A., & Lyng, J. G. (2009). A comparison of conventional and radio frequency defrosting of lean beef meats: Effects on water binding characteristics. *Meat Science*, *83*(2), 278-284.
- Gambuteanu, C., & Alexe, P. (2015). Comparison of thawing assisted by low-intensity ultrasound on technological properties of pork Longissimus dorsi muscle. *J Food Sci Technol*, *52*(4), 2130-2138.
- Guo, W., Llave, Y., Jin, Y., Fukuoka, M., & Sakai, N. (2017). Mathematical modeling of ohmic heating of two-component foods with non-uniform electric properties at high frequencies. *Innovative Food Science & Emerging Technologies*, *39*, 63-78.
- He, X., Jia, G., Tatsumi, E., & Liu, H. (2016). Effect of corona wind, current, electric field and energy consumption on the reduction of the thawing time during the high-voltage electrostatic-field (HVEF) treatment process. *Innovative Food Science & Emerging Technologies*, 135-140.
- He, X., Liu, R., Nirasawa, S., Zheng, D., & Liu, H. (2013). Effect of high voltage electrostatic field treatment on thawing characteristics and post-thawing quality of frozen pork tenderloin meat. *Journal of Food Engineering*, *115*(2), 245-250.
- Hu, L., Toyoda, K., & Ihara, I. (2008). Dielectric properties of edible oils and fatty acids as a function of frequency, temperature, moisture and composition. *Journal of Food Engineering*, *88*(2), 151-158.
- Icier, F., & Ilicali, C. (2005). The use of tylose as a food analog in ohmic heating studies.

- Journal of Food Engineering*, 69(1), 67-77.
- Icier, F., Izzetoglu, G. T., Bozkurt, H., & Ober, A. (2010). Effects of ohmic thawing on histological and textural properties of beef cuts. *Journal of Food Engineering*, 99(3), 360-365.
- James, S. J. (1999). Food refrigeration and thermal processing at langford, UK: 32 years of research. *Food and Bioproducts Processing*, 77(4), 261-280.
- Kentish, S., & Feng, H. (2014). Applications of power ultrasound in food processing. *Annual Review of Food Science & Technology*, 5(1), 263.
- Koray Palazoglu, T., & Miran, W. (2017). Experimental comparison of microwave and radio frequency tempering of frozen block of shrimp. *Innovative Food Science & Emerging Technologies*, 41, 292-300.
- Ku, S. K., Jeong, J. Y., Park, J. D., Jeon, K. H., Kim, E. M., & Kim, Y. B. (2014). Quality evaluation of pork with various freezing and thawing methods. *Korean Journal for Food Science of Animal Resources*, 34(5), 597-603.
- Li, Y., Li, F., Tang, J., Zhang, R., Wang, Y., Koral, T., & Jiao, Y. (2018). Radio frequency tempering uniformity investigation of frozen beef with various shapes and sizes. *Innovative Food Science & Emerging Technologies*, 48, 42-55.
- Liu, L., Llave, Y., Jin, Y., Zheng, D.-y., Fukuoka, M., & Sakai, N. (2017). Electrical conductivity and ohmic thawing of frozen tuna at high frequencies. *Journal of Food Engineering*, 197, 68-77.
- Liu, S., Ogiwara, Y., Fukuoka, M., & Sakai, N. (2014). Investigation and modeling of temperature changes in food heated in a flatbed microwave oven. *Journal of Food Engineering*, 131, 142-153.
- Llave, Y., Liu, S., Fukuoka, M., & Sakai, N. (2015). Computer simulation of radiofrequency defrosting of frozen foods. *Journal of Food Engineering*, 152(may), 32-42.
- Llave, Y., Mori, K., Kambayashi, D., Fukuoka, M., & Sakai, N. (2016). Dielectric properties and model food application of tylose water pastes during microwave thawing and heating. *Journal of Food Engineering*, 178, 20-30.
- Llave, Y., Terada, Y., Fukuoka, M., & Sakai, N. (2014). Dielectric properties of frozen tuna and analysis of defrosting using a radio-frequency system at low frequencies. *Journal of Food Engineering*, 139, 1-9.
- Luan, D., Tang, J., Liu, F., Tang, Z., Li, F., Lin, H., & Stewart, B. (2015). Dielectric properties of bentonite water pastes used for stable loads in microwave thermal processing systems. *Journal of Food Engineering*, 161, 40-47.
- Mousakhani-Ganjeh, A., Hamdami, N., & Soltanizadeh, N. (2015). Impact of high voltage electric field thawing on the quality of frozen tuna fish (*Thunnus albacares*). *Journal of Food Engineering*, 156, 39-44.
- Pham, Q. T. (2006). Modelling heat and mass transfer in frozen foods: a review. *International Journal of Refrigeration*, 29(6), 876-888.
- Richa, R., Shahi, N., Singh, A., Lohani, U., Omre, P., Kumar, A., & Bhattacharya, T. (2017). Ohmic heating technology and its application in meaty food: A review. *Advances in Research*, 10(4), 1-10.
- Ryynanen, S. (1995). The electromagnetic properties of food material: a review of the

- basic principles. *Journal of Food Engineering*, 26, 409-429.
- Seyhun, N., Ramaswamy, H. S., Zhu, S., Sumnu, G., & Sahin, S. (2012). Ohmic tempering of frozen potato puree. *Food and Bioprocess Technology*, 6(11), 3200-3205.
- Zhang, W., Luan, D., Tang, J., Sablani, S. S., Rasco, B., Lin, H., & Liu, F. (2015). Dielectric properties and other physical properties of low-acyl gellan gel as relevant to microwave assisted pasteurization process. *Journal of Food Engineering*, 149, 195-203.
- Zhu, S. M., Su, G. M., He, J. S., Ramaswamy, H. S., Le Bail, A., & Yu, Y. (2014). Water phase transition under pressure and its application in high pressure thawing of agar gel and fish. *Journal of Food Engineering*, 125, 1-6.

## **Chapter 2 Model food development for tuna (*Thunnus obesus*) in radio frequency and microwave tempering using grass carp mince**

### **2.1 Introduction**

Frozen seafood products are often tempered for further cutting or slicing processes. Compared to conventional tempering methods, e.g. air and water tempering, which usually take a relatively long time due to the slow heat transfer rates, radio frequency (RF) and microwave (MW) tempering methods are emerging and promising heating technologies with many potential applications (Bornhorst, Liu, Tang, Sablani, & Barbosa-Cánovas, 2017; B. Li & Sun, 2002; Llave, Terada, Fukuoka, & Sakai, 2014; Tang et al., 2008). RF and MW tempering are both dielectric tempering methods, which provide volumetric heating by converting electromagnetic energy to thermal energy inside the material (Ozkoc et al., 2014). Because of the volumetric and fast heating characteristics, RF and MW significantly improve the heating rate and retain the nutrients and quality of the fishery products (Di Rosa, Bressan, Leone, Falqui, & Chiofalo, 2019; Jiao, Tang, Wang, & Koral, 2018). However, the main challenge of dielectric tempering is the localized overheating caused by high electromagnetic field intensity focus due to shape and components of foods (Li et al., 2018). Experimentally obtaining the temperature distribution for optimization requires large amount of experimental replicates, which would increase the material cost, especially for the high value fishery products, e.g., tuna. Developing model foods with low cost, homogenous ingredients and comparable dielectric and thermal properties to the original food products could be a good alternative in initial studies as dummy loads for developing the processes (Luan et al., 2015; Wang et al., 2009).

In the dielectric-processing thawing and sterilization-g research field, some studies have been developed model foods. These studies revealed that model foods could be used to simulate various food materials being used as dummy loads for lowering potential test cost. However, only few model foods have been developed for tempering/thawing processes since it requires dielectric properties matching with the real foods under both frozen and unfrozen state. Thus, using low-cost fish with additives

as model foods for high-value fish could be an effective approach since fish, even in different species, may have similar components and physicochemical properties. Evaluating the properties of selected low-cost fish could be a better and reasonable starting point.

The general objective of this part of the study was to explore the feasibility of using grass carp mince as a model food to imitate the tuna tempering processes with RF and MW, and assess the additives influence on the temperature distributions of the developed model foods. Thus, this study aimed to: (1) determine the DPs of grass carp mince with different vegetable oil, methylcellulose (MC) and salt contents in the frequency range of 1-2500 MHz and at the temperatures from -40 to 40 °C; and (2) conduct RF (27.12 MHz) and MW (2450 MHz) tempering experiments to find the optimal composition of grass carp mince model food by comparing the heating patterns to that of tuna.

## **2.2 Materials and methods**

### **2.2.1 Materials preparation**

Frozen Bigeye Tuna (*Thunnus obesus*) was purchased from JINXIAN Co., Ltd., Shanghai, China, and the fresh grass carp was purchased from a local grocery store (No. 580 Guzong 99 Road, Nanhui New Town, Shanghai, China), transported to the laboratory in a cooler. The lateral part muscle was used for experiments. The grass carp was headed, skinned, cut into pieces, minced by hand, and different vegetable oil contents (1.0%, 2.0%, 4.0%, 6.0% and 8.0% wt), methylcellulose (MC, 9004-67-5, labtop Bio-Technology, Shanghai, China) contents (1.0%, 2.0%, 4.0%, 6.0% and 8.0% wt) and salt contents (0.25%, 0.5%, 1.0%, 2.0% and 4.0% wt) were added into the mince accordingly based on the experimental design. The additives were selected based on the literatures mentioned in the introduction section, which reported vegetable oil, MC and salt could efficiently adjust the dielectric properties of model foods. All samples prepared for RF and MW tempering experiments were frozen at -18 °C, cut into the size of 8×8×3 cm<sup>3</sup>, and then stored at -55 °C in a freezer for over 24 h (DW/BD-55W321EU1, Haier, Qingdao, China).

### 2.2.2 Composition determination

Both tuna and grass carp fillets were obtained and homogenized with a homogenizer (JR-12 800W, Shangxichu, Guangzhou, China) for determining their composition. The moisture content was determined with a constant mass method (AOAC 950.46) at 105 °C drying in an electric blast drying oven (Shanghai Boxun Industrial Co., Ltd. Medical Equipment Manufacturer, China). The fat content was determined with the Soxhlet extraction method (AOAC 960.39) in FOSS Soxtec™ 2050 automatic Soxhlet fat leaching instrument (Danish Fox Group Corporation, Denmark). The protein content was determined with the Kjeldahl method (AOAC 981.10) in FOSS Kjeltex™ 8400 fully automatic Kjeldahl analyzer (Danish Fox Group Corporation, Denmark). The ash content was determined by a dry ashing method (AOAC 920.153) at 550 °C in a muffle oven (Shanghai Jinghong Experimental Equipment Co., Ltd., China). All experiments were replicated three times.

### 2.2.3 Dielectric properties measurement

The dielectric properties, also called as relative complex permittivity ( $\epsilon^*$ ), can be described as a combination of the dielectric constant ( $\epsilon'$ ), which presents the ability to store electromagnetic energy, and the dielectric loss factor ( $\epsilon''$ ), which presents the ability to dissipate electromagnetic energy.

$$\epsilon^* = \epsilon' - j\epsilon'' \quad (2-1)$$

in which  $j=-1$ ,  $\epsilon^*$  is the relative complex permittivity,  $\epsilon'$  is the dielectric constant, and  $\epsilon''$  is the dielectric loss factor.

The dielectric properties of tuna and the developed model foods were measured with an open-ended probe (Agilent N1501A, Agilent Technologies Inc., San Jose, USA) connected with a network analyzer (Agilent E5071C, Agilent Technologies Inc., San Jose, USA). A custom-built temperature-holding sample holder ( $d = 2.5$  cm,  $h = 10$  cm) connected to an oil bath (PolyScience Products, Niles, USA) was used to hold the sample for dielectric property measurement at controlled temperatures. The measuring system was calibrated before each independent measurement to avoid system errors. The typical error of the system was about 5% following standard calibration procedures.

All samples were cut into a cylindrical shape with a diameter of 2.5 cm and height of 10 cm and fed into the sample holder. The sample temperature was monitored with a type-T thermocouple wire inserted into the sample geometrical center throughout the measurement process. The measurements were started when the temperature of the sample inside the measurement cell stabilized at -40 °C. Subsequent measurements were taken with a temperature range -40 ~ 40 °C by controlling the oil bath temperature. The detailed measurement system and procedures of experiments were described in Wang et al. (2008). The dielectric properties determination was within the frequency range of 1 ~ 2500 MHz and temperature range of -40 ~ 40 °C. All measurements were conducted in triplicate.

#### 2.2.4 Penetration depth

Penetration depth ( $d_p$ ) was defined as the depth in a material where the energy of a plane wave propagating perpendicular to the surface has decreased to  $1/e$  of the surface value. The penetration depths of tuna and the developed model foods at selected frequency bands were calculated with the following equation:

$$d_p = \frac{c}{2\pi f \sqrt{2\varepsilon' \left[ \sqrt{1+(\varepsilon''/\varepsilon')^2} - 1 \right]}} \quad (2-2)$$

where  $c$  is the speed of propagation of waves in vacuum, which is  $3 \times 10^8 \text{ m s}^{-1}$  and  $d_p$  is in m.

#### 2.2.5 Thermal properties

##### 2.2.5.1 Specific heat capacity

A Differential scanning calorimetry (DSC) with a liquid nitrogen cooling system (TA Instruments, Q2000 modulated, The United State) was used to determine the specific heat capacity of tuna and the selected model foods at a temperature range of -30 ~ 80 °C. Temperature and heat flow calibration was performed with indium and water before experiments. The reference example was considered as a hermetically sealed empty aluminum chamber. Liquid nitrogen was used as carrier gas. A clean aluminum chamber with 20 mg samples was hermetically sealed with the Tzero DSC press. After the samples were placed in a DSC unit, the system was first cooled down

to -30 °C with a heating rate of 5 °C/min, and heated from -30 to 80 °C with a heating rate of 1 °C/min. The heat flow curves presented the change of enthalpy values with temperature, and the specific heat capacity values were calculated from the curve.

### 2.2.5.2 Thermal conductivity

Choi and Okos (1986) developed mathematical models for prediction of thermal properties of water, protein, fat, carbohydrate, fiber and ash components as a function of temperature in the range of -40 ~ 150 °C. The models have been validated as effective by many literatures. The thermal conductivity of samples was calculated by the equations as follows:

$$k_{water} = 0.57109 + 1.7625 \times 10^{-3}T - 6.7036 \times 10^{-6}T^2 \quad (2-3)$$

$$k_{protein} = 0.20141 + 1.3874 \times 10^{-3}T - 4.3312 \times 10^{-6}T^2 \quad (2-4)$$

$$k_{fat} = 0.18071 + 2.7604 \times 10^{-3}T - 1.7749 \times 10^{-7}T^2 \quad (2-5)$$

$$k_{ash} = 0.32961 + 1.4011 \times 10^{-3}T - 2.9069 \times 10^{-6}T^2 \quad (2-6)$$

$$k_{ice} = 2.2196 - 6.2489 \times 10^{-3}T + 1.0154 \times 10^{-4}T^2 \quad (2-7)$$

where  $k$  is the thermal conductivity in W/m°C;  $T$  is the temperature in °C. In this study, the composition of tuna and its model foods were put into the equations, and their thermal conductivities at -40 °C ~ 40 °C were calculated.

## 2.2.6 Tempering experiment and temperature measurements

### 2.2.6.1 Radio frequency tempering

A 27.12 MHz RF heating system (Labotron 12, Sairem, France) was used for tempering experiments. The tempering experimental conditions were set as 600 W input power with an electrode gap of 7 cm. The applied voltage on the top electrode varied along the tempering process in the range of 1000 ~1500 V. The size of top electrode of RF system is 500 ×1050 mm<sup>2</sup>. The detailed information about RF system was described in Li at al. (2018). The RF heating cavity and sample location was showed in Fig. 2-1(a). The tempering time for each tuna and model food sample (size: 8×8×3 cm<sup>3</sup>) was set as 10 min until the sample center temperature reaching above -10 °C. The tempering time was obtained based on preliminary experimental results. Before the tempering

experiments, frozen samples were brought out of the freezer, and a  $\Phi 3$  mm hole was drilled at the geometrical center of each sample to allow insertion of temperature monitoring sensors. A fiber optic sensor (HQ-FTS-D1F00, Heqi guangdian, Shanxi, China) was inserted into the drilled hole for measuring the center temperature of samples during the RF tempering process. Right after tempering, the tempered sample was brought to an infrared camera (FLIR A655sc, Wilsonville, USA) for obtaining its surface temperature distribution. The experiment was replicated three times.

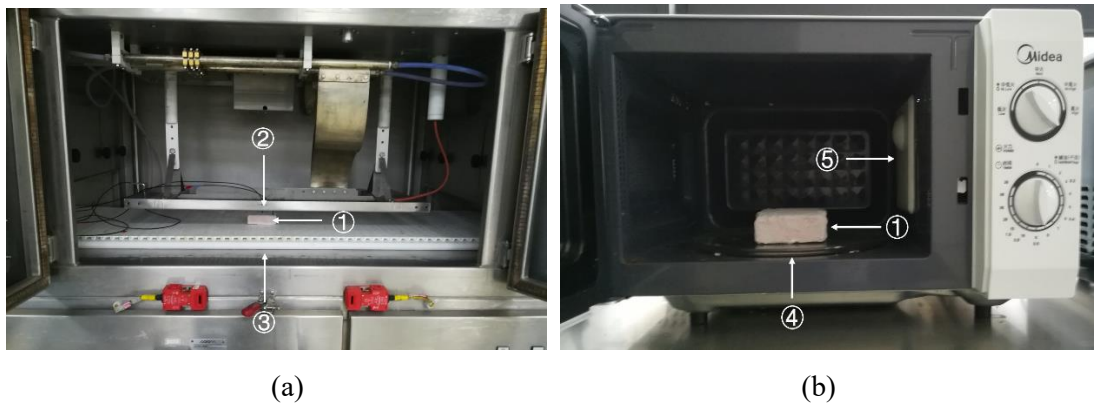


Fig. 2-1. Layout of (a) RF system (1. Sample; 2. Top electrode; 3. Bottom electrode) and (b) MW oven (1. Sample; 4. Turntable; 5. Magnetron) used for tempering experiments.

### 2.2.6.2 Microwave tempering

A 2450 MHz, 700 W microwave oven (M1-211A, Midea, Guangzhou, China) was used for the tempering experiments. The cavity size of the microwave oven is  $315 \times 202 \times 325$  mm<sup>3</sup> and the diameter of turntable is 270 mm. The samples were put into the cavity without any containers. The rotation speed of the turning table was 4 r/min in the MW tempering process. A picture of the oven cavity and sample location was showed in Fig. 2-1(b). The tempering time for each tuna and selected model food sample (size:  $8 \times 8 \times 3$  cm<sup>3</sup>) was set as 5 min in the thawing mode with 33% effective output power, which was suggested by the microwave oven manufacturer. During MW tempering process, the rotation of samples will twist the fiber optic sensor if inserting into the sample center to obtain the tempering temperature-time history. Thus, the center temperature of sample was measured every 1 min by stopping the experiment temporarily and quickly measured with a fiber optic sensor. Right after tempering, the tempered sample was brought to an infrared camera (FLIR A655sc, Wilsonville, OR,

USA) for obtaining its surface temperature distribution. The experiment was replicated three times.

### 2.2.7 Statistical analysis

Statistical analysis was performed using Microsoft office Excel 2016 and OriginPro 9.1. All experimental data were represented as mean or mean  $\pm$  standard deviation. A one way ANOVA test was conducted to determine the significance of the main effects using the LSD procedure to compare treatment means ( $p < 0.05$ ).

## 2.3 Results and discussion

### 2.3.1 Composition determination

The chemical composition of tuna and grass carp fish are shown in Table 2-1. The results showed that grass carp fish has a higher moisture content than of tuna. The fat content of grass carp was higher than of tuna while the protein content of grass carp was lower than tuna. The moisture, protein and fat content of tuna were 72.94%, 25.07% and 0.51%, respectively, while those of the grass carp fish were 80.43%, 18.24 and 0.97%. The composition of tuna and grass carp fish was similar to the reported in the literatures (Ashraf et al., 2011; Nurjanah et al., 2019), which showed 72.33 ~ 72.97% moisture, 21.47 ~ 25.86% protein and 0.60 ~ 2.38% fat of tuna and 74.30 ~ 78.79% moisture, 15.50 ~ 20.00% protein and 2.12 ~ 2.71% of grass carp fish. Liu, Fukuoka, and Sakai (2012) showed that moisture content was the most influential factor for the dielectric properties of fish flesh. Since the composition influenced dielectric properties of food material significantly, there was possibly a significant difference gap between both the dielectric constant and loss factor between the grass carp and the tuna, which could be made up by appropriate amount of additives addition.

Table 2-1 Chemical composition of tuna and grass carp fish

Sorts	Moisture content (%)	Fat content (%)	Protein content (%)	Ash content (%)
Lean Tuna	72.94 $\pm$ 0.11 <sup>a</sup>	0.51 $\pm$ 0.10 <sup>a</sup>	25.07 $\pm$ 0.19 <sup>a</sup>	1.30 $\pm$ 0.02 <sup>a</sup>
Grass Carp	80.43 $\pm$ 0.25 <sup>b</sup>	0.97 $\pm$ 0.07 <sup>b</sup>	18.24 $\pm$ 0.24 <sup>b</sup>	1.18 $\pm$ 0.07 <sup>a</sup>

## 2.3.2 Effect of additives on dielectric properties

### 2.3.2.1. Effect of oil content

The dielectric properties of grass carp, tuna, and the effect of oil content (1.0%, 2.0%, 4.0%, 6.0% and 8.0% wt) on the dielectric properties of grass carp mince at room temperature throughout the frequency range of 1 ~ 2500 MHz is shown in Fig. 2-2. The dielectric constant of tuna was lower than that of grass carp while the dielectric loss factor was higher than that of grass carp. Both dielectric constant and loss factor exponentially decreased from 1 to 300 MHz, and then the decreasing slope was slowed down from 300 to 1500 MHz until no significant change was found at 1500 ~ 2500 MHz. The dielectric constant decreased with increasing oil content at all frequencies, and the tendency of decline of samples with higher oil content were more significant. Dielectric properties of tuna and its model foods at 27.12 MHz and 2450 MHz at 20 °C is shown in Table 2-2. The dielectric constants at room temperature were reduced from 129.8 for grass carp without oil to 128.2, 125.3, 119.5, 117.2 and 114.9 for grass carp with 1.0%, 2.0%, 4.0%, 6.0% and 8.0% oil contents at 27.12 MHz, respectively. At 2450 MHz, the corresponding values were reduced from 61.9 for grass carp without oil to 60.0, 59.7, 57.9, 56.0 and 54.3 for grass carp with 1.0%, 2.0%, 4.0%, 6.0% and 8.0% oil contents, respectively. The dielectric constant of grass carp with 4.0% oil was found to be the closest to that of tuna. However, oil addition affected the dielectric loss factor of grass carp insignificantly.

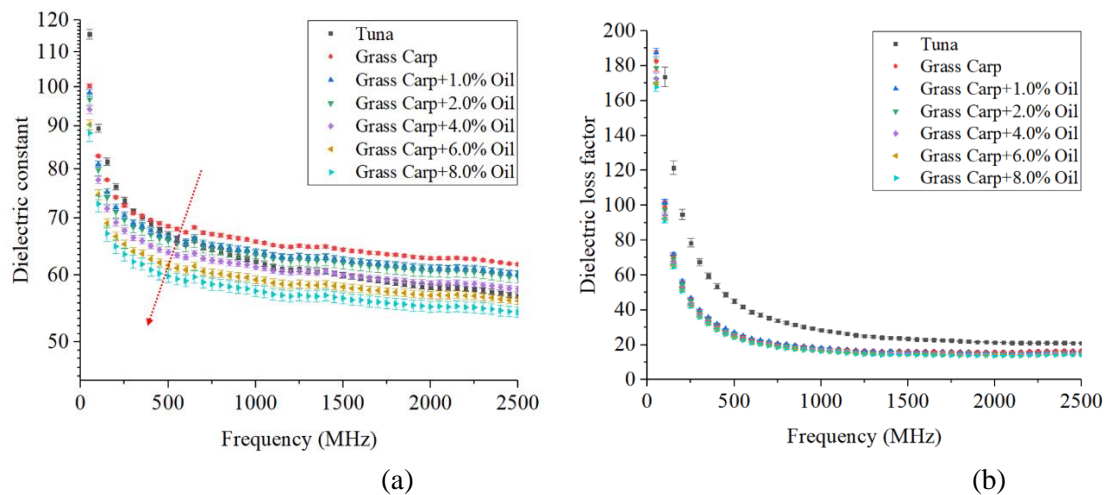


Fig. 2-2. Dielectric properties of tuna and grass carp with different vegetable oil content at frequency range of 1~2500 MHz at 20 °C

Table 2-2 Dielectric properties of tuna and its model foods at 27.12 MHz and 2450 MHz at 20 °C (MC: Methylcellulose)

Formulations	27.12 MHz		2450 MHz	
	$\epsilon'$	$\epsilon''$	$\epsilon'$	$\epsilon''$
Tuna	164.7 ± 2.5	552.8 ± 20.1	56.8 ± 0.4	21.0 ± 0.2
Grass Carp	129.8 ± 1.6	307.7 ± 9.9	61.9 ± 0.2	16.6 ± 0.2
Grass Carp+1% Oil	128.2 ± 1.4	315.9 ± 4.3	60.0 ± 0.5	15.8 ± 0.1
Grass Carp+2% Oil	125.3 ± 2.5	300.2 ± 9.7	59.7 ± 0.9	15.7 ± 0.3
Grass Carp+4% Oil	119.9 ± 1.6	289.2 ± 5.8	57.9 ± 0.4	15.2 ± 0.2
Grass Carp+6% Oil	117.2 ± 1.6	285.5 ± 0.9	56.0 ± 0.6	14.7 ± 0.1
Grass Carp+8% Oil	114.8 ± 2.5	281.7 ± 4.0	54.3 ± 0.8	14.3 ± 0.3
Grass Carp +1% MC	107.4 ± 0.9	437.3 ± 11.1	60.5 ± 0.3	18.2 ± 0.1
Grass Carp +2% MC	114.5 ± 1.4	539.6 ± 24.6	59.3 ± 0.2	19.3 ± 0.2
Grass Carp +4% MC	124.2 ± 1.1	688.4 ± 23.1	59.6 ± 1.2	21.3 ± 0.4
Grass Carp +6% MC	127.5 ± 5.8	783.6 ± 43.2	57.9 ± 0.3	22.4 ± 0.4
Grass Carp +8% MC	133.1 ± 2.6	902.4 ± 25.8	56.9 ± 1.6	23.6 ± 0.5
Grass Carp+0.25% NaCl	153.3 ± 1.2	467.7 ± 8.5	61.8 ± 0.2	18.5 ± 0.1
Grass Carp+0.5% NaCl	175.6 ± 2.2	628.3 ± 20.2	63.2 ± 0.3	20.8 ± 0.2
Grass Carp+1.0% NaCl	221.5 ± 2.7	987.3 ± 27.0	63.4 ± 0.5	25.4 ± 0.3
Grass Carp+2.0% NaCl	299.9 ± 6.1	1592.2 ± 49.1	61.4 ± 0.4	33.4 ± 0.6
Grass Carp+4.0% NaCl	450.2 ± 7.1	2731.3 ± 56.9	58.7 ± 0.5	48.4 ± 0.7
Grass Carp+4% Oil+4% MC+0% NaCl	115.0 ± 3.1	674.9 ± 24.7	56.0 ± 0.6	19.3 ± 0.5
Grass Carp+4% Oil+4% MC+0.5% NaCl	127.9 ± 0.2	931.8 ± 12.6	53.6 ± 0.1	22.6 ± 0.1
Grass Carp+4% Oil+4% MC+1.0% NaCl	138.8 ± 4.5	1191.9 ± 90.4	51.9 ± 1.4	25.6 ± 1.1
Grass Carp+4% Oil+4% MC+2.0% NaCl	165.7 ± 1.5	1784.1 ± 45.9	51.3 ± 0.2	32.7 ± 0.5

### 2.3.2.2. Effect of methylcellulose content

The effect of methylcellulose (MC) content (1.0%, 2.0%, 4.0%, 6.0% and 8.0% wt) on the dielectric properties of grass carp mince at room temperature and frequency of 1-2500 MHz is shown in Fig. 2-3. The dielectric constant of samples decreased with increasing MC content. As dielectric constant is usually mainly affected by the free water within the material, methylcellulose is a hydrophilic powder that tend to absorb free water and form gel network. Thus, the dielectric constant of grass carp mince decreased with increasing MC content (Chamchong & Datta, 1999; Curet, Rouaud, &

Boillereaux, 2008; Llave et al., 2016). However, the addition of MC increased the dielectric loss factor especially at low frequency ( $< 1000$  MHz). At 27.12 MHz, the dielectric loss factors of grass carp mince at room temperature increased from 307.7 to 437.3, 525.0, 688.4, 783.6 and 902.4 with 1.0%, 2.0%, 4.0%, 6.0% and 8.0% MC contents, respectively. At 2450 MHz, the loss factor of grass carp increased from 16.6 to 18.2, 19.3, 21.3, 22.4 and 23.6 for grass carp with 1.0%, 2.0%, 4.0%, 6.0% and 8.0% MC addition, respectively. This was because higher MC concentration led to higher ion concentration and the increment of loss factor. The result was similar to the effect of bentonite concentration in a model food reported by Luan et al. (2015), which showed that a higher bentonite concentration also led to lower dielectric constants and higher loss factors. It was observed that the dielectric loss factor of grass carp with 4.0% methylcellulose was the closest to that of tuna.

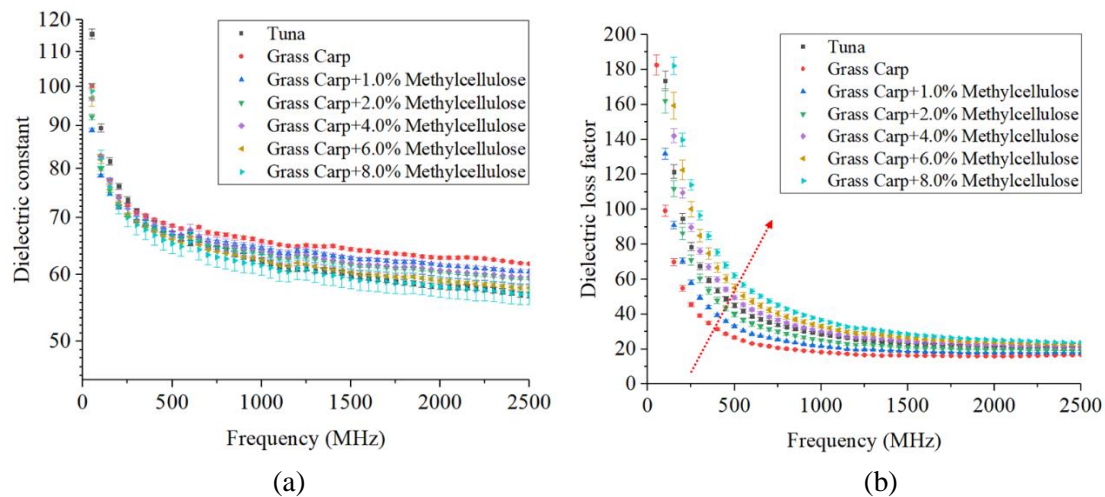


Fig. 2-3. Dielectric properties of tuna and grass carp with different methylcellulose content at the frequency range of 1~2500 MHz at 20 °C

### 2.3.2.3. Effect of salt content

The effect of salt content (0.25%, 0.5%, 1.0%, 2.0% and 4.0% wt) on the dielectric properties of grass carp mince at room temperature throughout the frequency range of 1-2500 MHz is shown in Fig. 2-4. The addition of salt significantly increased both the dielectric constant and the dielectric loss factor at 1000-2500 MHz. However, at 1000-2500 MHz, the dielectric constant first increased and then decreased with the increased salt concentration, among which, the dielectric constant of grass carp mince with 1.0% NaCl addition was found to be the highest. The addition of salt can increase the

solubility of protein and water retention and promote the formation of a protein-water matrix (Ahmed, Ramaswamy, & Raghavan, 2007; Calay, Newborough, Probert, & Calay, 1994; Feng et al., 2015; Ryynanen, 1995). The possible explanation is, with less than 1.0% salt addition, the protein molecules in mince were unfolded and the disulfide bonds were broken to form hydrophilic sulfhydryl groups, which would hold more free water inside the material and increase the dielectric constant. When the salt content increased above 1.0%, the myofilament lattice expanded due to the increased electrostatic repulsion by binding ions, which resulted in a lower water holding capacity and lower dielectric constant (Jiang, Nakazawa, Hu, Osako, & Okazaki, 2019). Comparing to the dielectric constant, the increasing rate of loss factor was significant as salt content increased. The dielectric loss factor increased with increasing salt content especially at 1000-2500 MHz, which indicated that ionic loss was the dominant loss mechanism at frequencies < 1000 MHz. The dielectric loss factors at room temperature increased from 307.7 to 467.7, 628.3, 987.3, 1592.2 and 2731.3 for grass carp with 0.25%, 0.5%, 1.0%, 2.0% and 4.0% salt contents at 27.12 MHz, respectively. Meanwhile, at 2450 MHz, the corresponding values increased from 16.6 for grass carp without addition to 18.5, 20.8, 25.4, 33.4 and 48.4 with 0.25%, 0.5%, 1.0%, 2.0% and 4.0% salt contents, respectively. This positive effect on the loss factor of increasing salt level was previously reported for salmon fillets with 0–0.5 g/100 g NaCl (Wang, Tang, Rasco, Kong, & Wang, 2008), surimi with 0–6 g/100 g NaCl (Calay et al., 1994), myofibrillar protein dispersions with 0.3-0.6 M NaCl (Feng et al., 2015), low-acyl gellan gel with 0-300 mM NaCl (Zhang et al., 2015) and tylose water pastes with 0.5-2.0% w.b. NaCl content (Llave et al., 2016).

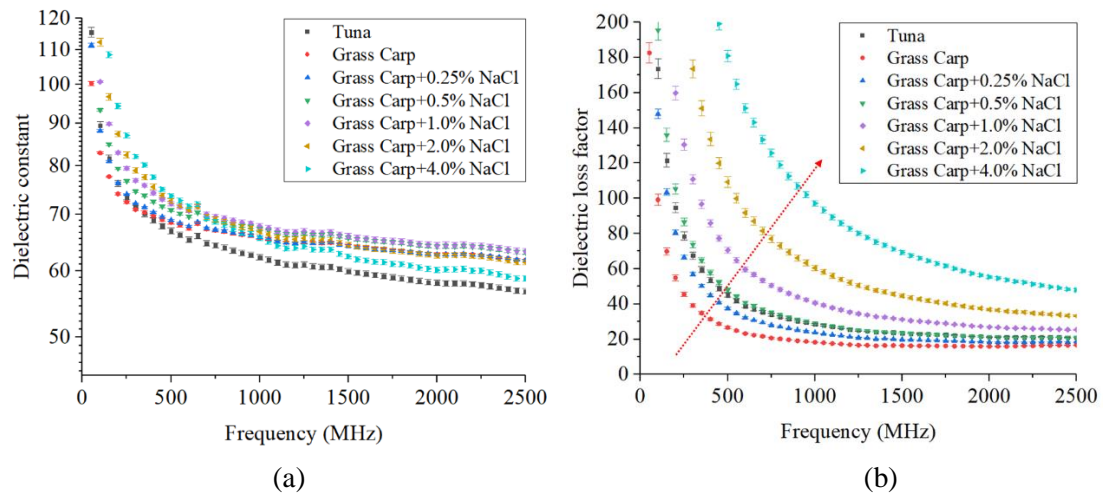


Fig. 2-4. Dielectric properties of tuna and grass carp with different salt content at frequency range of 1~2500 MHz at 20 °C

### 2.3.2.4 Effect of combined effect

The effect of salt content (0.5%, 1.0% and 2.0% wt) with 4% methylcellulose on the dielectric properties of grass carp at room temperature throughout the frequency range of 1-2500 MHz is shown in Fig. 2-5. The addition of salt increased the dissolved ions in the free water which reduced the polarization of water and the dielectric constant (Yaghmaee & Durance, 2002). Meanwhile, the loss factor increased with salt contents due to electrophoretic migration of dissolved ions. The result was similar to the literature (Bircan & Barringer, 1998). Moreover, the large basal surface structure of methylcellulose act as an emulsifier to combine oil and water molecules. Due to the interaction effects between the salt and vegetable oil, the effects of salt on the loss factor and oil on the dielectric constant were weakened a little. As a result, the dielectric properties of grass carp with 4.0% oil and 4.0% methylcellulose was the closest to that of tuna.

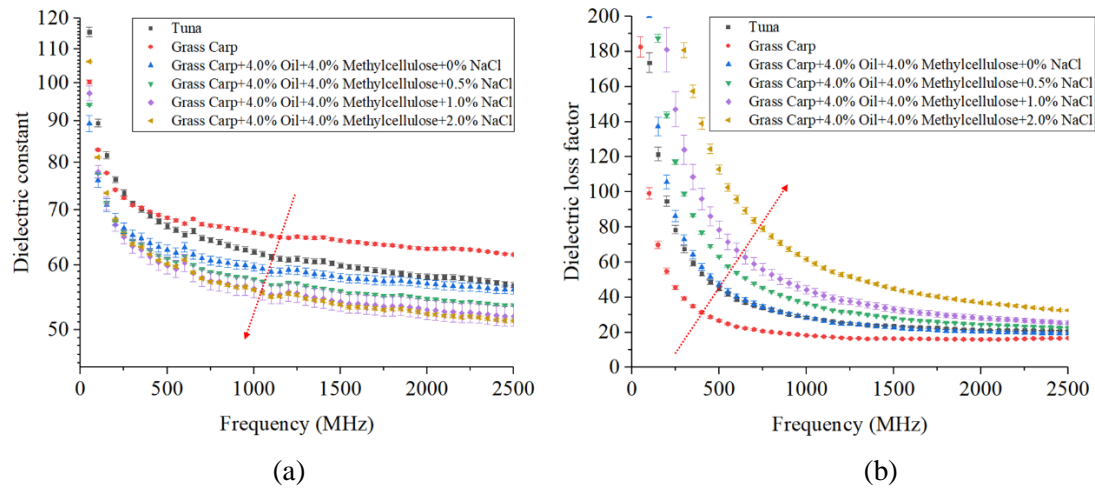
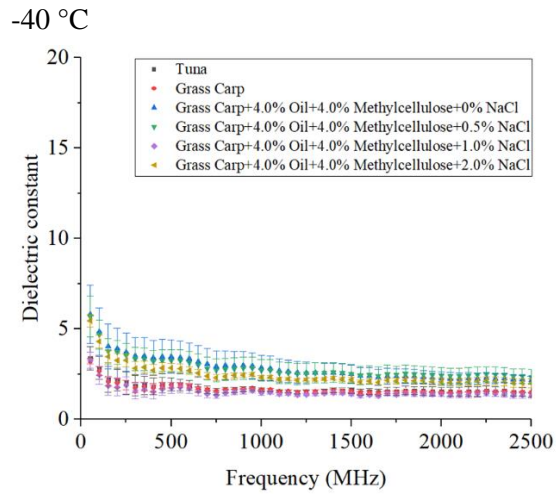


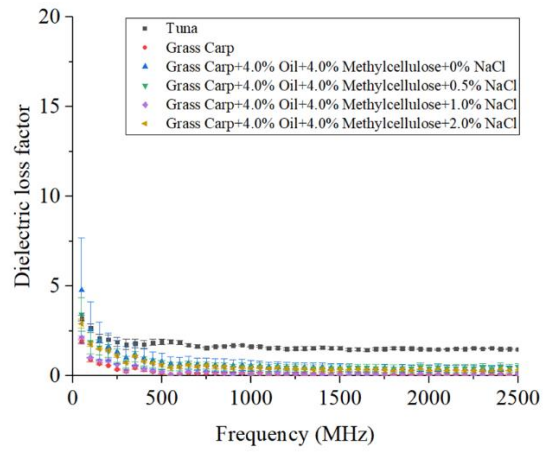
Fig. 2-5. Dielectric properties of tuna and model foods (grass carp with 4.0% oil, 4.0% methylcellulose and different salt contents) at frequency range of 1~2500 MHz at 20 °C

### 2.3.2.5. Effect of temperature

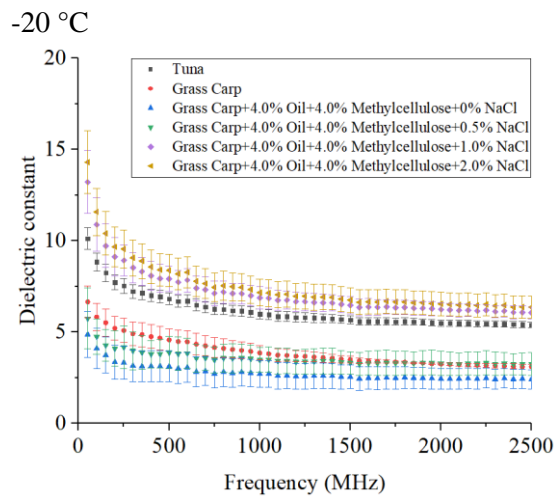
Fig. 2-6. shows the effect of temperature on the dielectric properties of the grass carp mince with 4% oil, 4% methylcellulose and different salt content (0%, 0.5%, 1.0% and 2.0% wt) within the frequency range of 1 ~ 2500 MHz. It was reported that the influence of temperature on the dielectric properties was depended on the frequency, the bound-water and free-water content ratio, and the ionic conductivity of the material (Calay et al., 1994). The results in Fig. 2-6 revealed that temperature had a significant influence on both dielectric constant and loss factor of the model foods. As salt content increased, the freezing point of fish samples decrease, thus the dielectric constant increased as salt content increased. The lower the temperature, the more proportion of water was frozen, and the reduced mobile water led to the lower dielectric properties compared to that at higher temperature. In general, both dielectric constant and loss factor increased as temperature increased from -40 to 40 °C, which was attributed to the increasing water dipole rotation and ionic conductivity (Kannan, Dev, Garipey, & Raghavan, 2013).



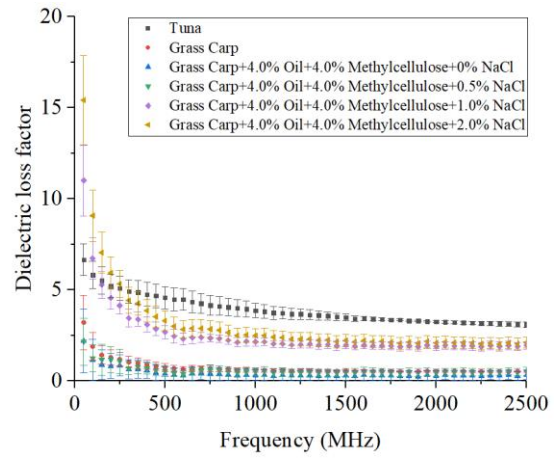
(a)



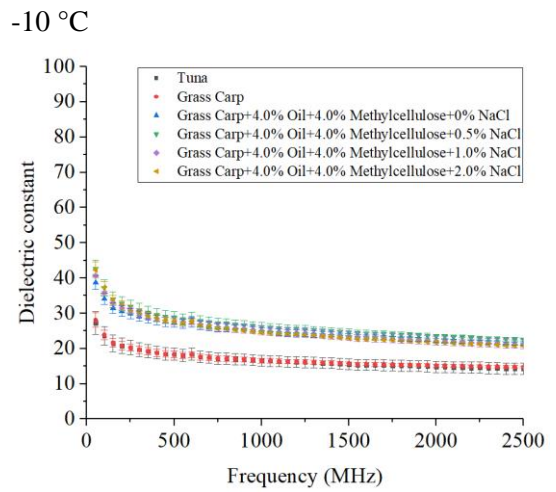
(b)



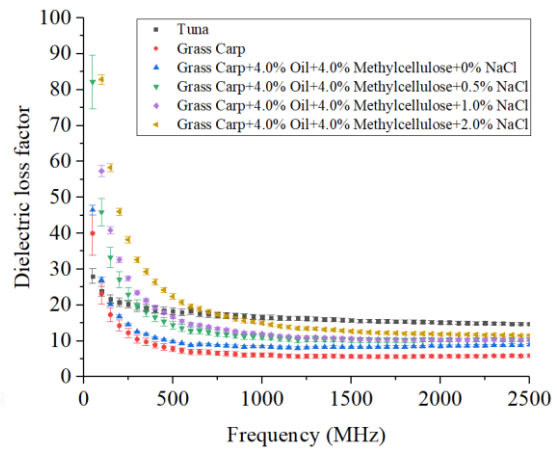
(c)



(d)



(e)



(f)

0 °C

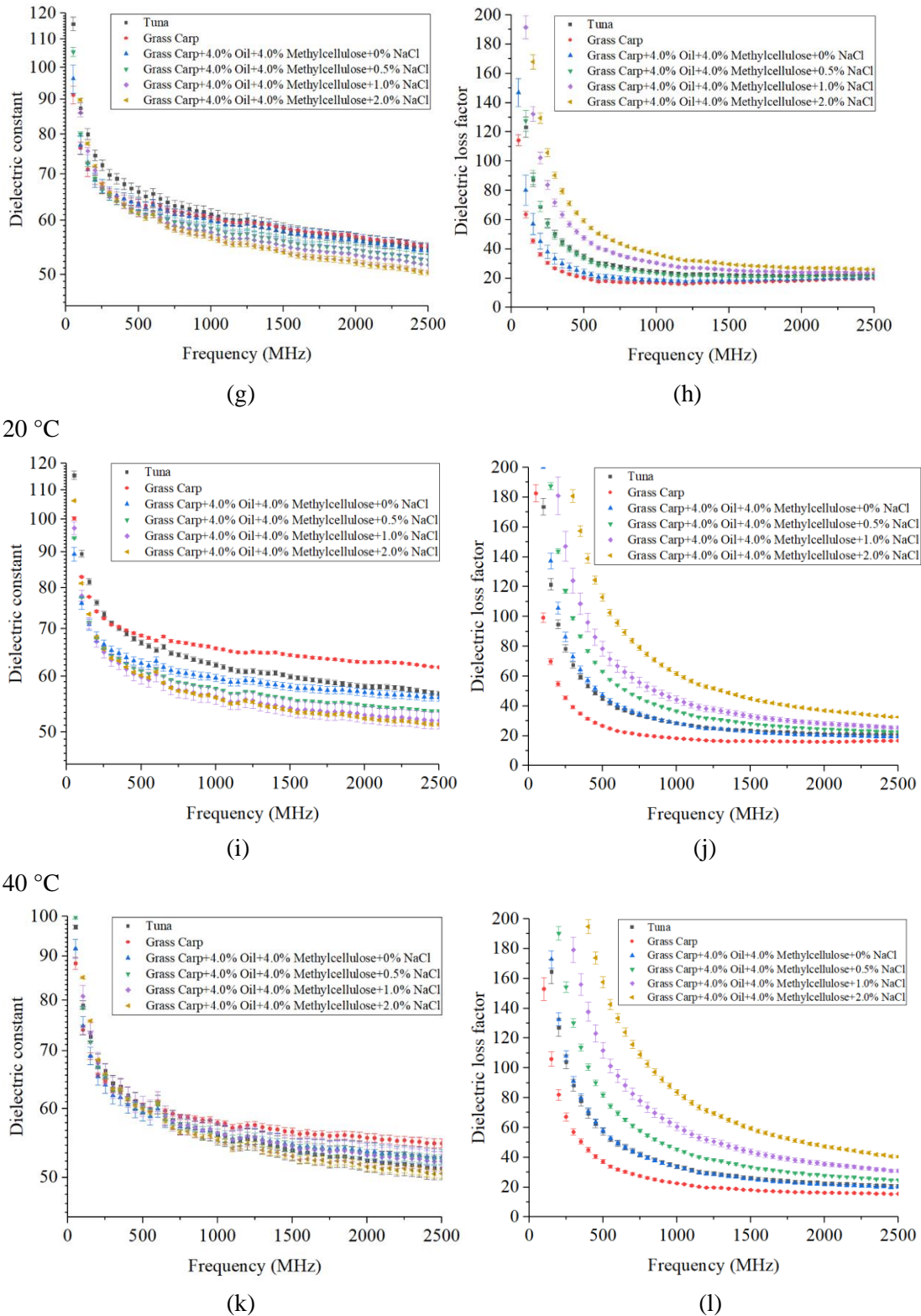
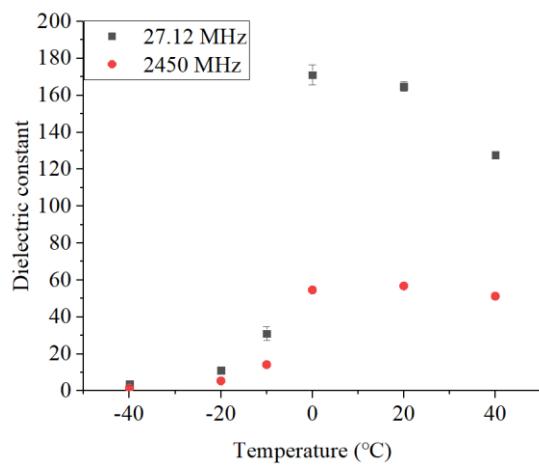


Fig. 2-6. Dielectric properties of tuna and model foods at frequency range of 1~2500 MHz at temperature range -40 ~ 40 °C

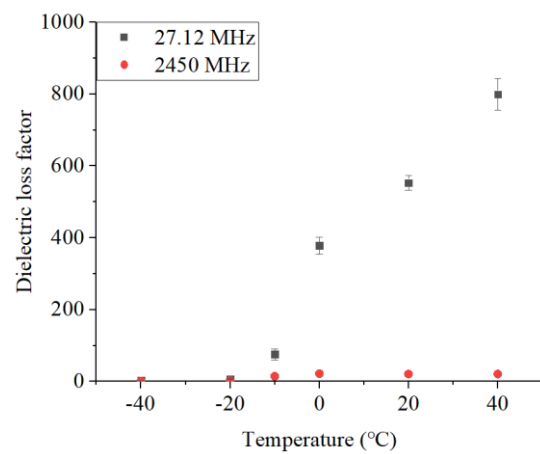
The changes in the dielectric properties of tuna and the developed model foods at -40 ~ 40 °C and frequencies of 27.12 and 2450 MHz are shown in Fig. 2-7. At frozen

state (-40 to -10 °C), the dielectric properties of all samples were not significantly different due to the limited amount of mobile water in frozen fish mince. The result was similar with the literature conducted by Llave et al. (2016). While at the phase change temperature (-10 to 0 °C), the dielectric properties increased significantly because of the increment in dipole molecules oscillation as free water amount increased. The loss factors sharply rose with the increasing salt contents over 0 °C due to the increment of electrophoretic migration with the addition of conductive charge carriers.

Tuna:

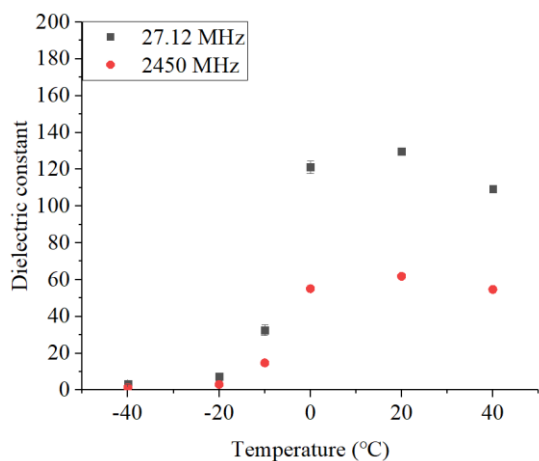


(a)

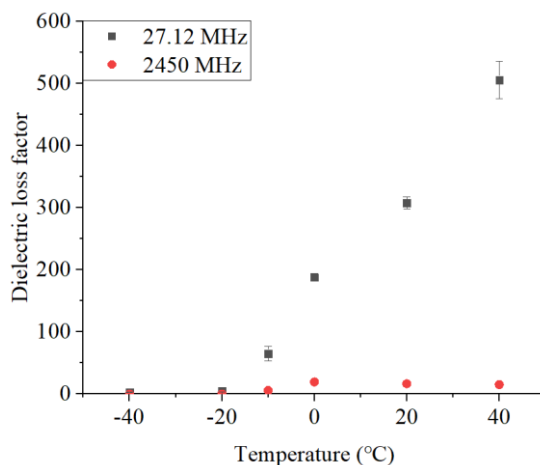


(b)

Grass Carp:

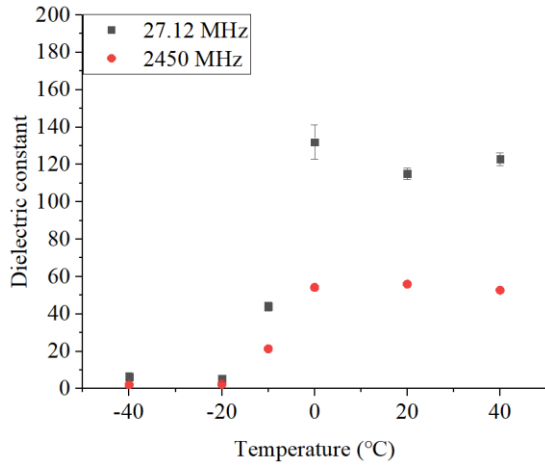


(c)

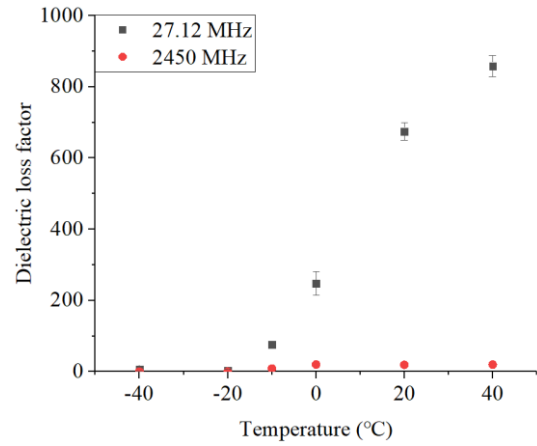


(d)

Grass Carp+4% Oil+4% Methylcellulose+0% NaCl:

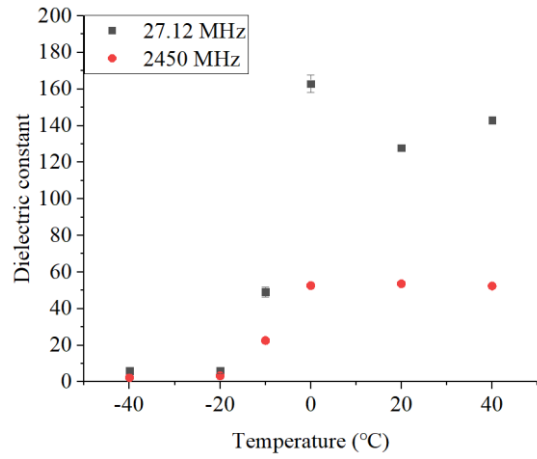


(e)

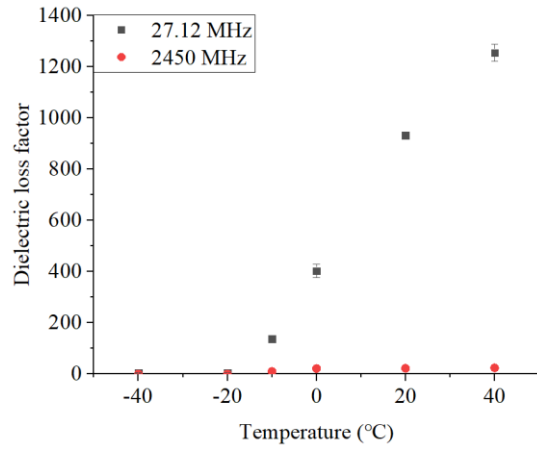


(f)

Grass Carp+4% Oil+4% Methylcellulose+0.5% NaCl:

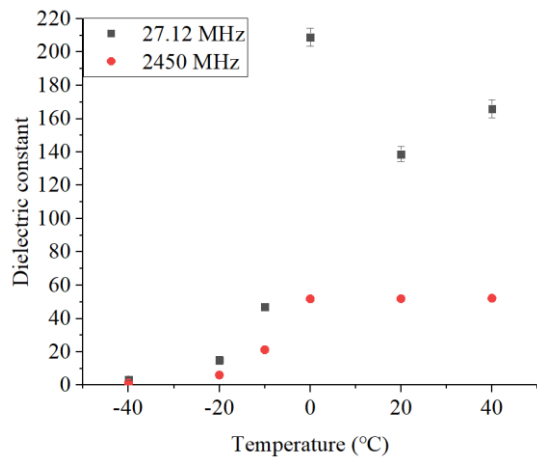


(g)

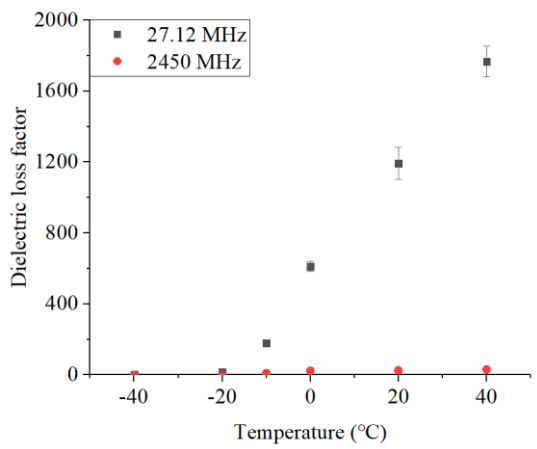


(h)

Grass Carp+4% Oil+4% Methylcellulose+1.0% NaCl:



(i)



(j)

Grass Carp+4% Oil+4% Methylcellulose+2.0% NaCl:

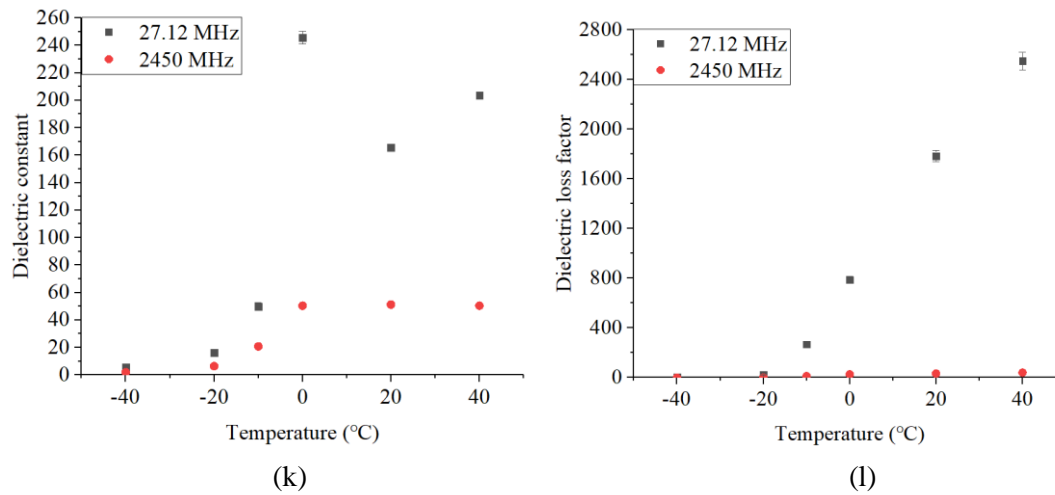


Fig. 2-7. Dielectric properties of tuna and grass carp with different salt content at temperature range -40 ~ 40 °C at 27.12 MHz and 2450 MHz

Table 2-3 Penetration depth of tuna and model foods at temperature range -40 ~ 40 °C at 27.12 MHz and 2450 MHz (MC: Methylcellulose)

Frequency (MHz)	Temperature (°C)	$d_p$ (cm)					
		Tuna	Grass Carp	Grass Carp+4% Oil+4% MC+0% NaCl	Grass Carp+4% Oil+4% MC+0.5% NaCl	Grass Carp+4% Oil+4% MC+1.0% NaCl	Grass Carp+4% Oil+4% MC+2.0% NaCl
27.12	-40	129.76	119.74	167.62	197.05	112.82	113.56
	-20	85.74	92.32	105.65	114.52	44.18	33.82
	-10	17.50	19.57	18.84	12.62	10.56	8.35
	0	7.97	12.31	10.23	7.56	5.96	5.18
	20	6.14	8.72	5.22	4.37	3.82	3.09
	40	4.77	6.17	4.57	3.72	3.11	2.57
2450	-40	11.74	15.32	17.59	17.03	15.61	9.13
	-20	1.51	6.59	10.90	7.32	2.58	2.44
	-10	0.55	1.31	1.04	0.92	0.90	0.80
	0	0.66	0.75	0.73	0.67	0.61	0.55
	20	0.71	0.93	0.77	0.64	0.56	0.45
	40	0.68	0.95	0.73	0.59	0.47	0.36

The penetration depth ( $d_p$ ) of tuna and the developed model foods in a temperature range from -40 to 40 °C at 27.12 and 2450 MHz were calculated (Table 2-3). In general,

the  $d_p$  of samples decreased at all frequencies with increasing temperature, especially at the frozen stage. Similar effects of temperature on  $d_p$  were reported for tylose water pastes by Llave et al. (2016). Frozen samples usually present a larger penetration depth due to their low dielectric constants comparing to those at unfrozen state. Moreover, samples showed a much larger penetration depth at 27.12 MHz than 2450 MHz, which agreed with the literature that penetration depth usually decreased with increasing frequency (Guan, Cheng, Wang, & Tang, 2004; Wang et al., 2009). Based on the results, it could be predicted that the tempering uniformity of fish samples at 27.12 MHz would possibly be better than that at 2450 MHz. The addition of oil and methylcellulose both increased the penetration depth of samples, and higher amount of salt addition decreased it due to the increased of dielectric loss factor (Wang, Tang, Liu, & Bohnet, 2018).

### **2.3.3 Effect of additives on thermal properties**

The thermal properties of foods were strongly dependent on their composition and temperature. The specific heat capacities of tuna and model food at temperature range -30 ~ 80 °C were showed in Fig. 2-8. The additives influenced the specific heat capacity significantly, especially at the temperature range of -10 ~ 0 °C. With the combined addition of oil, MC, and salt the specific heat capacity increased and the addition of salt reduced the peak temperature value, which indicated a decrease of phase change temperature. The specific heat capacity of the model food (grass carp with 4.0% oil, 4.0% MC and 1.0% NaCl) matched that of tuna well. Simdyankin and Bogdanov (2019) studied the thermal properties of hydrobionts' tissues in a freezing process. They found that the specific heat capacity increased due to the intensive ice formation in the tissues, and then decreased due to a significant decrease in the content of the liquid aqueous phase. Hassan and Ramaswamy (2011) found that addition of increasing sodium alginate in the treatment of meat and carrot resulted in a in the heat capacity, which was primarily attributed to the lowering of moisture content of the particles. The latent heat of tuna and its model foods was shown in Table 2-4. No significant difference was observed among different model foods. Wang et al. (2019) investigated

the thermal properties of mandarin fish soaking in sucrose and found no obvious difference for the therapy change.

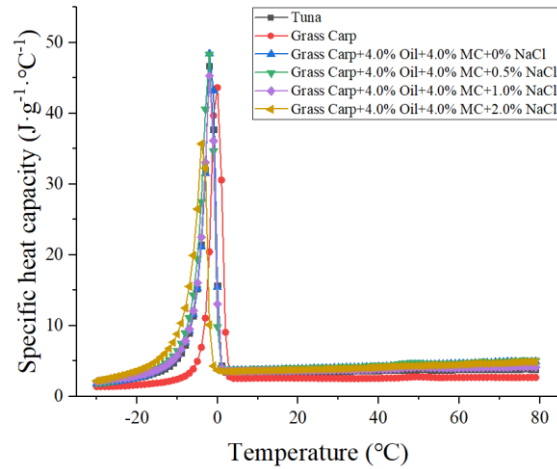


Fig. 2-8 Comparison of specific heat capacity of tuna and model food at temperature range -30 ~ 80 °C (MC: Methylcellulose)

Table 2-4 Comparison of latent heat of tuna and model foods around 0 °C

Material	Latent heat (J/g)
Tuna	162.65 ± 1.34 <sup>a</sup>
Grass Carp	192.85 ± 6.72 <sup>a</sup>
Grass Carp+4.0% Oil+4.0% MC+0% NaCl	142.40 ± 9.76 <sup>a</sup>
Grass Carp+4.0% Oil+4.0% MC+0.5% NaCl	156.15 ± 9.55 <sup>a</sup>
Grass Carp+4.0% Oil+4.0% MC+1.0% NaCl	153.95 ± 6.58 <sup>a</sup>
Grass Carp+4.0% Oil+4.0% MC+2.0% NaCl	127.80 ± 3.39 <sup>a</sup>

The thermal conductivities of tuna and model food at temperature range -40 ~ 40 °C were calculated and showed in Table 2-5. The thermal conductivity of frozen samples was higher than of unfrozen samples. The thermal conductivities of tuna at temperature -40 , -20, 0, 20, 40 °C were 1.96, 1.78, 1.07, 0.50, and 0.52, respectively, while those of grass carp were 2.15, 1.95, 1.16, 0.53, 0.55. The combined addition of oil, MC and salt significantly decreased the thermal conductivity of grass carp because of lowering water content, and the thermal conductivity of the model food (grass carp with 4.0% oil, 4.0% MC and 1.0% NaCl) matched that of tuna well. Salt did not influence the

thermal conductivities significantly since water is the predominant constituent in samples and significantly influences the thermal conductivity. Kumcuoglu, Turgut, and Tavman (2010) measured thermal conductivity values of meat samples with moisture contents between 4.73 and 79.47% and fat contents between 1.44 and 93.17% at a temperatures range of -30 ~ 25 °C. They found that thermal conductivities of frozen meat samples were higher than the ones in the unfrozen state because of higher thermal conductivity of ice compared with that of liquid water. Hassan and Ramaswamy (2011) investigated the thermo-physical properties of meat and carrot, based alginate particles as influenced by the formulation variables. They also found that the change of thermal conductivity values was mostly attributed to the change of moisture content, and little was caused by the other components.

Table 2-5 Comparison of thermal conductivities of tuna and model food at temperature range -40 ~ 40 °C (MC: Methylcellulose)

Temperature (°C)	Tuna	Grass Carp	Grass Carp +4.0% Oil+4.0% MC+0% NaCl	Grass Carp +4.0% Oil+4.0% MC +0.5% NaCl	Grass Carp +4.0% Oil+4.0% MC +1.0% NaCl	Grass Carp +4.0% Oil+4.0% MC +2.0% NaCl
-40	1.96	2.15	1.97	1.96	1.95	1.93
-30	1.86	2.04	1.88	1.87	1.86	1.84
-20	1.78	1.95	1.80	1.79	1.78	1.76
-10	1.72	1.88	1.73	1.72	1.71	1.69
0	1.07	1.16	1.07	1.06	1.06	1.04
10	0.48	0.51	0.47	0.47	0.47	0.46
20	0.50	0.53	0.49	0.48	0.48	0.47
30	0.51	0.54	0.50	0.49	0.49	0.49
40	0.52	0.55	0.51	0.51	0.50	0.50

### 2.3.4 Temperature distributions

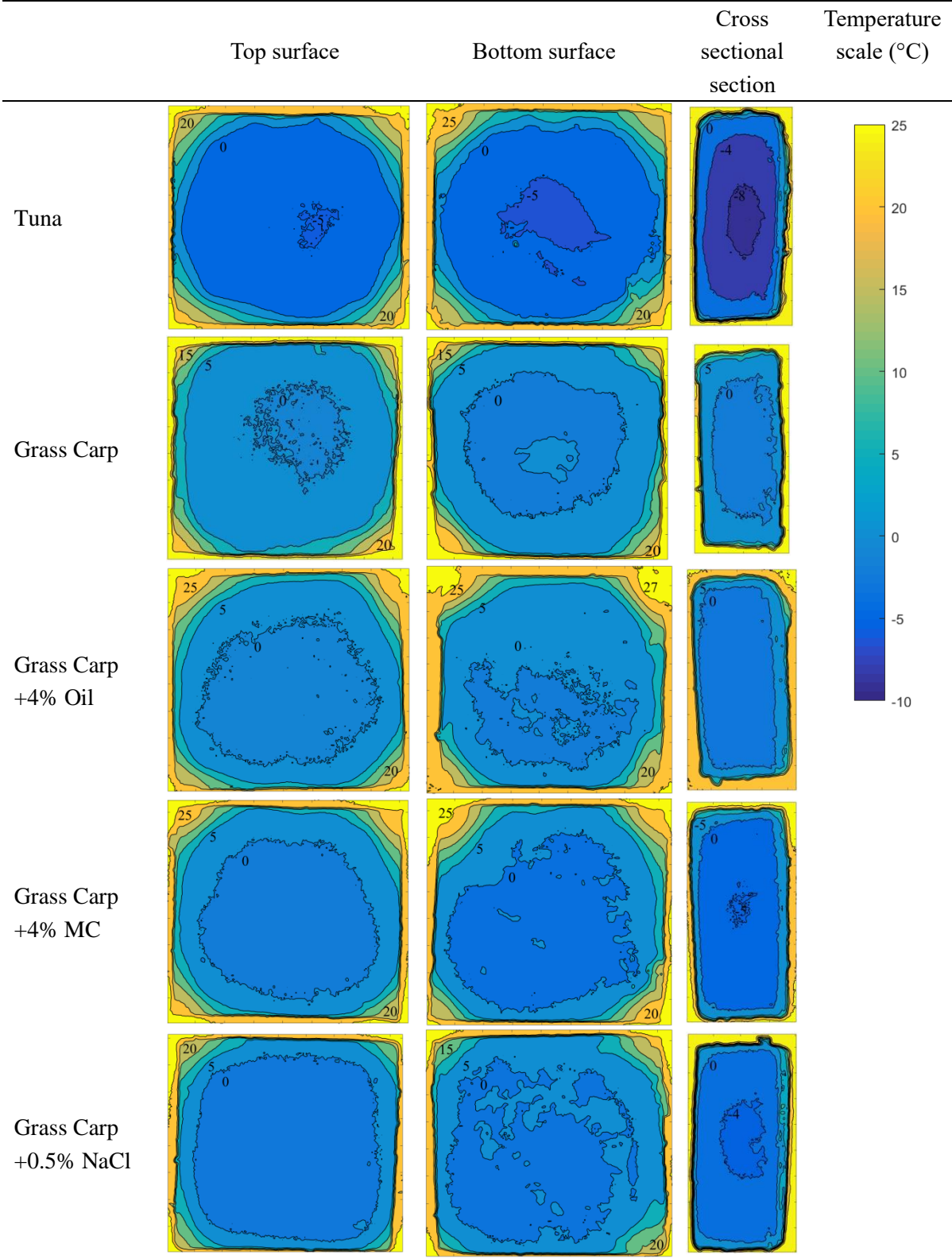
#### 2.3.4.1 Temperature distributions after RF tempering

Temperature distributions on the top surface, bottom surface and longitudinal section surface of tuna and the model food samples after RF tempering are shown in Fig. 2-9. The temperature distributions of tuna mince, grass carp mince, grass carp

mince with only one additive (4% oil or 4% MC), and grass carp mince added both 4% oil and 4% MC with different salt content (0%, 0.5%, 1.0% and 2.0% wt) were compared to obtain the optimized model food composition. All samples showed that the temperature at the sample corners was higher than the other locations because the higher electromagnetic field intensity at these locations where the surfaces converged caused more severe localized heating (Jiao, Tang, Wang, & Koral, 2014; Liu, Ogiwara, Fukuoka, & Sakai, 2014). The difference between the maximum and minimum temperature ( $\Delta T$ ) on the surface of the tuna mince was 34.0 °C, which was significantly greater than that of the original grass carp mince, 26.1 °C. The cold spot temperature of the tuna mince was -9.3 °C while that of the grass carp mince was -2.2 °C.

Adding 4.0% oil to the grass carp mince increased the hot spot temperature at the sample corners for -4 °C, but barely affected the cold spot temperature. However, adding 4% oil and 4% Methylcellulose to the grass carp mince reduced the tempering rate, and decreased the cold spot temperature to -5.4 °C. However, adding 0.5%, 1.0%, and 2.0% salt significantly decreased the cold spot temperatures to -5.1, -7.3, and -8.8 °C, and decreased the hot spot temperatures to 19.6, 18.5, and 16.1 °C, respectively.

The addition of different salt content significantly influenced the temperature distribution of mince during RF tempering. The cold spot temperatures of the grass carp mince with 4% oil and 4% methylcellulose with 0%, 0.5%, 1.0%, and 2.0% salt decreased to -6.4, -6.9, -8.2, and -10.7 °C, and the  $\Delta T$  values of them increased to 34.4, 34.7, 34.1, and 35.5 °C, respectively. Therefore, the hot spot temperature, cold spot temperature and  $\Delta T$  of grass carp mince with 4% oil, 4% MC and 1.0% salt addition were 25.9, -8.2, 34.1 °C, which was close to that of tuna mince, 24.7, -9.3, 34.4 °C.



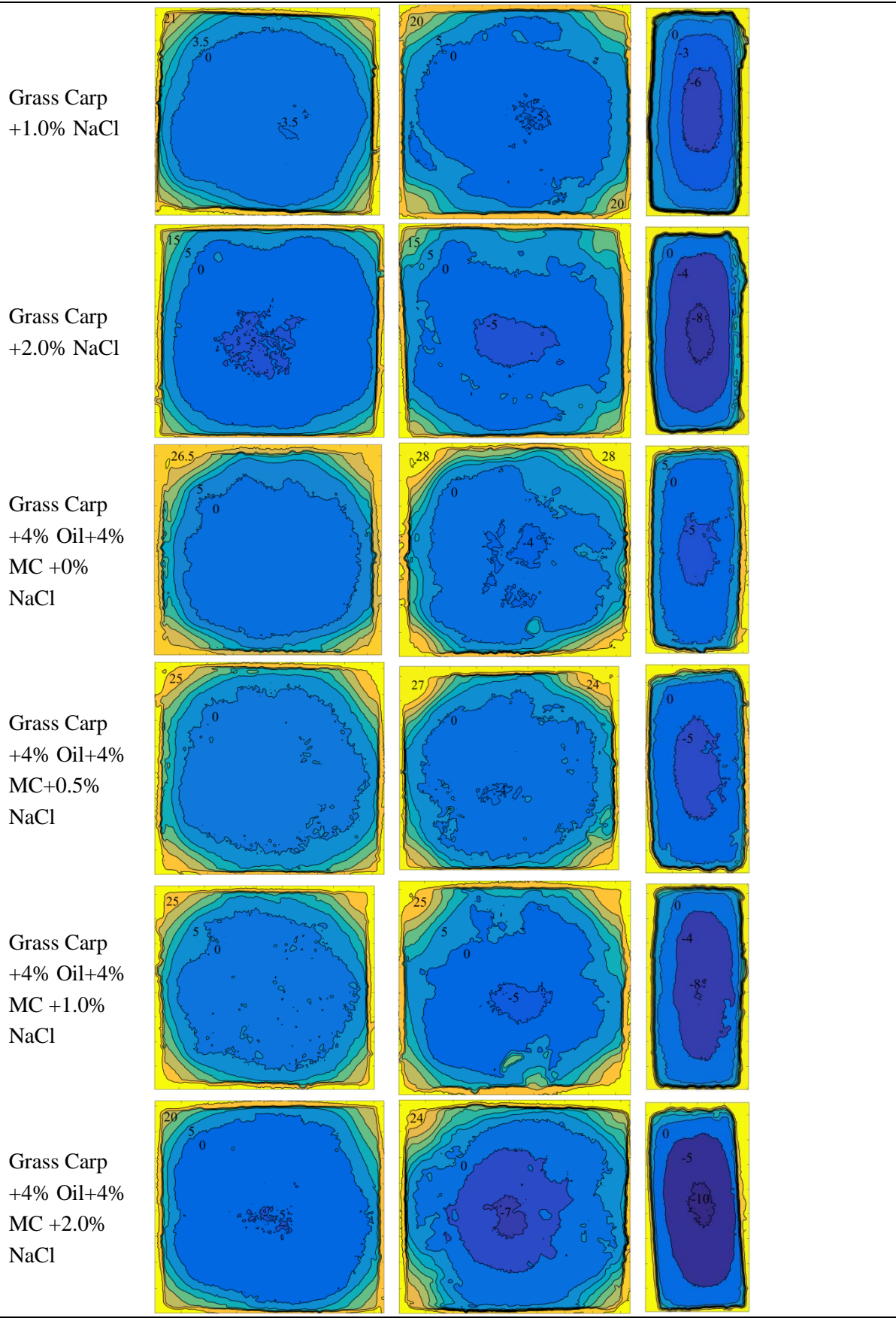


Fig. 2-9. Comparison of temperature distributions of top surface, bottom surface and longitudinal section of tuna and model foods after RF tempering 10 minutes

The time-temperature profiles at the sample center of tuna and its model foods (grass carp with 4.0% oil, 4.0% MC and various salt content) during RF tempering were showed in Fig. 2-10. The final center temperature matched well with that of the infrared images. The addition caused a significant decrease of the RF tempering rate. After 10 min RF tempering, the center temperature of grass carp was  $-5.1\text{ }^{\circ}\text{C}$ , and that of the grass carp with 4.0% oil, 4.0% MC and 1.0% NaCl reached at  $-10.5\text{ }^{\circ}\text{C}$ , which was closer to that of tuna ( $-10.9\text{ }^{\circ}\text{C}$ ). Thus, the temperature profile of grass carp mince with 4% oil, 4% MC and 1.0% salt addition matched the temperature profile of tuna mince.

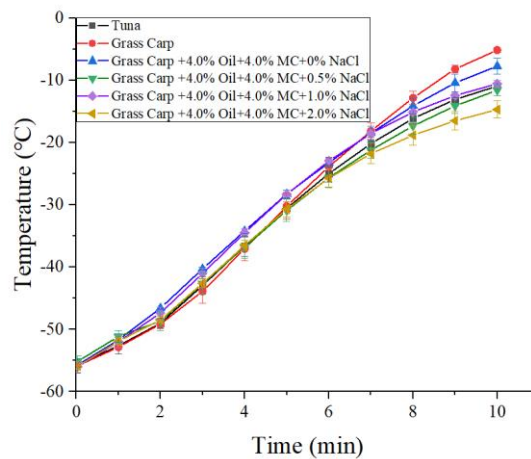


Fig. 2-10. Comparison of time-temperature profiles of tuna and model food at center during 10 min RF tempering (MC: Methylcellulose)

### 2.3.4.2 Temperature distributions during MW tempering

The time-temperature profiles of tuna and its model foods at center during 5 min MW tempering were showed in Fig. 2-11. The sample center temperature all matched with those in the thermal images. No significance on the center temperature was found among the model food composition in MW tempering. After 5 min MW tempering, the center temperatures of products were all below  $0\text{ }^{\circ}\text{C}$ .

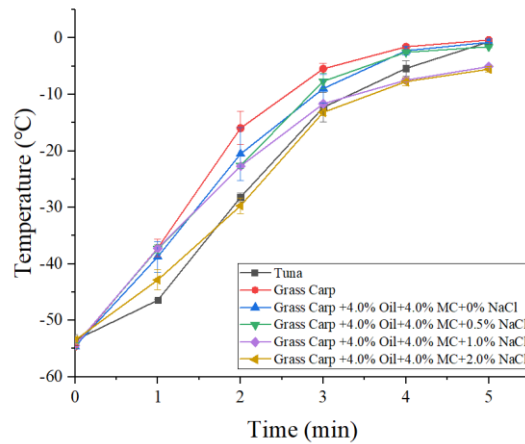
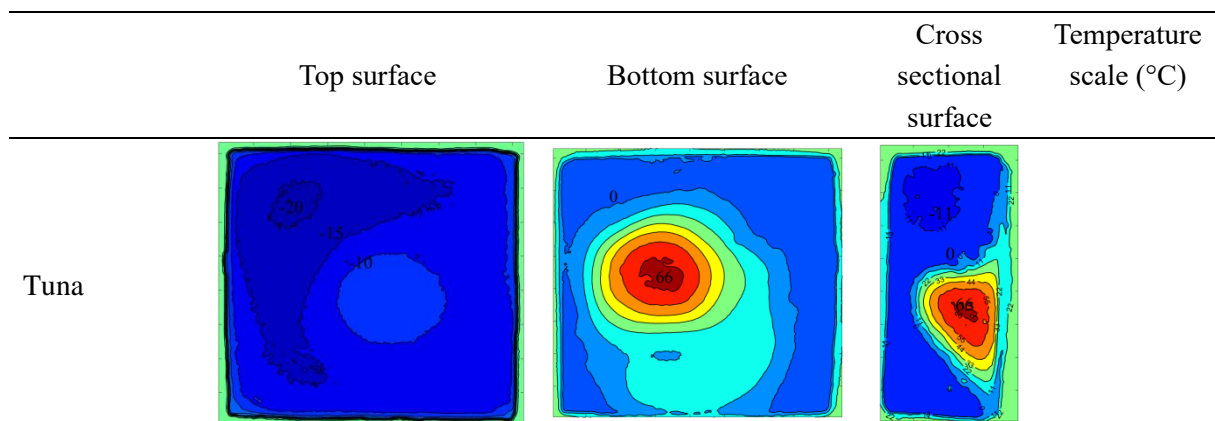
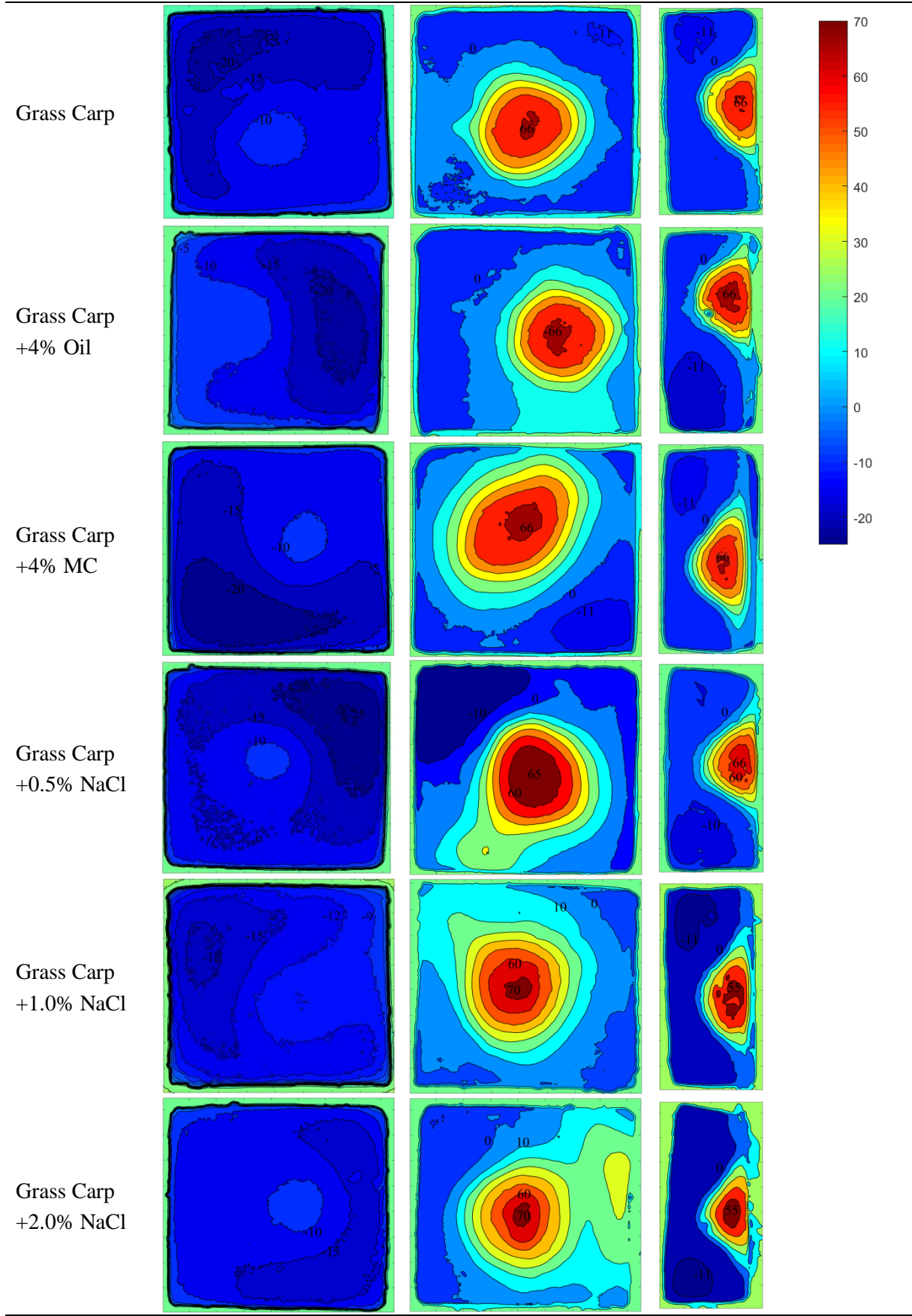


Fig. 2-11. Comparison of time-temperature profiles of tuna and model food at center during MW tempering (MC: Methylcellulose)

Temperature distributions on the top surface, bottom surface and longitudinal section (internal surface after a vertical bisection) of tuna and its model food after microwave tempering are shown in Fig. 2-12. The hot spot occurred near the bottom surface which was not in the geometric center of the samples while the cold spot occurred near the top surface close to edges or corners after microwave heating, which was different than the RF tempering. The bottom centers of the samples were already cooked, which reached 66 °C while the top surfaces were still frozen, which remained at -20 °C. This is partly due to the limited penetration depth of microwave resulted in a localized heating, and the thawed parts becomes a much greater absorber of electromagnetic energy (Chamchong & Datta, 1999). Similar results were reported by Llave et al. (2016), who studied microwave thawed and cooked tuna fillets and found the hot spot occurred at the bottom center and a large temperature difference (around 100 °C) existed between the hot and cold spots. However, there were also previous studies (Akkari, Chevallier, & Boillereaux, 2005; Chamchong & Datta, 1999) of microwave thawing showing the hot spot at the top surfaces. This is possibly because the sample was put in a self-designed container for microwave heating which influenced the heating pattern of the samples. Llave et al. (2016) also reported a similar heating pattern. Moreover, higher concentration of added salt increased the tempering rate and decreased the areas of frozen parts. Meanwhile, with multiple component

addition, the higher concentration of added salt showed the larger temperature gap. The  $\Delta T$  values of the grass carp mince with 4% oil, 4% MC and 0%, 0.5%, 1.0%, 2.0% salt were 83.8, 89.7, 91.7, 93.6 °C, respectively after 5 min of MW tempering. Chamchong and Datta (1999) reported that the non-uniformity of temperature increased with time during MW thawing of tylose paste. The reason was MW energy absorption at the thawed parts was higher than that in the frozen parts because salt addition exaggerated the “shield” effect and produced more severe temperature non-uniformity. In this study, the hot spot temperature at the bottom and the cold spot temperature at the top surface of grass carp mince with 4% oil, 4% MC and 1.0% salt addition were 71.2 °C and -21.7 °C, which were the closest to that of tuna, which were 69.6 °C and -21.2 °C, respectively. Thus, the grass carp mince with 4% oil, 4% MC and 1.0% salt was found as the optimum composition of model food for tuna. This result was slightly different from the best matching DPs of grass carp mince, which was 4% oil, 4% MC and 0% salt. This is because the dielectric properties matching was never perfect for both dielectric constant and loss factor, which could only provide a general range of guidance for model food development. Furthermore, samples were tempered unevenly in MW experiments is because the penetration depth of the thawed parts in the fish sample dramatically reduced which caused localized heating at certain locations of the sample.





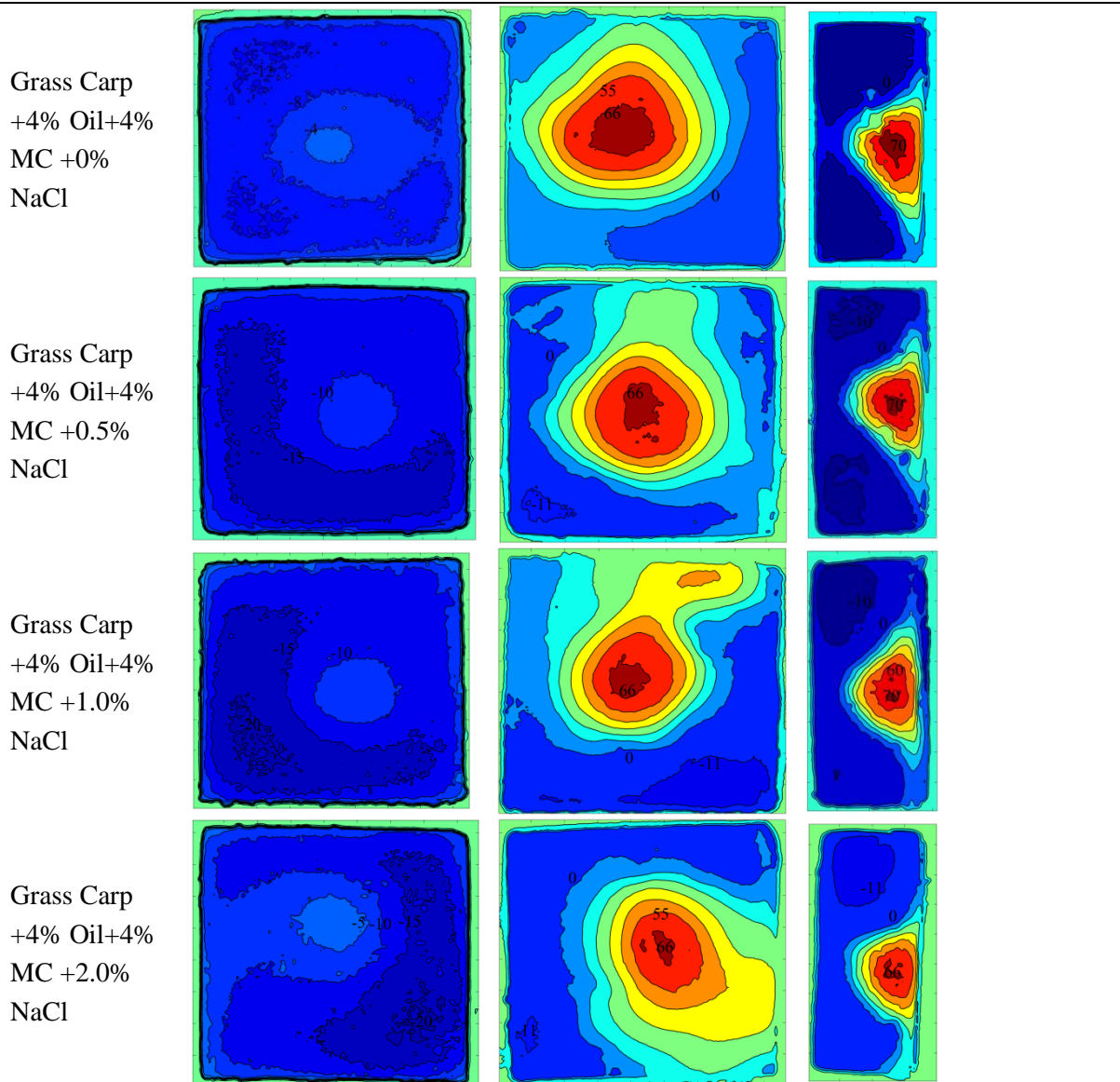


Fig. 2-12. Comparison of temperature distributions of top surface, bottom surface and longitudinal section of tuna and model foods after microwave tempering 5 minutes

## 2.4 Conclusions

The addition of oil decreased the dielectric constant of model foods at the range of 1-2500 MHz. The addition of methylcellulose increased the dielectric loss factor especially at low frequency (<1000 MHz). Salt addition significantly increased both the dielectric constant and the dielectric loss factor. However, the dielectric constant decreased with more than 1.0% salt. At frequency over 1000 MHz. As a result, the grass carp mince with 4.0% oil and 4.0% methylcellulose was close that of tuna on dielectric properties at both RF and MW frequencies.

From RF and MW tempering experiment validation, the temperature distribution

of grass carp mince with 4.0% Oil, 4.0% Methylcellulose and 1.0% salt addition matched that respective temperature distribution of tuna mince during RF and MW tempering. The temperature uniformity of tuna and its model food in RF tempering was better than those in MW tempering. The penetration depth at RF range was much larger than that at microwave frequencies, which allows radio frequency become a more appropriate tempering methods for frozen fish. In future MW experiment, optimizing the size, especially the thickness of the target tempering products and MW tempering parameters would be important to develop a reasonable tempering process with better temperature uniformity.

This study provides a basis for the development of model food based on the low-cost fish and its feasibility of substitution to explore tuna thawing and tempering. The model food developed in this study was low cost, easy to prepare and had comparable dielectric properties to tuna, which was experimentally proved to be effective in temperature distribution. In the future work, it is desirable to conduct numerical simulations to facilitate optimizing the amount of the additives in the model food with the best matching of dielectric and thermal properties to the target food.

## References

- Ahmed, J., Ramaswamy, H. S., & Raghavan, V. G. S. (2007). Dielectric properties of butter in the MW frequency range as affected by salt and temperature. *Journal of Food Engineering*, 82(3), 351-358. doi:10.1016/j.jfoodeng.2007.02.049
- Akkari, E., Chevallier, S., & Boillereaux, L. (2005). A 2D non-linear “grey-box” model dedicated to microwave thawing: Theoretical and experimental investigation. *Computers & Chemical Engineering*, 30(2), 321-328. doi:10.1016/j.compchemeng.2005.09.008
- Ashraf, M., Zafar, A., Rauf, A., Mahboob, S., Naureen, A., & Qureshi, N. (2011). Nutritional Values of Wild and Cultivated Silver Carp (*Hypophthalmichthys molitrix*) and Grass Carp (*Ctenopharyngodon idella*). *International Journal of Agriculture and Biology*, 13, 1560-8530.
- Bircan, C., & Barringer, S. A. (1998). Salt-starch interactions as evidenced by viscosity and dielectric property measurements. *Journal of Food Science*, 63(6), 983-986. doi:10.1111/j.1365-2621.1998.tb15838.x
- Bornhorst, E. R., Liu, F., Tang, J., Sablani, S. S., & Barbosa-Cánovas, G. V. (2017). Food Quality Evaluation using Model Foods: a Comparison Study between Microwave-Assisted and Conventional Thermal Pasteurization Processes. *Food and Bioprocess Technology*, 10(7), 1248-1256. doi:10.1007/s11947-017-1900-9
- Calay, R. K., Newborough, W., Probert, D., & Calay, P. S. (1994). Predictive equations for the dielectric properties of foods. *International Journal of Food Science and Technology*, 29(6), 699-713. doi:10.1111/j.1365-2621.1994.tb02111.x
- Chamchong, M., & Datta, A. K. (1999). Thawing of Foods in a Microwave Oven: I. Effect of Power Levels and Power Cycling. *Journal of Microwave Power and Electromagnetic Energy*, 34(1), 9-21. doi:10.1080/08327823.1999.11688384
- Choi, Y. H., & Okos, M. (1986). Effects of temperature and composition on the thermal conductivity and thermal diffusivity of some food components. *Journal of Food Process and Applications*, 1(1), 93-101.
- Curet, S., Rouaud, O., & Boillereaux, L. (2008). Microwave tempering and heating in a single-mode cavity: Numerical and experimental investigations. *Chemical Engineering and Processing: Process Intensification*, 47(9-10), 1656-1665. doi:10.1016/j.cep.2007.09.011
- Curet, S., Rouaud, O., & Boillereaux, L. (2013). Estimation of dielectric properties of food materials during microwave tempering and heating. *Food and Bioprocess Technology*, 7(2), 371-384. doi:10.1007/s11947-013-1061-4
- Di Rosa, A. R., Bressan, F., Leone, F., Falqui, L., & Chiofalo, V. (2019). Radio frequency heating on food of animal origin: a review. *European Food Research and Technology*, 245(9), 1787-1797. doi:10.1007/s00217-019-03319-8
- Feng, D., Xue, Y., Li, Z., Wang, Y., Yang, W., & Xue, C. (2015). Dielectric properties of myofibrillar protein dispersions from Alaska Pollock (*Theragra chalcogramma*) as a function of concentration, temperature, and NaCl concentration. *Journal of Food Engineering*, 166, 342-348. doi:10.1016/j.jfoodeng.2015.06.038

- Guan, D., Cheng, M., Wang, Y., & Tang, J. (2004). Dielectric properties of mashed potatoes relevant to Microwave and Radio frequency Pasteurization and Sterilization Processes. *Food Science*, 69(1), FEP30-FEP37. doi:10.1111/j.1365-2621.2004.tb17864.x
- Hassan, H. F., & Ramaswamy, H. S. (2011). Measurement and targeting of thermophysical properties of carrot and meat based alginate particles for thermal processing applications. *Journal of Food Engineering*, 107(1), 117-126. doi:10.1016/j.jfoodeng.2011.05.028
- Jiang, Q., Nakazawa, N., Hu, Y., Osako, K., & Okazaki, E. (2019). Microstructural modification and its effect on the quality attributes of frozen-thawed bigeye tuna (*Thunnus obesus*) meat during salting. *LWT-Food Science and Technology*, 100, 213-219. doi:10.1016/j.lwt.2018.10.070
- Jiao, Y., Tang, J., Wang, S., & Koral, T. (2014). Influence of dielectric properties on the heating rate in free-running oscillator radio frequency systems. *Journal of Food Engineering*, 120, 197-203. doi:10.1016/j.jfoodeng.2013.07.032
- Jiao, Y., Tang, J., Wang, S., & Koral, T. (2018). Radio-Frequency Applications for Food Processing and Safety. *Annual Review of Food Science and Technology*, 9, 105-127. doi:10.1146/annurev-food-041715-033038
- Kannan, S., Dev, S. R. S., Garipey, Y., & Raghavan, G. S. V. (2013). Effect of radiofrequency heating on the dielectric and physical properties of eggs. *Progress in Electromagnetics Research*, 51, 201-220. doi:10.2528/PIERB13031812
- Kumcuoglu, S., Turgut, A., & Tavman, S. (2010). The Effects of Temperature and Muscle Composition on the Thermal Conductivity of Frozen Meats. *Journal of Food Processing and Preservation*, 34(3), 425-438. doi:10.1111/j.1745-4549.2008.00347.x
- Li, B., & Sun, D. (2002). Novel methods for rapid freezing and thawing of foods – a review. *Journal of Food Engineering*, 54(3), 175-182. doi:10.1016/S0260-8774(01)00209-6
- Li, Y., Li, F., Tang, J., Zhang, R., Wang, Y., Koral, T., & Jiao, Y. (2018). Radio frequency tempering uniformity investigation of frozen beef with various shapes and sizes. *Innovative Food Science & Emerging Technologies*, 48, 42-55. doi:10.1016/j.ifset.2018.05.008
- Liu, S., Fukuoka, M., & Sakai, N. (2012). Dielectric properties of fish flesh at microwave frequency. *Food Science and Technology Research*, 18(2), 157-166. doi:10.3136/fstr.18.157
- Liu, S., Ogiwara, Y., Fukuoka, M., & Sakai, N. (2014). Investigation and modeling of temperature changes in food heated in a flatbed microwave oven. *Journal of Food Engineering*, 131, 142-153. doi:10.1016/j.jfoodeng.2014.01.028
- Llave, Y., Mori, K., Kambayashi, D., Fukuoka, M., & Sakai, N. (2016). Dielectric properties and model food application of tylose water pastes during microwave thawing and heating. *Journal of Food Engineering*, 178, 20-30. doi:10.1016/j.jfoodeng.2016.01.003
- Llave, Y., Terada, Y., Fukuoka, M., & Sakai, N. (2014). Dielectric properties of frozen

- tuna and analysis of defrosting using a radio-frequency system at low frequencies. *Journal of Food Engineering*, 139, 1-9. doi:10.1016/j.jfoodeng.2014.04.012
- Luan, D., Tang, J., Liu, F., Tang, Z., Li, F., Lin, H., & Stewart, B. (2015). Dielectric properties of bentonite water pastes used for stable loads in microwave thermal processing systems. *Journal of Food Engineering*, 161, 40-47. doi:10.1016/j.jfoodeng.2015.02.014
- Nurjanah, Abdullah, A., Naibaho, I., Kartikayani, D., Nurilmala, M., Yusfiandayani, R., & Sondita, M. F. A. (2019). Fish quality and nutritional assessment of yellowfin tuna (*Thunnus albacares*) during low temperature storage. *IOP Conference Series: Earth and Environmental Science*, 404. doi:10.1088/1755-1315/404/1/012074
- Ozkoc, S. O., Sumnu, G., & Sahin, S. (2014). Recent developments in microwave heating. In *Emerging Technologies for Food Processing* (pp. 361-383).
- Ryynanen, S. (1995). The electromagnetic properties of food material: a review of the basic principles. *Journal of Food Engineering*, 26, 409-429. doi:10.1016/0260-8774(94)00063-F
- Simdyankin, A., & Bogdanov, V. (2019). Thermal properties of commercial hydrobionts' tissues in the freezing process. *Foods and Raw Materials*, 247-254. doi:10.21603/2308-4057-2019-2-247-254
- Tang, Z., Mikhaylenko, G., Liu, F., Mah, J.-H., Pandit, R., Younce, F., & Tang, J. (2008). Microwave sterilization of sliced beef in gravy in 7-oz trays. *Journal of Food Engineering*, 89(4), 375-383. doi:10.1016/j.jfoodeng.2008.04.025
- Wang, J., Tang, J., Liu, F., & Bohnet, S. (2018). A New Chemical Marker-Model Food System for Heating Pattern Determination of Microwave-Assisted Pasteurization Processes. *Food and Bioprocess Technology*, 11(7), 1274-1285. doi:10.1007/s11947-018-2097-2
- Wang, L., Shi, L., Jiao, C., Wu, W., Li, X., Wang, J., . . . Zhang, M. (2019). Effects of different sugars on the thermal properties and microstructures of Mandarin fish (*Siniperca chuats*). *Lwt*, 99, 84-88. doi:10.1016/j.lwt.2018.09.031
- Wang, Y., Tang, J., Rasco, B., Kong, F., & Wang, S. (2008). Dielectric properties of salmon fillets as a function of temperature and composition. *Journal of Food Engineering*, 87(2), 236-246. doi:10.1016/j.jfoodeng.2007.11.034
- Wang, Y., Tang, J., Rasco, B., Wang, S., Alshami, A. A., & Kong, F. (2009). Using whey protein gel as a model food to study dielectric heating properties of salmon (*Oncorhynchus gorbuscha*) fillets. *LWT - Food Science and Technology*, 42(6), 1174-1178. doi:10.1016/j.lwt.2009.01.005
- Yaghmaee, P., & Durance, T. D. (2002). Predicative equations for dielectric properties of NaCl, D-sorbitol and sucrose solutions and surimi at 2450 MHz. *Journal of Food Science*, 67(6), 2207-2211. doi:10.1111/j.1365-2621.2002.tb09528.x
- Zhang, W., Luan, D., Tang, J., Sablani, S. S., Rasco, B., Lin, H., & Liu, F. (2015). Dielectric properties and other physical properties of low-acyl gellan gel as relevant to microwave assisted pasteurization process. *Journal of Food Engineering*, 149, 195-203. doi:10.1016/j.jfoodeng.2014.10.014

## **Chapter 3 Numerical simulation of RF tempering tuna process with different electrodes and sample shapes**

### **3.1 Introduction**

RF temper the frozen sample fast and volumetrically since the waves penetrate food directly and generate volume heat, which is suitable for tempering of bulk frozen products and has the potential for industrialization. During RF processing, the size of the sample located between the electrodes and its electromagnetic characteristics (permeability and permittivity), geometrical configuration of the sample, distance between the electrodes, distance between the top electrode and the sample have a certain effect on power absorption (and heat generation within), as well as on the heating rates and temperature uniformity (Erdogdu, et al., 2016; Uyar, Rahmi, Erdogdu, Ferruh, Marra, & Francesco, 2014; Uyar, et al., 2015). Temperature uniformity of the samples is a major focus in the recent studies (Ferrari-John, Katrib, Palade, Batchelor, Dodds, & Kingman, 2016), and various approaches have been applied for this purpose including the physical property of the surrounding container (Huang, Marra, & Wang, 2016). It is easy to appear the phenomenon of edge and corner overheating. Therefore, it is crucial to analyze and study the temperature distribution of the material during RF heating. Through establishment of finite element model, the process of RF tempering of tuna can be analyzed more finely and precisely than by experiments besides the electromagnetic field and internal temperature distribution.

In this study, a numerical simulation model of RF tempering tuna process was established, and the effects of different electrode (plane electrode, electrode with needle type surface, electrode with pyramid type surface) and different sample shapes (rectangular, cylindrical) on the RF tempering process were compared. The changes of electromagnetic field and temperature field were analyzed in detail to explore a more variety of RF thawing process.

### **3.2 Materials and methods**

#### **3.2.1 Materials preparation**

Frozen Bigeye tuna (*Thunnus obesus*) was purchased from JINXIAN Co., Ltd.,

Shanghai, China, transported to the laboratory in a cooler. The lateral part muscle was used for experiments. All samples prepared for RF tempering experiments were cut into pieces, minced by the meat grinder, frozen at -18 °C, cut into the size of 8×8×3 cm<sup>3</sup>, and then stored at -35 °C in a freezer for over 24 h (DW/BD-55W321EU1, Haier, Qingdao, China).

### 3.2.2 Radio frequency tempering of tuna

The minced tuna samples of 8×8×3 cm<sup>3</sup> were tempered by a 27.12 MHz, 50 Ω RF heating system (Labotron 12, Sairem, France). In the RF tempering process, the input power was 600W and the height of the dielectric electrode was 7 cm. Before tempering, holes of Φ 3mm were drilled into the samples with an electric drill to facilitate the insertion of optical fibers (HQ-FTS-D1F00, Heqi guangdian, Shanxi, China) in the experiment. The positions of the holes were the geometric center of the sample and the corner position (1 cm from the edge and 0.5 cm from the upper surface).

In the experiment, the sample was taken out of the refrigerator at -35 °C, the optical fiber sensors were quickly inserted into the pre-drilled hole. Then put the sample into the RF heater and turn on. When the center temperature of the sample reached -4 °C, turn off the RF heater. Right after tempering, the tempered sample was brought to an infrared camera (FLIR A655sc, Wilsonville, USA) for obtaining its surface temperature distribution. The experiment was replicated three times.

## 3.3 Computer simulation

### 3.3.1 Computer simulation of the tempering tuna process

The RF tempering tuna process involves a multi-physical field coupled with electromagnetic and heat transfer.

Maxwell equation can be used to describe the electric field intensity distribution during electromagnetic conduction. Under the assumption of quasi-static state, Maxwell equation can be simplified to Laplace equation, which can be effectively used in RF electromagnetic field. Laplace's equation is expressed as follows:

$$-\nabla \cdot ((\sigma + j2\pi\epsilon_0\epsilon') \nabla V) = 0 \quad (3-1)$$

where

$\sigma$  is the electrical conductivity of the food material ( $\text{S m}^{-1}$ )

$$j = \sqrt{-1}$$

$V$  is the electric potential across the electrode gap (V)

The total heat balance during RF heating is described by the following equation:

$$\rho C_p \frac{\partial T}{\partial t} = \nabla \cdot k \nabla T + Q \quad (3-2)$$

where

$\rho$  is the density ( $\text{kg m}^{-3}$ )

$t$  is the time (s)

$T$  is the temperature (K)

$k$  is the thermal conductivity ( $\text{W}^{-1} \text{m} \text{ } ^\circ\text{C}$ )

$C_p$  is the specific heat capacity ( $\text{J}^{-1} \text{kg} \text{ } ^\circ\text{C}$ ) and  $Q$  is the amount of electromagnetic power converted to heat, as the following equation:

$$Q = 2\pi f \varepsilon_0 \varepsilon'' |\vec{E}|^2 \quad (3-3)$$

where

$f$  is the working frequency of the RF equipment (Hz)

$\varepsilon_0$  is the permittivity of electromagnetic wave in free space ( $8.85 \times 10^{-12} \text{F/m}$ )

$|\vec{E}|$  is the electric field intensity in the food material (V/m). The equation is

expressed as follows as follows:

$$\varepsilon \nabla \cdot \vec{E} + \vec{E} \cdot \nabla = 0 \quad (3-4)$$

The heat convection between food and the atmosphere is described by the following equation:

$$-k \nabla T = h(T - T_{\text{air}}) \quad (3-5)$$

$h$  is the convective heat transfer coefficient ( $\text{Wm}^{-2} \text{K}^{-1}$ )

$T_{\text{air}}$  is the atmospheric temperature ( $^\circ\text{C}$ )

### 3.3.2 Modeling

A finite element method (FEM) software COMSOL Multiphysics® (COMSOL Multiphysics 5.2, Burlington, MA, USA) was employed to simulate the RF tempering

process. The joule heating module, which conjugates the electromagnetic heating with the heat transfer modules, was selected to simulate the RF tempering processes. The computation was conducted on a Dell workstation with two dual core Intel Xeon CPU 2.60 GHz processors, 128 GB RAM on a Microsoft Windows Server 2012 R2 standard operation system.

The geometry model of RF heating chamber is shown as Fig. 3-1. All domains in the model were set using a free-dissecting tetrahedral mesh, and the meshing size for them were selected as “fine”. The model was solved with the default direct solver, and the time step used in this study was 1 s.

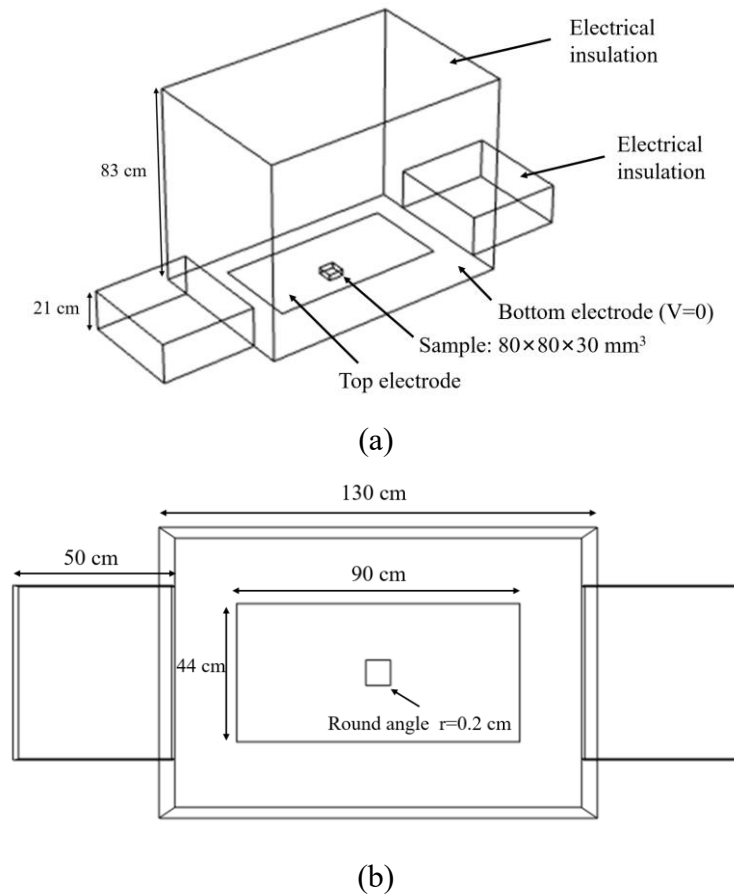


Fig. 3-1 Geometry model of RF heating chamber (a. Main view b. Top view)

Selection of simulated voltage values:

During the operation of the RF system, it is difficult to determine the electrode voltage in the high-frequency high-voltage electric field, so the formula derivation method was used to predict the electrode voltage (Alfaifi, et al., 2014; Choi & Konrad, 1991; Huang, Zhu, Yan, & Wang, 2015):

$$V = (d_{air}\sqrt{(\varepsilon')^2 + (\varepsilon'')^2} + d_{mat})\left(\sqrt{\frac{\rho C_p}{\pi f \varepsilon_0 \varepsilon''} \frac{dT}{dt}}\right) \quad (3-6)$$

where  $d_{air}$  is the gap from the top electrode to the top surface of the material (m)  
 $d_{mat}$  is the material height (m)

The voltage changes constantly in the process of RF tempering, and the voltage directly affects the heating rate. According to the voltage derivation Eqs. (3-6), the heating rate of the material also affects the voltage. In this simulation, the heating rate of the center of the material was selected, and then the voltage was deduced by the formula. Combined with the experiment results, the final simulated voltage was determined (0~500 s: 4000 V, 500 s ~ the end: 4400 V).

The parameter conditions for simulating the tuna tempering process are shown in Table 3-1.

Table 3-1 Parameters used in the model.

Parameter	Value
Sample initial temperature	-35 [°C]
Surrounding temperature	20 [°C]
Sample thermal conductivity	in 2.2.3 Table 2-5
Sample dielectric properties	in 2.2.2.5 Fig. 2-7 (a) (b)
Sample specific heat	in 2.2.3 Fig. 2-8
Frequency	27 [MHz]
Electrode voltage	4000~4400 [V]
Convective heat transfer coefficient	15 [W·m <sup>-2</sup> ·K]
Electrode gap	7 [cm]

### 3.3.3 Different electrode shapes

Different electrode shapes (plane electrode, electrode with needle type surface, and electrode with pyramid type surface)

Plane electrode: 90×44 cm<sup>2</sup>

Electrode with needle type surface:  $90 \times 44 \text{ cm}^2$ , a needle is a combination of a cylinder and a cone (cylinder: Radius=20 mm, Height=10 mm, cone: Radius=20 mm, Height=10 mm).

Electrode with pyramid type surface:  $90 \times 44 \text{ cm}^2$ , the pyramid is a quadrilateral cone (base side length  $L=10 \text{ mm}$ , height  $H=20 \text{ mm}$ ).

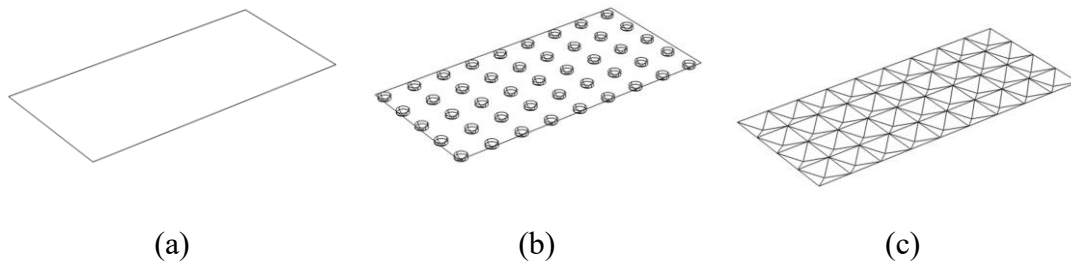


Fig. 3-2 Different shaped electrode plates (a. Plane electrode; b. Electrode with needle type surface; c. Electrode with pyramid type surface)

### 3.3.4 Different sample shapes

Different sample shapes (rectangular or cylindrical)

rectangular:  $80 \times 80 \times 30 \text{ mm}^3$

cylindrical:  $R=45 \text{ mm}$ ,  $H=30 \text{ mm}$

### 3.3.5 Temperature Uniformity Index (TUI)

The effect of tempering uniformity of the material can be used as the Temperature Uniformity Index (TUI) with the following equation:

$$TUI = \frac{\int |T - T_{tg}| dV_{vol}}{(T_{tg} - T_{initial}) V_{vol}} \quad (3-7)$$

where

$T$  is the local temperature in the food ( $^{\circ}\text{C}$ )

$T_{tg}$  is the target tempering temperature ( $^{\circ}\text{C}$ )

$T_{initial}$  is the initial temperature of the food ( $^{\circ}\text{C}$ )

$V_{vol}$  is the volume of the food ( $\text{m}^3$ )

### 3.4 Results and discussion

#### 3.4.1 Simulated and experimental results of tuna tempering process

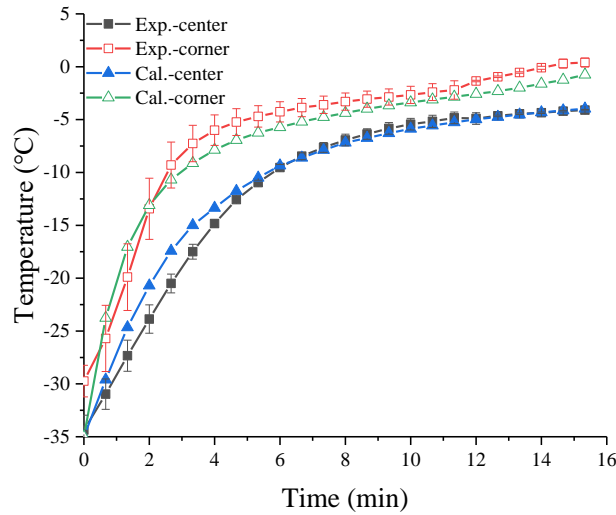


Fig. 3-3 Comparison of experimental (exp.) and simulated (cal.) values of RF tempering temperature rise curve of tuna

The comparison between the experimental and simulated values of tuna RF tempering rate is shown in Fig. 3-3. In the experiment, when the center temperature reached the target temperature of  $-4\text{ }^{\circ}\text{C}$ , the corner temperature was  $0.4\text{ }^{\circ}\text{C}$  at 920 s. In the simulation, at 912 s, the center temperature reached the target temperature of  $-4\text{ }^{\circ}\text{C}$  and the corner temperature was  $-0.9\text{ }^{\circ}\text{C}$ . Meanwhile, at 920 s, the center temperature of the simulated value reached  $-3.9\text{ }^{\circ}\text{C}$ , the corner temperature was  $-0.7\text{ }^{\circ}\text{C}$ . The overall trend of the simulated values was similar with that of the experimental values, so the simulation had the potential to replace the experiment to explore the RF tempering tuna.



rectangular material, the deflection angle of the electric field was the largest at the corner. Uyar, et al. (2014) found a similar result by using RF to heat meat cubes and simulating the effect of sample load with respect to the position of the electrodes on power absorption and heating rate of the material. When the electromagnetic wave entered the material, the electric field distribution in the middle part of the meat sample was relatively uniform, but the electric field in the corner of the sample was distorted, so the electric field intensity at the corner and edge was higher.

For the cylindrical material, the deflection angle of the electric field was the largest at the edge, where the upper and lower bottom surfaces were connected to the side surface. The non-uniform absorption of electromagnetic wave energy by materials was the main factor for the uneven temperature distribution of tempered samples. There was a great difference in the electromagnetic wave energy absorption of materials under different electrode plates, and the electromagnetic wave energy absorption of the two shapes of materials was the most uniform under the electrode with needle type surface.

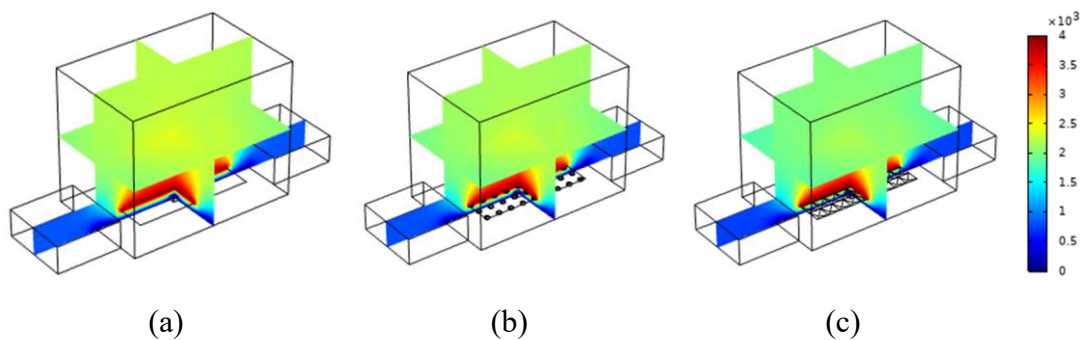


Fig. 3-5 Electric field intensity ( $\text{V m}^{-1}$ ) distribution inside the RF heating cavity with different shapes of electrode plates (a. Plane electrode; b. Electrode with needle type surface; c. Electrode with pyramid type surface)

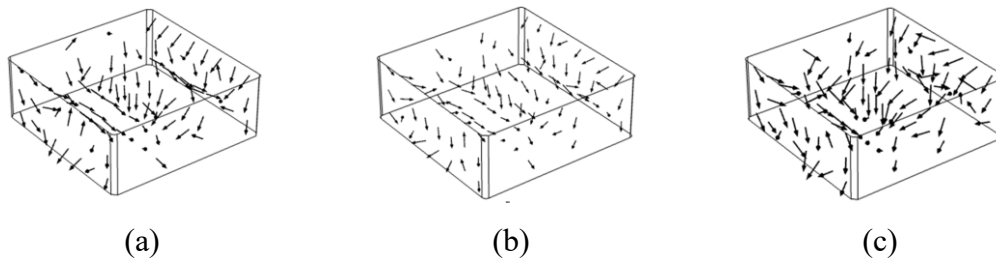


Fig. 3-6 Electric field intensity ( $V m^{-1}$ ) distribution of rectangular materials under different shapes of electrode plates (a. Plane electrode; b. Electrode with needle type surface; c. Electrode with pyramid type surface)

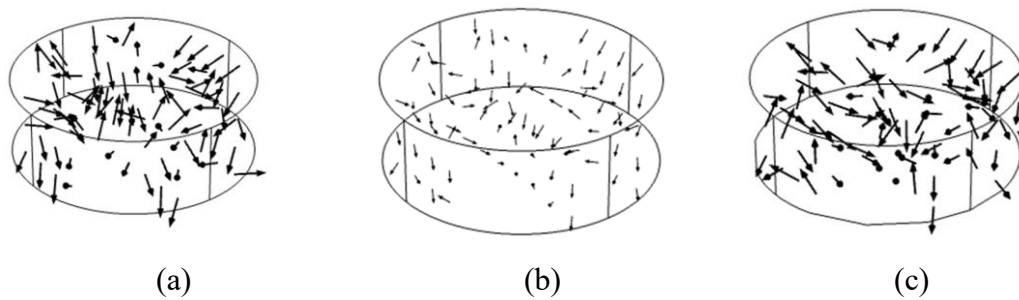


Fig. 3-7 Electric field intensity ( $V m^{-1}$ ) distribution of cylindrical materials under different shapes of electrode plates (a. Plane electrode; b. Electrode with needle type surface; c. Electrode with pyramid type surface)

### 3.4.3 Temperature rise curve under different electrode plates

Tempering rate of rectangular materials under different shapes of electrodes is shown in Fig. 3-8. For rectangular materials, to reach the target temperature  $-4\text{ }^{\circ}\text{C}$ , the plane electrode, the needle-shaped electrode, the pyramid-shaped electrode took 912 s, 657 s and 629 s, respectively. And the corner temperature was  $-0.9\text{ }^{\circ}\text{C}$ ,  $-2.0\text{ }^{\circ}\text{C}$  and  $-0.2\text{ }^{\circ}\text{C}$ , respectively. The temperatures at the corners were higher than those at the center of the sample. This could be due to increased electric field distribution as a result of deflection of electric fields at the corners and edges of the products (Marra, LuZhang, & G.Lyng, 2009; Tiwari, Wang, Tang, & Birla, 2011).

Compared with the plane electrode, the tempering rates of the material under the needle-shaped and pyramid-shaped electrode were faster.

Tempering rate of cylindrical materials under different shapes of electrodes is shown in Fig. 3-9. For cylindrical materials, to reach the target temperature  $-4\text{ }^{\circ}\text{C}$ , the plane electrode, the needle-shaped electrode, the pyramid-shaped electrode took 958 s, 722 s and 732 s, respectively. And the edge temperature was  $4.0\text{ }^{\circ}\text{C}$ ,  $0.0\text{ }^{\circ}\text{C}$  and  $3.7\text{ }^{\circ}\text{C}$ , respectively. Compared with the plane electrode, the tempering rates of the material under the needle-shaped and pyramid-shaped electrode were faster. And the edge temperature of the cylindrical material was higher than the corner temperature of the rectangular material under the three different shapes of electrodes during the tempering process.

Generally, under the electrode with needle type surface, the tempering time of rectangular and cylindrical materials was the shortest, and the temperature difference between center and corner is the smallest. Under three different shapes of electrodes, the tempering time of cylindrical materials was longer than that of rectangular materials.

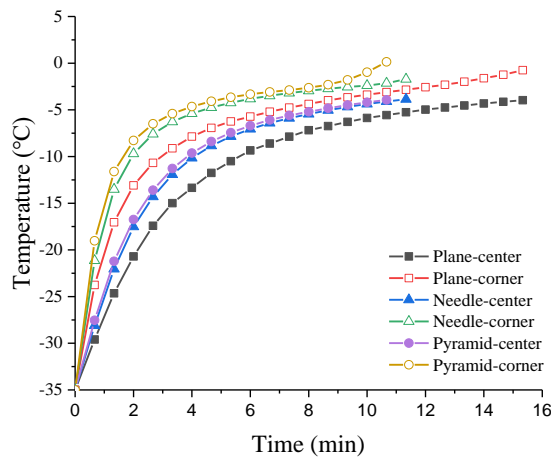


Fig. 3-8 Tempering temperature rise curve of rectangular materials under different shapes of electrode plates

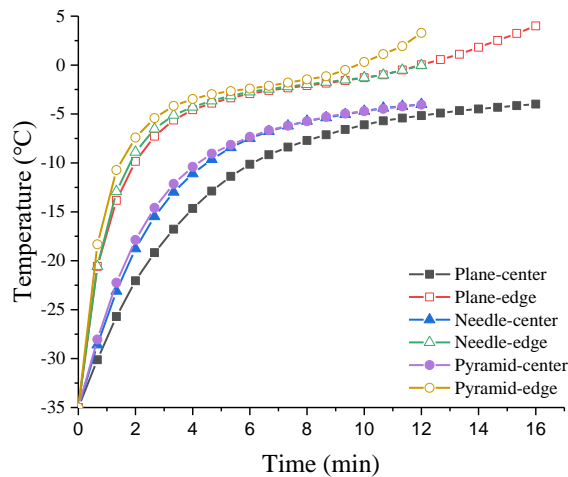


Fig. 3-9 Tempering temperature rise curve of cylindrical materials under different shapes of electrode plates

### 3.4.4 Temperature distribution under different electrode plates

Tempering rate of rectangular materials under different shapes of electrodes is shown in Fig. 3-10. The hot spot temperatures of rectangular materials after RF thawing under plane, needle-shaped and pyramid-shaped electrodes were 42.5 °C, 23.1 °C and 29.7 °C, respectively. Under the RF tempering of three different shapes of electrodes, the uniformity of the top surface of the rectangular material was less than that of the bottom surface. The temperature distribution of the longitudinal section was uniform, and all areas were concentrated near the target tempering temperature. Moreover, the cold points of the top, bottom, and longitudinal section of the rectangular material all appeared in the center of the surface, and the hot spots all appeared in the corner of the surface.

Generally, the RF tempering uniformity under the needle-shaped electrode was the best, followed by the pyramid-shaped and plane electrode. For rectangular materials, there was corner overheating in RF tempering under three different shapes of electrodes, which was due to the deflection and deformation of the electric field near the corners of the material, and the accumulation of electromagnetic energy in the corners of the material and thermal escape makes the corner temperature increase. Bedane, Chen, Marra, and Wang (2017) carried out an experimental study for RF thawing with

movement on a conveyor belt and reported a temperature uniformity with the reduced overheating on the corners of the sample compared to the stationary case. This result was concluded based on the increased electric field absorption in the stationary sample due to the deflection of the electric field along the corners and edges, and the movement of the sample might have changed these deflections.

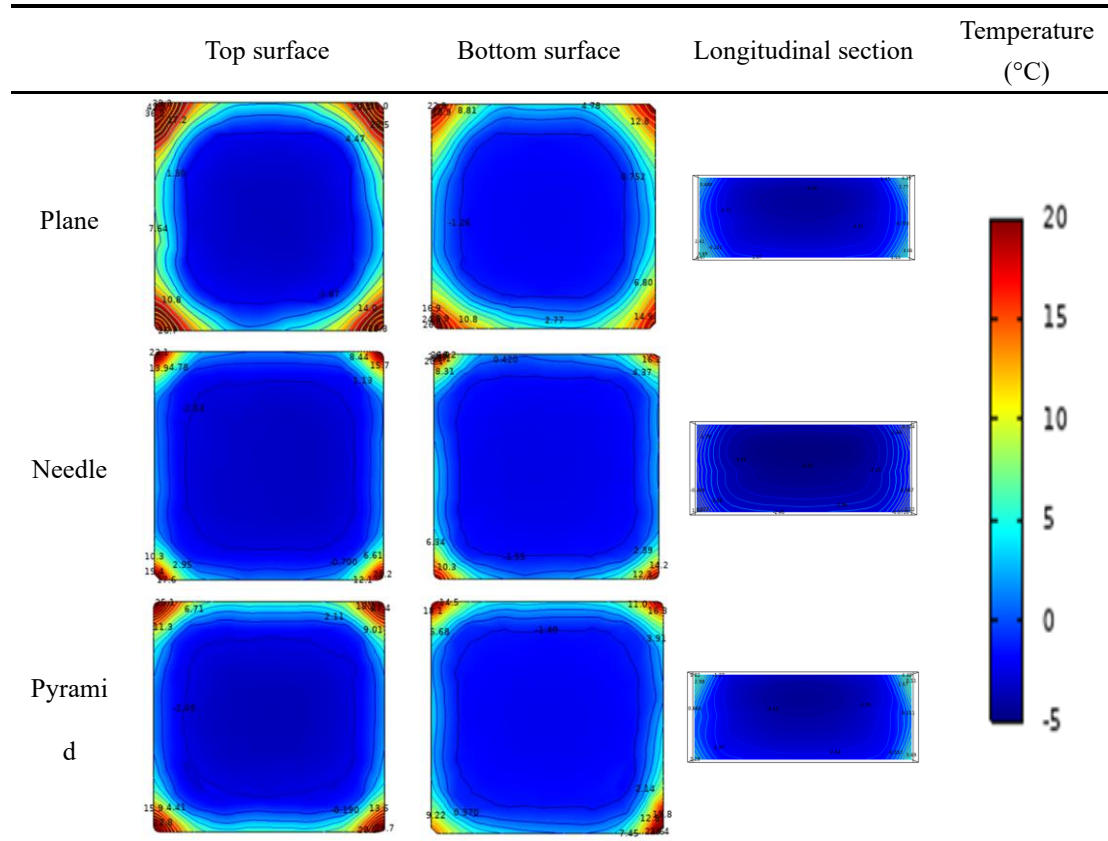


Fig. 3-10 Temperature distribution of rectangular materials after RF tempering under different shapes of electrode plates

Tempering rate of cylindrical materials under different shapes of electrodes is shown in Fig. 3-11. The hot spot temperatures of the cylindrical material after RF tempering under the plane, needle-shaped and pyramid-shaped electrodes were 12.4 °C, 2.9 °C and 3.1 °C, respectively. Under the RF tempering of three different shapes of electrodes, the uniformity of the top surface of the cylindrical material was less than that of the bottom surface. The temperature distribution of the longitudinal section was uniform and all areas were concentrated near the target tempering temperature. Moreover, the cold points of the top, bottom, and longitudinal section of the rectangular material all appeared in the center of the surface, and the hot spots all appeared in the

edge of the surface. Generally, the RF tempering uniformity under the needle-shaped electrode was the best, followed by the pyramid-shaped and plane electrode. The comparison of temperature distributions under different electrode plates indicated that RF tempering under the needle-shaped electrode reduced the difference between hot and cold temperatures.

Under the RF tempering of three different shapes of electrodes, the overheating areas of cylindrical materials were less than those of rectangular materials, and the uniformity was better.

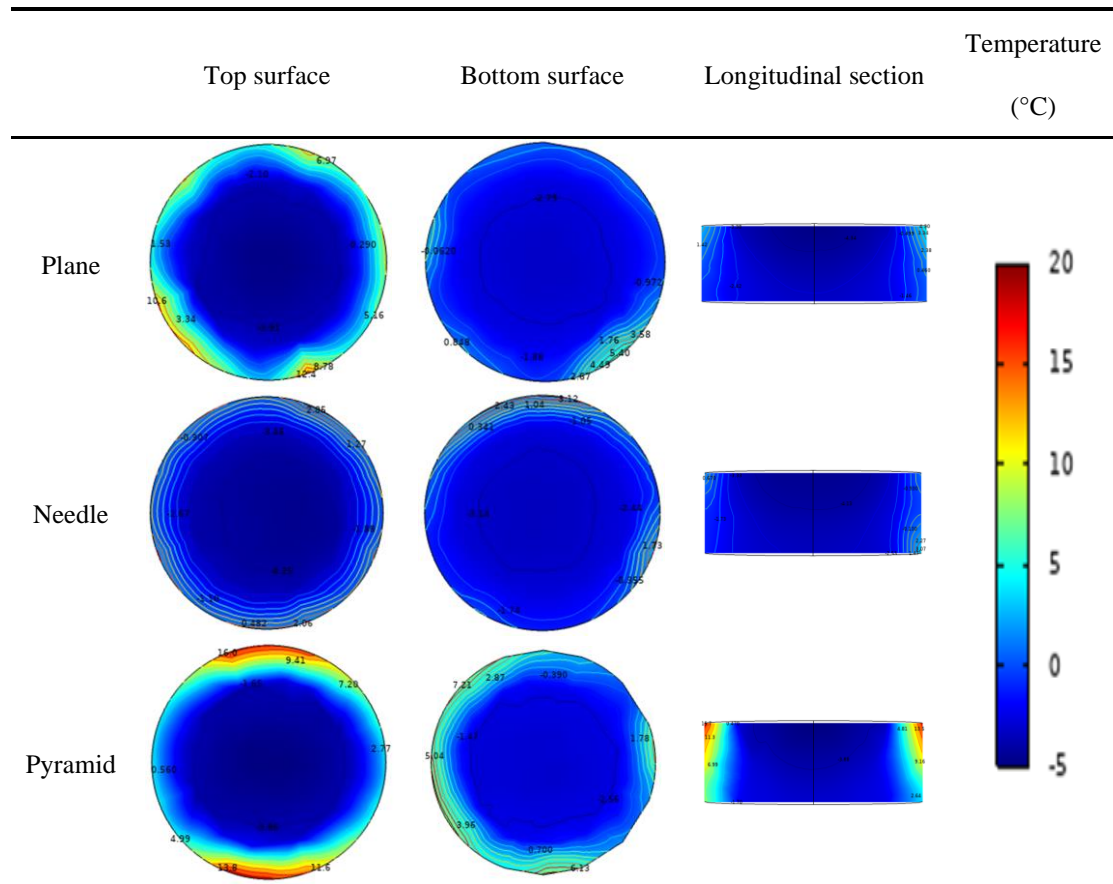


Fig.3-11 Temperature distribution of cylindrical materials after RF tempering under different shapes of electrode plates

### 3.4.5 Tempering uniformity evaluation under different electrode plates

The TUI values of materials after RF-tempering calculated from the temperature uniformity formula were shown in Table 3-2. The lower value indicates the higher temperature uniformity after tempering. The simulation results show that when the target temperature (center temperature  $-4\text{ }^{\circ}\text{C}$ ) was reached, the volume uniformity of

the tuna under the plane, needle-shaped and pyramid-shaped electrodes were 0.051, 0.045, 0.101. The uniformity of the materials of the two shapes materials was higher under the needle-shaped electrode, followed by the plane plate and the pyramid-shaped electrodes. The electrode shapes changed the electric field distribution within the system resulting in the changes of power absorption and heating uniformity of the sample.

Table 3-2 TUI values of materials after RF thawing under different shapes of electrode plates

	Plane	Needle-shaped	Pyramid-shaped
Rectangular	0.099	0.078	0.109
Cylindrical	0.051	0.045	0.101

### 3.5 Conclusion

In this study, the finite element model of RF tempering was established by coupling electromagnetic field and solid heat transfer. The computer simulation values were close to the experimental values, indicating that the model could used for the study of RF tempering tuna process and could effectively predict the tempering process and temperature distribution.

In the process of RF tempering, the electric field intensity distribution in the heating cavity was uneven, and the electrode plates of three different shapes (plane, needle-shaped, pyramid-shaped) had great influence on the electric field distribution. The shape of the electrode plate has a significant effect on the RF tempering process of the material, and the material absorbs the electromagnetic wave energy more evenly under the needle plate. The heating rate and temperature distribution of materials with different shapes (rectangular and cylinders) were different under three different shapes of electrodes. Among them, the RF tempering uniformity of rectangular s and cylinders under needle-shaped electrode was the best.

## References

- Alfaifi, B., Tang, J., Jiao, Y., Wang, S., Rasco, B., Jiao, S., & Sablani, S. (2014). Radio frequency disinfestation treatments for dried fruit: Model development and validation. *Journal of Food Engineering*, *120*, 268-276.
- Bedane, T. F., Chen, L., Marra, F., & Wang, S. (2017). Experimental study of radio frequency (RF) thawing of foods with movement on conveyor belt. *Journal of Food Engineering*, *201*, 17-25.
- Choi, C. T. M., & Konrad, A. (1991). Finite element modeling of the RF heating process. *IEEE Transactions on Magnetics*, *27*(5), 4227-4230.
- Erdogdu, Ferruh, Sarghini, Fabrizio, Uyar, Rahmi, Marra, & Francesco. (2016). Computer simulation of radio-frequency heating applied to block-shaped foods: Analysis on the role of geometrical parameters. *Food and Bioproducts Processing. Transactions of the Institution of Chemical Engineers, Part C*, *98*, 310-319.
- Ferrari-John, R. S., Katrib, J., Palade, P., Batchelor, A. R., Dodds, C., & Kingman, S. W. (2016). A Tool for Predicting Heating Uniformity in Industrial Radio Frequency Processing. *Food & Bioprocess Technology*, *9*(11), 1-9.
- Huang, Z., Marra, F., & Wang, S. (2016). A novel strategy for improving radio frequency heating uniformity of dry food products using computational modeling. *Innovative Food Science & Emerging Technologies*, *34*, 100-111.
- Huang, Z., Zhu, H., Yan, R., & Wang, S. (2015). Simulation and prediction of radio frequency heating in dry soybeans. *Biosystems Engineering*, *129*, 34-47.
- Marra, F., LuZhang, & G.Lyng, J. (2009). Radio frequency treatment of foods: Review of recent advances. *Journal of Food Engineering*, *91*(4), 497-508.
- Tiwari, G., Wang, S., Tang, J., & Birla, S. L. (2011). Analysis of radio frequency (RF) power distribution in dry food materials. *Journal of Food Engineering*, *104*(4), 548-556.
- Uyar, Rahmi, Erdogdu, Ferruh, Marra, & Francesco. (2014). Effect of load volume on power absorption and temperature evolution during radio-frequency heating of meat cubes: A computational study. *Food and Bioproducts Processing. Transactions of the Institution of Chemical Engineers, Part C*, *92*(3), 243-251.
- Uyar, Rahmi, Palazoglu, T., Koray, Farag, Karim, W., Bedane, & Tesfaye. (2015). Radio-frequency thawing of food products - A computational study. *Journal of Food Engineering*.

## **Chapter 4 Ohmic tempering of minced tuna and its model food made with Allaska pollock surimi – Evaluation of electrical conductivities**

### **4.1 Introduction**

Ohmic heating (OH) process is one of the electrical heating methods based on the passage of the electrical current through a product that serves as an electrical resistance, and the electrical energy is converted to heat energy within the food product. Thus, the EC of foodstuff is defined to be as a significant parameter with a major influence on the OH performance (Hosain, Adel, Farzad, Hadi, & Hosain, 2011). For fish samples, their composition, muscle types, and physical properties of the samples, as well as the temperature and frequency levels of the applied processes have been reported to influence their EC values (Jin, Cheng, Fukuoka, & Sakai, 2015; Jin, Jiang, Jiao, Llave, Fukuoka, & Sakai, 2020; Liu, et al., 2017). Liu, et al. (2017) examined the EC values of different tuna muscle types (dorsal, lateral, and ventral) between frequencies of 50 Hz and 20 kHz and temperature of  $-30\text{ }^{\circ}\text{C}$  to  $20\text{ }^{\circ}\text{C}$ . They found that the dorsal muscle containing higher moisture content and lower fat content contributed to a higher EC value while the ventral muscle showed the opposite. Jin, et al. (2015) evaluated the effect of muscle type, current direction, and the presence of muscle membranes on the EC values of yellowtail fillets during OH process. It was reported that the muscle membrane had a significant influence on the EC values, and the EC of yellowtail fillets in parallel current direction to the fish muscle was higher than in series direction. Cevik and Icier (2018) investigated the effect of fat content (2, 10, and 18%) and voltage gradient ( $10, 13, \text{ and } 16\text{ V cm}^{-1}$ ) on the EC of frozen minced beef meat during ohmic thawing and found that the EC values of frozen minced beef meat decreased as the fat content increased for the same voltage gradient. Uemura, Noguchi, Park, and Kim (1994) evaluated the OH of minced fish (Alaska pollock) heated up to  $90\text{ }^{\circ}\text{C}$  at the frequency range  $50\text{ Hz} \sim 10\text{ kHz}$  and showed that the used frequency made a big impact on the EC values, the heating rate, and the dielectric loss of the samples, being the biggest values at the frequency of 10 kHz.

OH has advantages such as high heating rate, high energy efficiency, volumetric

heating, and no waste water (Hosain, et al., 2011). However, some OH literatures have reported the occurrence of nonuniform temperature distribution because of some foodstuff regions have different EC values, due to the heterogeneous distribution of muscle and the presence of connective and adipose tissues in meat and fish products (Bozkurt & Icier, 2012; Icier, et al., 2010; Jin, et al., 2015; Liu, et al., 2017; Yildiz-Turp, Sengun, Kendirci, & Icier, 2013). Moreover, for thawing-tempering process the local overheating in the food material occurred because of the high differences between the EC values of thawed and unthawed parts. Therefore, to promote more uniform thawing-tempering process, it had been reported to be necessary to apply suitable voltages gradient, provide homogenous samples, and facilitate electrode-sample contact (Döner, Çokgezme, Çevik, Engin, & İçier, 2020). However, experimental determination of the optimum parameters of OH process requires many replicates and consumes energy and time, which increase the cost, especially for high-value fishery products such as the case of frozen tuna blocks. In this sense, the development of model foods to conduct experimental work with low cost, avoiding the random variability in composition/structure of natural resources, and providing similar EC values to the target food products could be a good alternative in initial studies as dummy loads for developing the process (Luan, et al., 2015; J. Wang, Tang, Liu, & Bohnet, 2018).

In the electro-processing thawing and heating research field, some studies have been developed model foods such as (Cong, Liu, Tang, & Xue, 2012; Icier & Ilicali, 2005; Llave, Mori, Kambayashi, Fukuoka, & Sakai, 2016; Y. Wang, Tang, Rasco, Wang, Alshami, & Kong, 2009). These studies revealed that model foods could be used to simulate various food materials being used as dummy loads for lowering potential test cost. However, only few studies assessed the feasibility of model food for OT or thawing. Thus, it is believed that using pollock surimi as a base to develop a model food for high-value fishery products, such as tuna for sushi and sashimi consumption during OT process can be an effective approach. The purpose of this work was to evaluate the use of Alaska pollock surimi as a model food to simulate minced lean tuna by exploring the influence of salt added on the EC of pollock surimi and conducting appropriate

control of the voltage gradient during OT. Thus, this study aimed to: (1) evaluate the EC values of minced lean tuna at the temperature range of  $-40\text{ }^{\circ}\text{C}$  to  $10\text{ }^{\circ}\text{C}$  and at the frequency range of 50 Hz to 20 kHz; (2) determine the EC of pollock surimi with 0%, 0.25%, 0.5%, 1.0%, and 2.0% salt at the same processing conditions as the minced lean tuna; (3) find the optimum voltage control during OT process at 20 kHz; and (4) determine the optimum experimental parameters of pollock surimi as a model food of minced lean tuna by comparing their performance during OT at 20 kHz in terms of temperature profiles and distributions and closeness of their EC values.

## 4.2 Material and methods

### 4.2.1 Material preparation

Frozen bigeye tuna (*Thunnus obesus*) muscles were used as raw material which was purchased directly from a fish market in Misaki, Japan. The fish was caught by longline fishing, frozen onboard, shipped frozen by air-blast method to the laboratory, and then kept in a deep freezer at  $-60\text{ }^{\circ}\text{C}$ . Detail information was shown by Jiang, Jia, Nakazawa, Hu, Osako, and Okazaki (2019). Commercial frozen Alaska pollock (AP) (*Theragra chalcogramma*) surimi (FA grade) was provided by Glacier Fish Company (Seattle, WA, USA). After delivery to the laboratory, 10 kg block of surimi was cut into small pieces ( $\sim 500\text{ g}$ ), vacuum packaged, and stored in a refrigerator ( $-60\text{ }^{\circ}\text{C}$ ). Detail information was shown by Nguyen, Park, Liqiong, Nakazawa, Osako, and Okazaki (2020). The physicochemical composition of both tuna and pollock surimi samples are shown in Table 4-1. These were examined by Japan Food Research Laboratories, a general incorporated foundation (Tokyo, Japan). Although the tuna sample had higher protein and fat content than pollock surimi, and the sodium and salt equivalent of pollock surimi were higher than tuna, the moisture content of them were similar.

Table 4-1. Intrinsic composition of lean tuna and Allaska pollock surimi.

Sorts	Energy (kcal/100g)	Moisture content (%)	Protein content (%)	Fat content (%)	Ash content (%)	Carbohydrate content (%)	Sodium (%)	Salt equivalent (%)
Tuna	106	74.4	23.8	1.2	1.2	0	0.0314	0.0798
Pollock Surimi	102	73.9	17.0	0.1	0.7	8.4	0.166	0.422

Before experimentation, samples were thawed in a refrigerator at 4 °C overnight, and separately homogenized at 1500 rpm for 3.5 min at 4 °C using a vacuum mixer (UMC-5, Stephan Machinery Corp., Hameln, Germany). For pollock surimi, different salt content (0%, 0.25%, 0.5%, 1.0%, and 2.0%) was added. Mixed samples (approximately 30 g) were carefully filled into a polystyrene container (30×30×30 mm<sup>3</sup>) of 2.5 cm thickness to avoid air bubbles. Two titanium plate electrodes (30 mm width, 100 mm height, and 0.5 mm thickness) were placed at opposite sides of the container and pressed to the surface of the samples by using an external mechanical press manually adapted (see Fig. 4-1). Under these conditions, the whole container-sample-electrodes components of the system were deep frozen at –40 °C in an air blast freezer (KQF-5AL, Air Operation Technologies, Inc., Japan) for > 3 h and stored at –40 °C in a freezer (CR-221BSE, TOSHIBA, Japan). This procedure assures a firm contact between the samples and the electrode surfaces for posterior OH experiments (Liu et al. 2017; Llave et al. 2018).

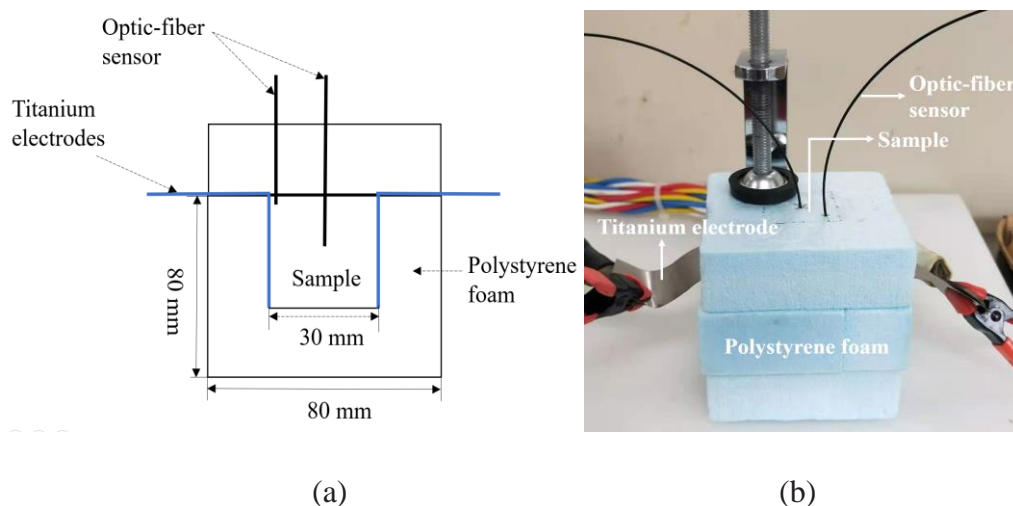


Fig. 4-1. (a) Schematic diagram of the fiber-optic temperature sensor in the sample.  
 (b) Picture of the sample setup for OT experiment.

#### 4.2.2 Temperature monitoring

For the EC measurement, frozen samples were brought out of the freezer, and a hole of 1.6 mm diameter was drilled at the center of each sample to allow insertion of K-type thermocouple connected to a temperature data logger (HIOKI LR8431,

MEMORY HiLOGGER) for temperature recording. The samples were put into a constant-temperature and constant-humidity chamber (SH-241, ESPEC Corp., Japan) to equilibrate the sample temperature to -40 °C, -30 °C, -20 °C, -10 °C, -7 °C, -6 °C, -5 °C, -4 °C, -3 °C, -2 °C, -1 °C, 0 °C, 5 °C, 10 °C, and measure the corresponding EC values.

For the OT experiments, frozen samples were brought out of the freezer, and 1.6 mm holes of diameter were drilled at the center and corner (5 mm apart from edges and 2 mm apart from the top surface) of each sample to allow the insertion of two temperature fiber-optic sensors connected to a temperature measuring system (FTC-DIN-ST-PH, Photon Control, Canada). The schematic diagram of the temperature monitoring in the sample and the sample setup for the OT experiment are shown in Fig. 4-1. Experiments were conducted until the sample center temperature reached -4 °C. Right after tempering, an infrared thermal camera (Thermo GEAR G120EX, Nippon Avionics Co., Ltd., Japan) was used to capture the top surface temperature distribution of the tempered samples within 10 s. Calibration of the infrared camera was performed under controlled conditions with several blackbody reference sources and an emissivity of 0.95.

#### 4.2.3 Measurement of EC

A LCR meter (HiTESTER3532-50, HIOKI Co. Ltd., Japan) was used to measure the electrical resistance of samples. The electrical resistances were measured from -40 °C to 10 °C within the frequency range of 50 Hz to 20 kHz. All experiments were conducted in triplicates.

The EC ( $\sigma$ , S m<sup>-1</sup>) was determined with the geometrical parameters of the sample and the resistance using the equation below:

$$\sigma = \frac{1}{R} \times \frac{L}{A} \quad (4-1)$$

where R is the resistant of the sample ( $\Omega$ ); L is the gap between the two electrodes (m); A is the cross-sectional area of one surface of the sample (m<sup>2</sup>) in direct contact to the electrode.

The LCR meter was used to measure the impedance (Z), reactance (X), and

resistance ( $R_s$  and  $R_p$ , when considering series and parallel circuits, respectively) for the calculation of EC value. Although the temperature increases during OH of biological materials is due to resistance ( $R$ ) not impedance ( $Z$ ), it might be convenient to use  $Z$  value instead of  $R$  value when  $Z = R$ , especially at high frequency (higher than 1 kHz), as suggested by Liu, et al. (2017). Among lower frequency range,  $R_p$  was greater than  $R_s$ , and this difference increased as frequency decreased, which was due to the electrical disposition of resistor and capacitors in the parallel and serial electrical connection, where the resistance value was in the range  $R_p > Z > R_s$  until the reactance values become 0. Beyond this point, it has been reported that  $R_p = Z = R_s$  (Llave, Udo, Fukuoka, & Sakai, 2018) for the case of OH of beef at 20 kHz and analysis of EC at low and high frequencies. However, in this research, due to the use of surimi and minced muscle, the direction of membrane in the fish muscle has been previously broken during the homogenization step or before, thus series and parallel of current direction was not taken into consideration. For this reason, the calculation of EC values was based on the impedance ( $Z$ ) of the samples.

#### **4.2.4 Experimental tempering using an OH system**

The samples were filled into the container and tempered just to  $-4\text{ }^{\circ}\text{C}$ . All experiments were conducted in triplicates. The voltage was applied to the electrodes using a voltage regulated Joule heating machine (FJB-5.5, Frontier Engineering Co., Ltd., Japan) at a frequency of 20 kHz. The amount of heat generated is related to the electric current induced by the voltage gradient in the field and the EC of materials (Icier, et al., 2005). Higher voltage usually results in higher heating rate but worse tempering uniformity. Thus, several different voltages and its combination were selected for exploring the most appropriate voltage for samples during OT. The voltage applied was one step (400 V:  $-35\text{ }^{\circ}\text{C} \sim -4\text{ }^{\circ}\text{C}$  or 200 V:  $-35\text{ }^{\circ}\text{C} \sim -4\text{ }^{\circ}\text{C}$ ), two steps (400 V+200 V:  $-35\text{ }^{\circ}\text{C} \sim -15\text{ }^{\circ}\text{C}$  and  $-15\text{ }^{\circ}\text{C} \sim -4\text{ }^{\circ}\text{C}$ , respectively) and three steps (400 V+200 V+100 V:  $-35\text{ }^{\circ}\text{C} \sim -20\text{ }^{\circ}\text{C}$ ,  $-20\text{ }^{\circ}\text{C} \sim -10\text{ }^{\circ}\text{C}$  and  $-10\text{ }^{\circ}\text{C} \sim -4\text{ }^{\circ}\text{C}$ , respectively).

#### **4.2.5 Statistical analysis**

Statistical analyses were performed using Microsoft office Excel 2016 and

OriginPro 9.1. All experimental data was presented as mean or mean  $\pm$  standard deviation.

### **4.3 Results and discussion**

#### **4.3.1 EC values of minced tuna and model foods blocks**

##### **4.3.1.1 Effect of temperature on EC**

EC is the intrinsic and basis electrical property of foodstuffs during OH process that is essential for analyzing the heat penetration and the uniformity of the temperature distribution. Considering the temperature dependance of the EC values, the relationship between EC and temperature was investigated in multiple ranges. The EC values of minced tuna at the frequency range of 50 Hz ~ 20 kHz and temperature range of  $-40 \sim 10$  °C are showed in Fig. 4-2. There was nearly no change of the EC values within the temperature range of  $-40 \sim -20$  °C. However, the EC values increased linearly with temperature from  $-20$  to  $-10$  °C, exponentially with temperature from  $-10$  to  $0$  °C, and polynomially with temperature from  $0$  to  $10$  °C. As example, the EC values of minced tuna at the temperatures of  $-40$ ,  $-20$ ,  $-10$ ,  $-5$ ,  $0$ ,  $5$ , and  $10$  °C were 0.00003, 0.0009, 0.007, 0.08, 0.37, 0.41, and 0.47 S m<sup>-1</sup>, respectively at 50 Hz; while at 20 kHz were 0.0001, 0.001, 0.007, 0.09, 0.44, 0.52, and 0.60 S m<sup>-1</sup>, respectively. In Fig. 4-2b, the temperature dependency of EC values showed a faster increasing trend with rising frequency. In other words, the temperature dependency was highly sensitive at higher frequencies compared to lower frequencies.

The EC values of pollock surimi (without any salt addition) at similar frequency and temperature range used for minced lean tuna are showed in Fig. 4-3. At 50 Hz, the EC values of pollock surimi at the temperatures of  $-40$ ,  $-20$ ,  $-10$ ,  $-5$ ,  $0$ ,  $5$ , and  $10$  °C were 0.0000007, 0.00004, 0.002, 0.02, 0.13, 0.18, and 0.19 S m<sup>-1</sup>, respectively. At 20 kHz, the values were 0.00004, 0.0001, 0.002, 0.02, 0.14, 0.19, and 0.22 S m<sup>-1</sup>, respectively. In general, the EC values of pollock surimi were almost half of the EC values of minced lean tuna at the investigated temperature range.

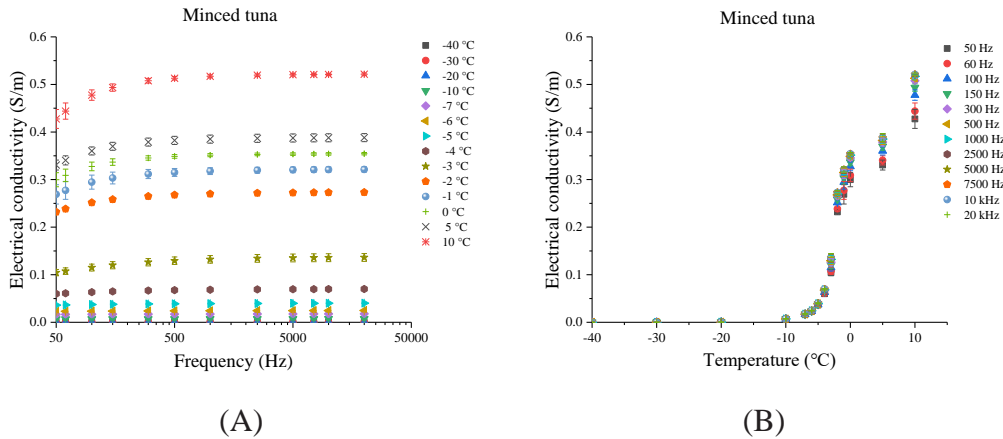


Fig. 4-2. Electrical conductivity of minced tuna at the frequency range of 50 Hz ~ 20 kHz and the temperature range of  $-40 \sim 10 \text{ }^{\circ}\text{C}$ . A: at several temperatures, B: at several frequencies.

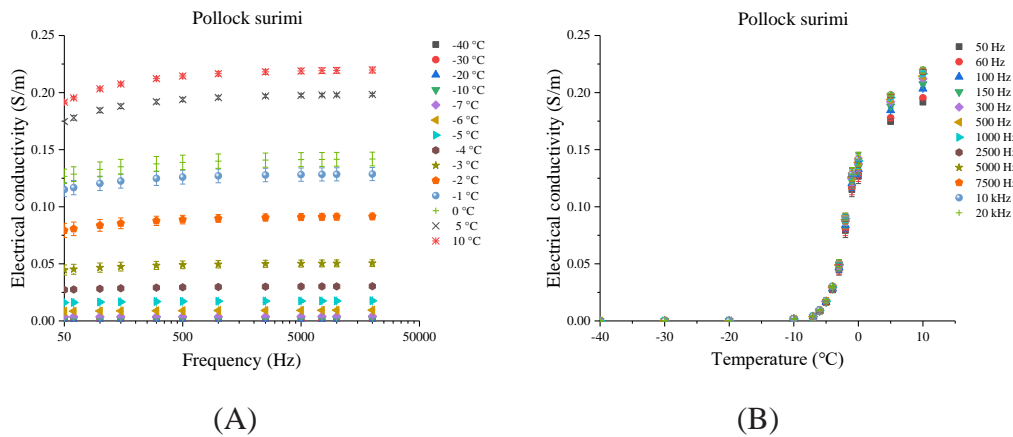


Fig. 4-3. Electrical conductivity of pollock surimi (without salt) at the frequency range of 50 Hz ~ 20 kHz and the temperature range of  $-40 \sim 10 \text{ }^{\circ}\text{C}$ . A: at several temperatures, B: at several frequencies.

For both samples, the EC values at temperatures below  $-20 \text{ }^{\circ}\text{C}$  were less than  $0.005 \text{ S m}^{-1}$ . These values agreed with the EC values of lean tuna flesh muscle ( $1.34 \times 10^{-4} \text{ S m}^{-1}$  to  $0.458 \text{ S m}^{-1}$  at the temperature range of  $-30 \text{ }^{\circ}\text{C}$  to  $20 \text{ }^{\circ}\text{C}$ , respectively) reported by (Liu, et al., 2017). They claimed that at lower temperatures, mobile water was gradually frozen, and the ion movement was restricted as the temperature decreased (below  $-20 \text{ }^{\circ}\text{C}$ ). Rahman (2010) reported that during the thawing of frozen foods, water molecules change from solid to liquid phase, which contributed to the increased mobility of electrical components; thus, a steep increase of EC values is observed. Seyhun, et al. (2012) investigated the change of EC values of potato puree with variable salt contents (0.5%~1.0% salt) at different frequencies (10~30 kHz) during ohmic

thawing from  $-16$  to  $0$  °C. They reported that the change of EC values with temperature was linear at lower temperature and exponential when the temperature reached to initial thawing temperatures. Cevik, et al. (2018) determined the change of effective EC of frozen minced beef meat with different fat contents (2~18%) during ohmic thawing by applying different voltage gradients ( $10\sim 16$  V  $\text{cm}^{-1}$ ) from  $-18$  to  $-1$  °C. They reported that the EC change was linear at temperature range from  $-18$  to  $-9.5$  °C, exponential at temperature range from  $-9.5$  °C to  $-4$  °C and polynomial above  $-4$  °C. A similar behavior was also obtained in the present study for both samples.

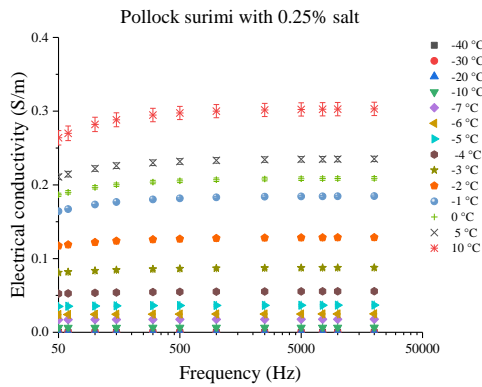
#### **4.3.1.2 Effect of frequency on EC**

In general, the EC values slightly increased with increasing frequency at the constant temperature, specially below 1 kHz (Fig. 4-2a and Fig. 4-3a). The influence of frequency on EC values changes was less pronounced than temperature effect. From Fig. 4-2a, it can be observed that the EC values of minced tuna at  $-10$  °C and frequencies of 50, 500, 1000, 10000, and 20000 Hz were 0.0068, 0.0070, 0.0071, 0.0072, and 0.0074  $\text{S m}^{-1}$ , respectively, and 0.4274, 0.5131, 0.5171, 0.5211, and 0.5215  $\text{S m}^{-1}$ , respectively, at  $10$  °C. In Fig. 4-3, the EC values of pollock surimi at the same frequencies and  $-10$  °C were 0.0016, 0.0016, 0.0016, 0.0017, and 0.0018  $\text{S m}^{-1}$ , respectively; while at  $10$  °C, the EC values were 0.1917, 0.2145, 0.2189, 0.2194, and 0.2198  $\text{S m}^{-1}$ , respectively.

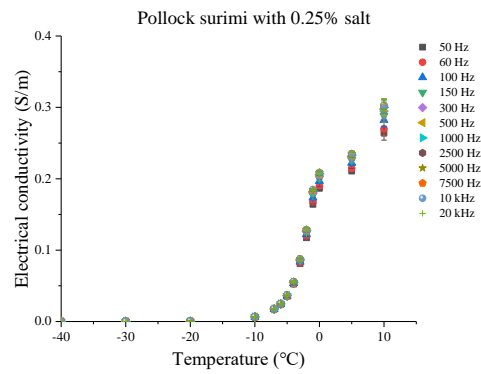
In general, the EC values of pollock surimi were lower than that of minced tuna at frequencies from 50 Hz to 20 kHz. It was noted that higher frequencies caused more active motion of ions, and the difference between high and low frequencies was more pronounced as temperature raised, especially above  $0$  °C. These characteristics of the EC values with frequency are similar as those reported by Lee, Ryu, and Kang (2013). They investigated the effect of frequency alternating current during OH from  $20$  to  $90$  °C on the heating rate, the inactivation of food-borne pathogens, and the quality of tomato-based salsa. They reported that the EC values of the samples were higher at high-frequency range (1 to 20 kHz) than at low-frequency range (below 500 Hz).

### 4.3.1.3 Effect of salt concentration on EC

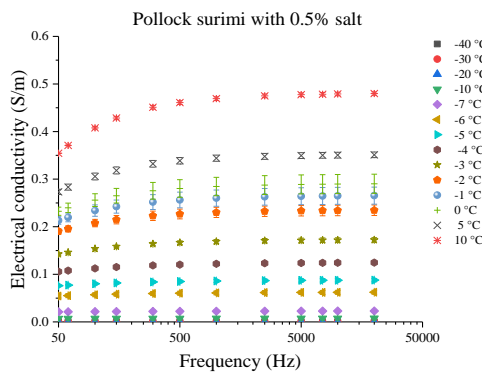
EC values of pollock surimi with different salt content (0%, 0.25%, 0.5%, 1.0%, and 2.0%) at the frequency range of 50 Hz ~ 20 kHz and temperature range of  $-40 \sim 10$  °C are showed in Fig. 4-4. It can be observed that the EC values of pollock surimi increased with an increase in salt content. The influence of salt addition on EC values of pollock surimi was greater above 0 °C, especially at high salt content and higher frequencies. It can be due to the well know effect of the addition of salt on the ionic conduction. Guo et al. (2017) reported that the salt dependency of EC values was highly sensitive at higher frequencies compared to lower frequencies.



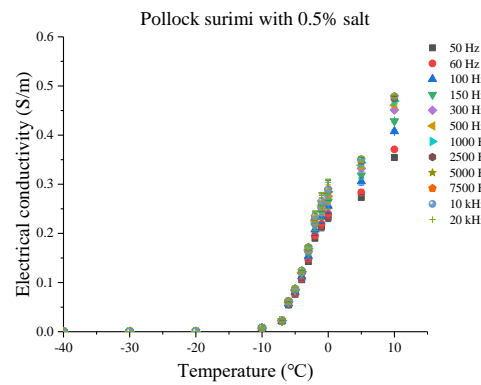
(a)



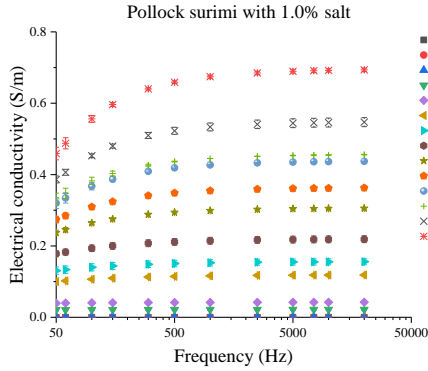
(b)



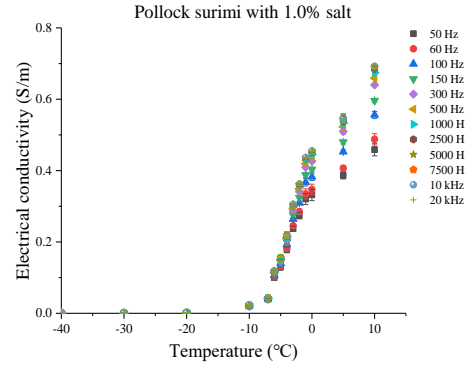
(c)



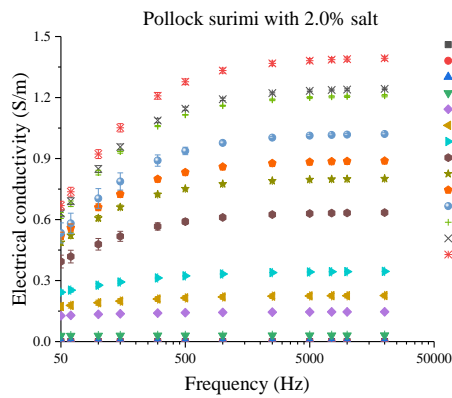
(d)



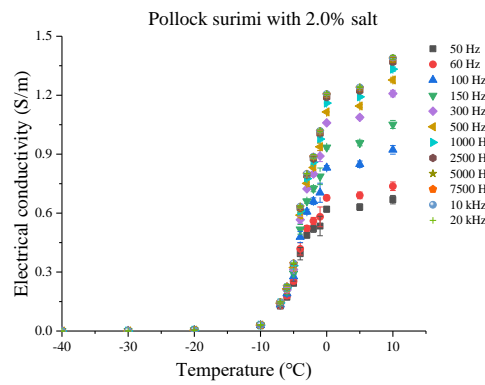
(e)



(f)



(g)



(h)

Fig. 4-4. Electrical conductivity of pollock surimi with different salt contents (0.25%, 0.5%, 1.0%, and 2.0%) at frequency range of 50 Hz~20 kHz and temperature range of  $-40 \sim 10$  °C.

In Fig. 4-5a, the EC values of minced tuna and pollock surimi with different salt contents at the temperature range of  $-40 \sim 10$  °C at 50 Hz are showed. At the initial temperature of  $-40$  °C, the EC values of pollock surimi with 0%, 0.25%, 0.5%, 1.0%, and 2.0% salt were  $9.01 \times 10^{-7}$ ,  $2.19 \times 10^{-6}$ ,  $2.56 \times 10^{-6}$ ,  $4.23 \times 10^{-6}$ , and  $6.23 \times 10^{-6}$  S m<sup>-1</sup>, respectively; while at the final temperature of 10 °C the EC values were 0.19, 0.26, 0.35, 0.46, and 0.67 S m<sup>-1</sup>, respectively. However, at 20 kHz (Fig. 4-5b) higher EC values for pollock surimi with 0%, 0.25%, 0.5%, 1.0%, and 2.0% salt were observed such as  $4.24 \times 10^{-5}$ ,  $4.81 \times 10^{-5}$ ,  $5.31 \times 10^{-5}$ ,  $5.88 \times 10^{-5}$ , and  $1.39 \times 10^{-4}$  S m<sup>-1</sup> at  $-40$  °C and 0.22, 0.30, 0.48, 0.69, and 1.39 S m<sup>-1</sup> at 10 °C, respectively. Higher EC values at 20 kHz than at 50 Hz can be due to the resistance to the movement of ions at higher frequencies are less pronounced than at lower frequencies (Guo, Llave, Jin, Fukuoka,

& Sakai, 2017).

For both cases, the EC values of pollock surimi with 0.5% salt were the closest to the EC values of minced tuna. For example, at 20 kHz and  $-40$ ,  $-20$ ,  $-10$ ,  $-5$ ,  $0$ ,  $5$ , and  $10$  °C, they were  $0.00005$ ,  $0.0003$ ,  $0.007$ ,  $0.09$ ,  $0.02$ ,  $0.35$ , and  $0.48$  S m $^{-1}$ , respectively, while for minced tuna at the same temperatures and frequencies, the EC values were  $0.00006$ ,  $0.0005$ ,  $0.007$ ,  $0.04$ ,  $0.35$ ,  $0.39$ , and  $0.52$  S m $^{-1}$ , respectively.

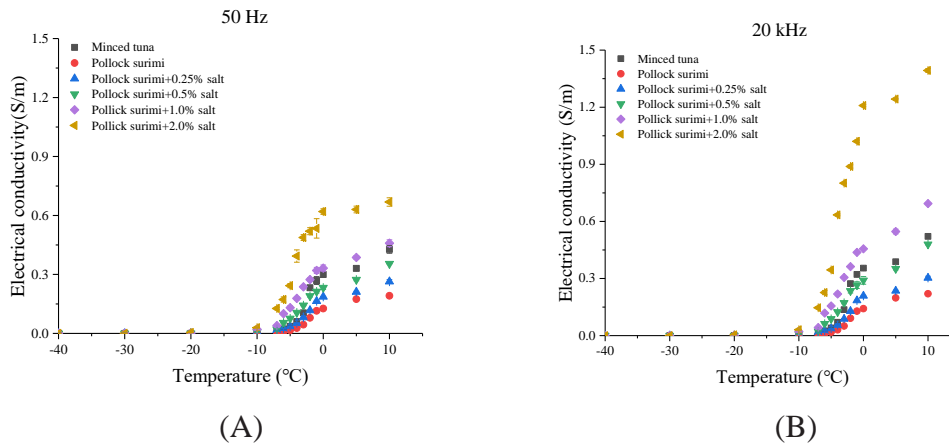


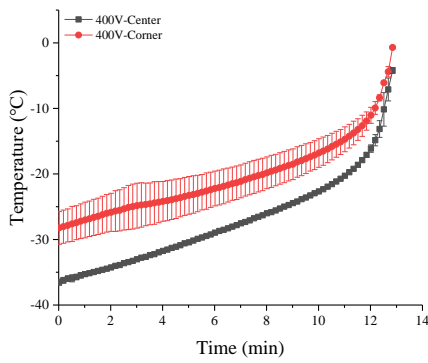
Fig. 4-5. Comparison of electrical conductivities of minced tuna and pollock surimi with different salt contents at temperature range of  $-40 \sim 10$  °C. A: at 50 Hz and B: at 20 kHz.

### 4.3.2 Experimental voltage gradient control during OT

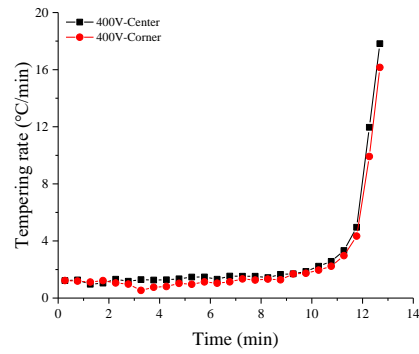
Several approaches in voltage gradient control during OT were tested using the lean minced tuna sample described in this section.

#### 4.3.2.1 Temperature history

Time-temperature profiles of minced tuna during OT at 400V ( $-35 \sim -4$  °C) are shown in Fig. 4-6 (a) for center and corner positions. It took 12.85 min for the center and 12.68 min for the corner of the sample to reach  $-4$  °C. The temperature increased linearly below  $-15$  °C and then sharply increased above  $-15$  °C. The tempering rates of minced tuna under the same conditions are shown in Fig. 4-6 (b). It is showed that the OT rate for the center position was below  $2.0$  °C min $^{-1}$  before 10.1 min (at  $-22.3$  °C). Then, it increased to  $3.18$  °C min $^{-1}$  at  $-20.3$  °C,  $7.68$  °C min $^{-1}$  at  $-15.5$  °C, and  $18.24$  °C min $^{-1}$  at  $-10.2$  °C.

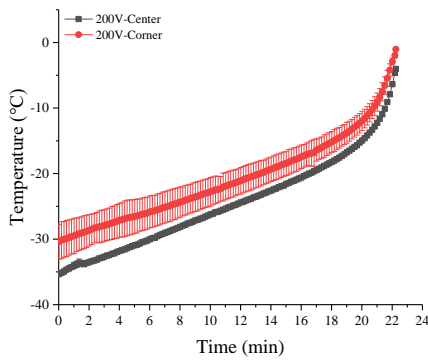


(A)

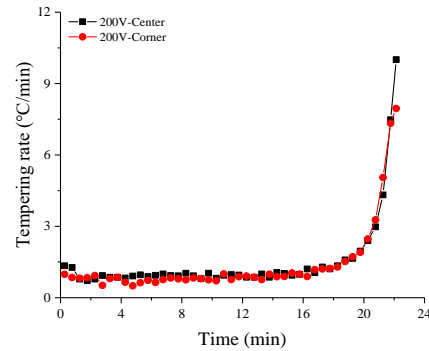


(B)

Fig. 4-6. (A) Time-temperature profiles and (B) average tempering rate of minced tuna during OT process under a controlling voltage at 400 V ( $-35 \sim -4$  °C).



(A)



(B)

Fig. 4-7. (A) Time-temperature profiles and (B) average tempering rates of minced tuna during OT process under a controlling voltage at 200 V ( $-35 \sim -4$  °C).

Time-temperature profiles of minced tuna during OT at 200V ( $-35 \sim -4$  °C) are shown in Fig. 4-7 (a) for center and corner positions. It took 22.25 min for the center and 21.85 min for the corner of the sample to reach  $-4$  °C, and then the temperature increased linearly below  $-10$  °C and sharply increased above  $-10$  °C. Although the initial temperature difference between the center and corner was  $4.93$  °C, at the end of the process it was  $2.99$  °C (when the tuna sample reached the target temperature of  $-4$  °C). The initial sample surface temperature was higher than that of center, which was caused by the exposure of sample's surface in the environment and inevitable heat transfer when the sample was took from the refrigerator and fitted into the heating device. The OT rate before 20.1 min was below  $2.0$  °C  $\text{min}^{-1}$  (at  $-14.9$  °C), and  $1.17$  °C  $\text{min}^{-1}$ ,  $2.13$  °C  $\text{min}^{-1}$ , and  $6.18$  °C  $\text{min}^{-1}$  at  $-20.2$  °C,  $-15.0$  °C, and  $-10.1$  °C, respectively.

The voltage gradient was statistically significant on the OT time and rate. Darvishi (2012) used five different voltages (6, 8, 10, and 14 V cm<sup>-1</sup>) at 50 Hz to ohmically heat tomato paste. They found that OH times were dependent on the voltage gradient used and reported that the time of tomato paste from 26 °C to 96 °C decreased from 235 s to 38 s as the voltage gradient increased from 6 to 14 V cm<sup>-1</sup>. Nistor, Botez, Luca, Mocanu, and Timofti (2013) determined the temperature variation of apple puree treated by OH with different voltage gradients (15, 17, 17.5, and 20 V cm<sup>-1</sup>). They reported that the processing time depended on the voltage gradient, and the heating time from 20 °C to above 60 °C was 300 s with a higher voltage gradient of 20 V cm<sup>-1</sup> while the heating time was more than 1200 s with a lower voltage gradient of 15 V cm<sup>-1</sup>. Fattahi and Zamindar (2020) applied three different voltages (40, 50, and 60 V) and three different concentrations (0.3, 0.4, and 0.5% w/v) of brine solution to improve immersion ohmic thawing of frozen tuna fish cubes. They observed that the immersion ohmic thawing process at 50 V in saline concentration of 0.3% w/v resulted in the faster thawing process. In the present study, a similar result has been observed concluding that the voltage gradients played a major role in OT times. However, it has been reported that higher voltages caused current density and amplifier the temperature nonuniformity in OH (Icier, et al., 2010). Therefore, the voltage needs to be decreased in order to control the temperature increasing homogeneously with the aim to preserve the food quality and nutrition (Chai & Park, 2007; Icier, et al., 2010; Yildiz-Turp, et al., 2013).

In this study, several experiments adjusting the applied voltage during OT process have been evaluated and results are shown as follows. In Fig. 4-8, the time-temperature profiles of minced tuna under controlling voltage of 400V+200V at the temperature range of -35 ~ -15 °C and -15 ~ -4 °C, respectively, are shown. Above -15 °C, the tempering rate smoothly decreased by the voltage control (reduction from 400 V to 200 V), being more pronounced at surface position. As a result, it took 16.1 min for the center position to reach the target temperature, while 15.7 min for the surface position. At the target temperature, the temperature difference between the center and corner positions was 3.42 °C. A three-step voltage control (400V+200V+100V: -35 ~ -20°C,

-20 ~ -10 °C, and -10 ~ -4 °C, respectively) during OT process of minced tuna was conducted and the time-temperature profiles at center and surface positions are shown in Fig. 4-9. Results shown a significant decrease in the OT rate around -10 °C and -16 °C, where the voltage was reduced from 400V to 200V and then to 100V, respectively. It took 18.2 min for the center position to reach the target temperature, while 17.3 min for the surface position.

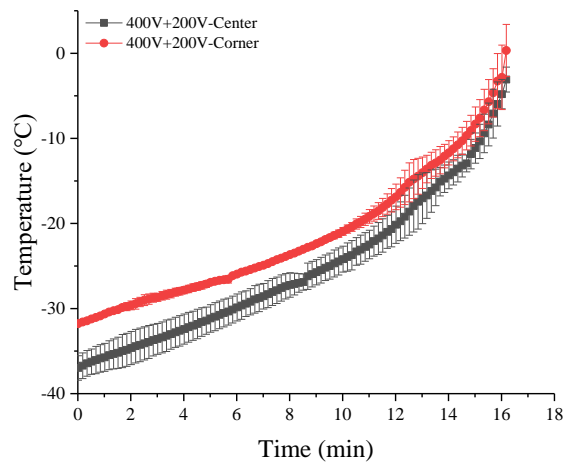


Fig. 4-8. Time-temperature profiles of minced tuna during OT process under the controlling voltage (400V+200V: -35 ~ -15 °C and -15 ~ -4 °C)

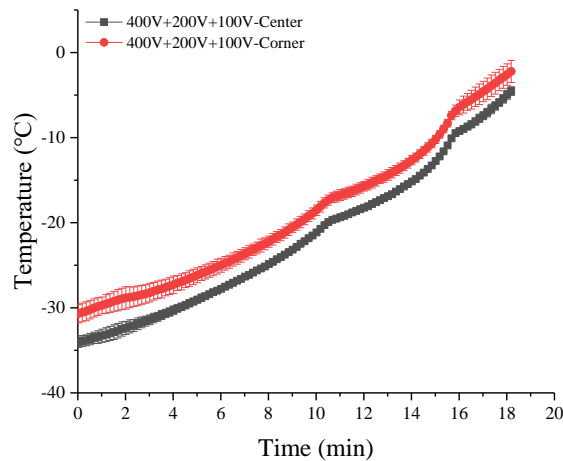


Fig. 4-9. Time-temperature profiles of minced tuna during OT process under controlling voltage at 400 V (-35 ~ -20°C), 200 V (-20 ~ -10 °C), and 100 V (-10 ~ -4 °C).

In Fig. 4-10, the time-temperature profiles of tuna under several controlling voltage steps (400V from -35 to -4 °C, 200V from -35 to -4 °C, 400V+200V from -

35 to  $-15\text{ }^{\circ}\text{C}$  and  $-15$  to  $-4\text{ }^{\circ}\text{C}$ , respectively, and 400V+200V+100V from  $-35$  to  $-20\text{ }^{\circ}\text{C}$ ,  $-20$  to  $-10\text{ }^{\circ}\text{C}$ , and  $-10$  to  $-4\text{ }^{\circ}\text{C}$ , respectively) are shown. These voltage control methods were adjusted based on the results observed for the EC changes (reported above). Compared to the results of one or two steps voltage control during OT, although the three steps method took more time to reach the target temperature, it shown more uniform tempering process, judged based on the smaller differences between temperatures at center and corner positions.

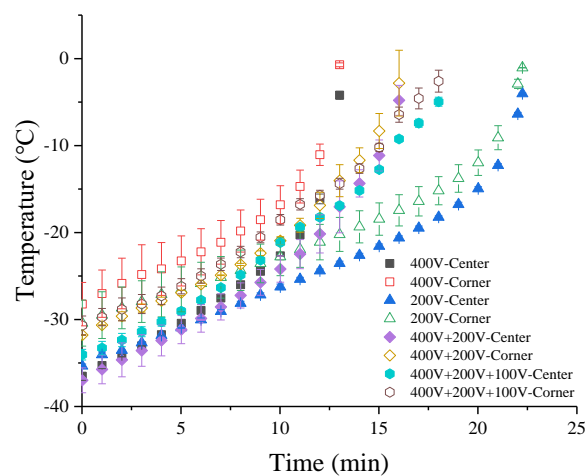


Fig. 4-10. Time-temperature profiles of minced tuna during OT process under several controlling voltage (400 V:  $-35 \sim -4\text{ }^{\circ}\text{C}$ ; 200 V:  $-35 \sim -4\text{ }^{\circ}\text{C}$ ; 400 V+200 V:  $-35 \sim -15\text{ }^{\circ}\text{C}$  and  $-15 \sim -4\text{ }^{\circ}\text{C}$ , respectively; 400 V+200 V+100 V:  $-35 \sim -20\text{ }^{\circ}\text{C}$ ,  $-20 \sim -10\text{ }^{\circ}\text{C}$ , and  $-10 \sim -4\text{ }^{\circ}\text{C}$ , respectively).

The comparison of the time-temperature profiles of minced tuna and model foods under the same three steps controlling voltage method (400V,  $-35 \sim -20\text{ }^{\circ}\text{C}$ ; 200V,  $-20 \sim -10\text{ }^{\circ}\text{C}$ ; 100V,  $-10 \sim -4\text{ }^{\circ}\text{C}$ ) is shown in Fig. 4-11. It took 32.5 min for the pollock surimi (without salt) and 19.5 min for the pollock surimi with 0.5% salt added to reach the target temperature ( $-4\text{ }^{\circ}\text{C}$ ). Salt concentration played a significant role on the decrease of OT time of pollock surimi because salt increased the ion mobility which increased the EC specially above  $-10\text{ }^{\circ}\text{C}$ . Seyhun et al. (2012) tempered frozen potato puree from  $-16$  to  $0\text{ }^{\circ}\text{C}$  using OH and found that the tempering times with 0.5% salt concentration at frequency of 10, 20, and 30 kHz were 72%, 67%, and 57% longer than

that with 1.0% salt concentration, respectively. They emphasized the strong influence of salt concentration on tempering time and the addition of salt significantly enhances OT rate. Duguay, Ramaswamy, Zareifard, Zhu, Grabowski, and Marcotte (2015) evaluated the ohmic behavior of cabbage (50% v/v) and radish (50% v/v) with different salt concentrations (0.50, 1.00, 1.50, and 1.85%) at different voltages (65, 80, 100, 120, and 135 V) from 30 to 70 °C. The results showed that samples heated under 1.5% salt and 120 V or 1.00% salt and 135 V conditions resulted in the shortest processing time.

Moreover, from Fig. 4-11 it can be observed that the time-temperature profiles of pollock surimi with 0.5% salt nearly matched the profiles of minced tuna (approximately similar time to reach the target temperature  $\approx 18.2$  min at the center position) by the application of the three steps voltage control during OT process. In addition, the temperature difference between the center and corner positions at the final temperature of pollock surimi with 0.5% salt was 7.41 °C while that of tuna was 2.37 °C. This may be because the specific heats between them were different. The higher specific heat would be higher at the higher moisture contents in sample, and salts resulted in the reduction of specific heat because the sodium chloride ions interact with the water molecules (Abudagga & Kolbe, 1997; Jaczynski & Park, 2010; Muramatsu, et al., 2015). Thus, the temperature at the corner positions at final was higher than that of tuna.

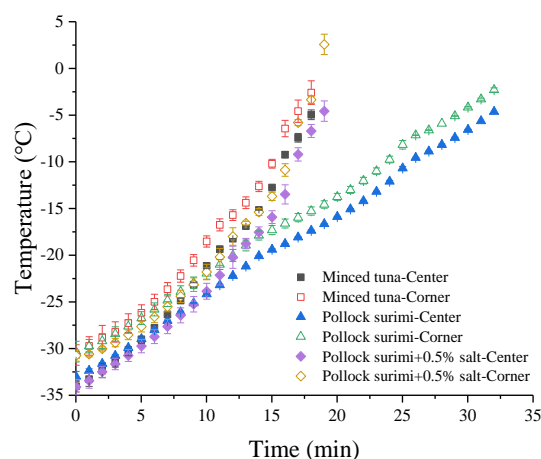


Fig. 4-11. Time-temperature profiles of minced tuna and the model food (with 0.5% and without salt) during OT process under the controlling voltage in three steps (400 V,  $-35 \sim -20$  °C; 200 V,  $-20 \sim -10$  °C; 100 V,  $-10 \sim -4$  °C).

#### 4.3.2.2 Temperature distributions

Temperature distributions of minced tuna under the controlling voltage in different methods (400V,  $-35 \sim -4$  °C; 200V,  $-35 \sim -4$  °C; 400V+200V,  $-35 \sim -15$  °C and  $-15 \sim -4$  °C, respectively; 400V+200V+100V:  $-35 \sim -20$ °C,  $-20 \sim -10$  °C, and  $-10 \sim -4$  °C, respectively) are shown in Fig. 4-12. Results showed that the temperature distribution of the minced tuna was more uniform after an OT process conducted by controlling the applied voltage in three steps. The corner temperatures were slightly higher than center temperature values, and the mean difference between corner and center temperatures of top surface was approximately 10.5 °C under the controlling voltage in three steps. The temperature changes in the treated samples during OT process is mainly related to the electric field and the heat transfer process. It is believed that the application of voltage gradient in several steps decreased the negative effect of multicomponent materials as the fishery products used in this study on current intensity and resulted in more uniform temperature distributions. By applying voltage gradient throughout OT process, the tempering rate can be regulated resulting in an effective method to reduce overheating. In addition, the method of three-steps voltage gradient could keep the appearance of the sample better than by using the other methods. The importance to consider the use of technologies that apply moderate temperatures and short process time to produce high-quality food has been reported in the literature (Knirsch, Alves dos Santos, Martins de Oliveira Soares Vicent, & Vessoni Penna, 2010). Döner, et al. (2020) analyzed the effects of voltage gradient (10, 13, and 16 V cm<sup>-1</sup>), electrode type and sample shape of minced beef on temperature distribution during OT process. They found that the voltage had a significant effect on temperature homogeneity ( $p < 0.05$ ) and that the maximum temperature and the average temperature values increased as the voltage increased, which can be explained by local fast generation rates for different structures in the sample and the neglected effects of heat conduction at these related regions ( $p < 0.05$ ). Çelebi and İcier (2014) have investigated the OT of minced meat samples at different voltage gradients (10, 15, and 20 V cm<sup>-1</sup>) and found that the surface temperature was higher for higher voltage gradients and that

lower voltage gradients could make the temperature distribution more homogeneous. Similar results were obtained in the present study. Miao, Chen, and Noguchi (2007) investigated the ohmic thawing process of pollock (*Theragra chalcogramma*) surimi from  $-24\text{ }^{\circ}\text{C}$  to  $-2\text{ }^{\circ}\text{C}$  and found that a homogeneous temperature distribution in frozen surimi was obtained with a salt solution below 4.0% by applying 20 V at 60 Hz.

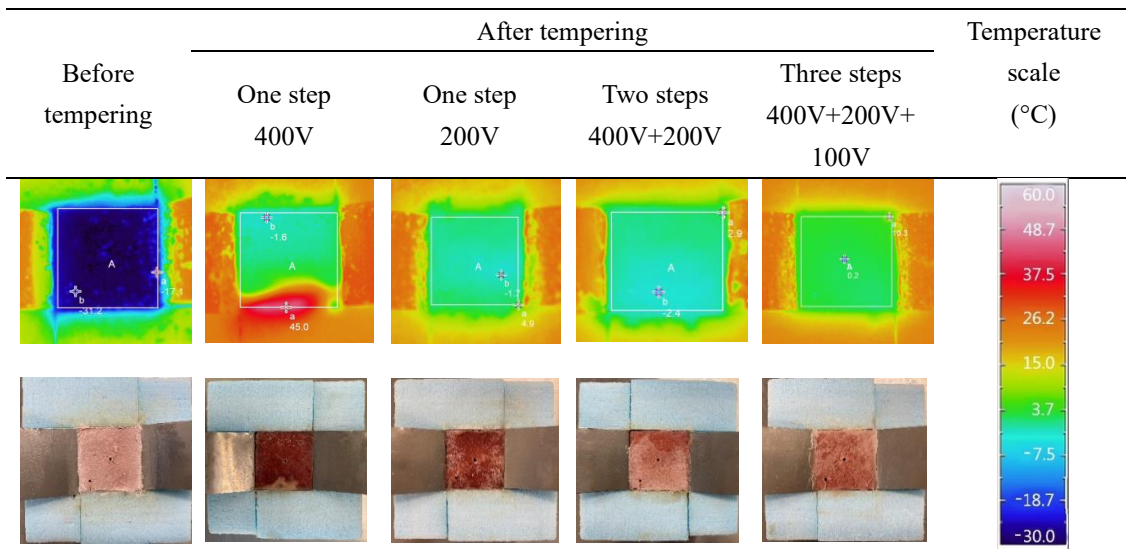


Fig. 4-12. Temperature distributions on the top surface of minced tuna under several controlling voltage approaches during OT process (400 V,  $-35 \sim -4\text{ }^{\circ}\text{C}$ ; 200 V,  $-35 \sim -4\text{ }^{\circ}\text{C}$ ; 400 V+200 V,  $-35 \sim -15\text{ }^{\circ}\text{C}$  and  $-15 \sim -4\text{ }^{\circ}\text{C}$ , respectively; 400 V+200 V+100 V:  $-35 \sim -20\text{ }^{\circ}\text{C}$ ,  $-20 \sim -10\text{ }^{\circ}\text{C}$ , and  $-10 \sim -4\text{ }^{\circ}\text{C}$ , respectively) and their respective digital pictures.

The comparison of temperature distributions of minced tuna and surimi-based model food under the controlling voltage in three steps (400V,  $-35 \sim -20\text{ }^{\circ}\text{C}$ ; 200V,  $-20 \sim -10\text{ }^{\circ}\text{C}$ ; 100V,  $-15 \sim -4\text{ }^{\circ}\text{C}$ ) is shown in Fig. 4-13. It is showed that the temperature distributions of all samples were uniform after an OT process under the controlling voltage in three steps. In the evaluated cases shown in Fig. 4-13, the cold points occurred in the center of top surface while the hot points occurred in the corner. The mean differences between corner and center temperatures of minced tuna, pollock surimi and pollock surimi with 0.5% salt were approximately similar, being  $10.5\text{ }^{\circ}\text{C}$ ,  $8.2\text{ }^{\circ}\text{C}$ , and  $9.8\text{ }^{\circ}\text{C}$ , respectively. Although salt increased the temperature difference between the hot and cold points, an addition of salt content of 0.5% to the pollock surimi gave a better agreement with the minced tuna results as was discussed in this study.

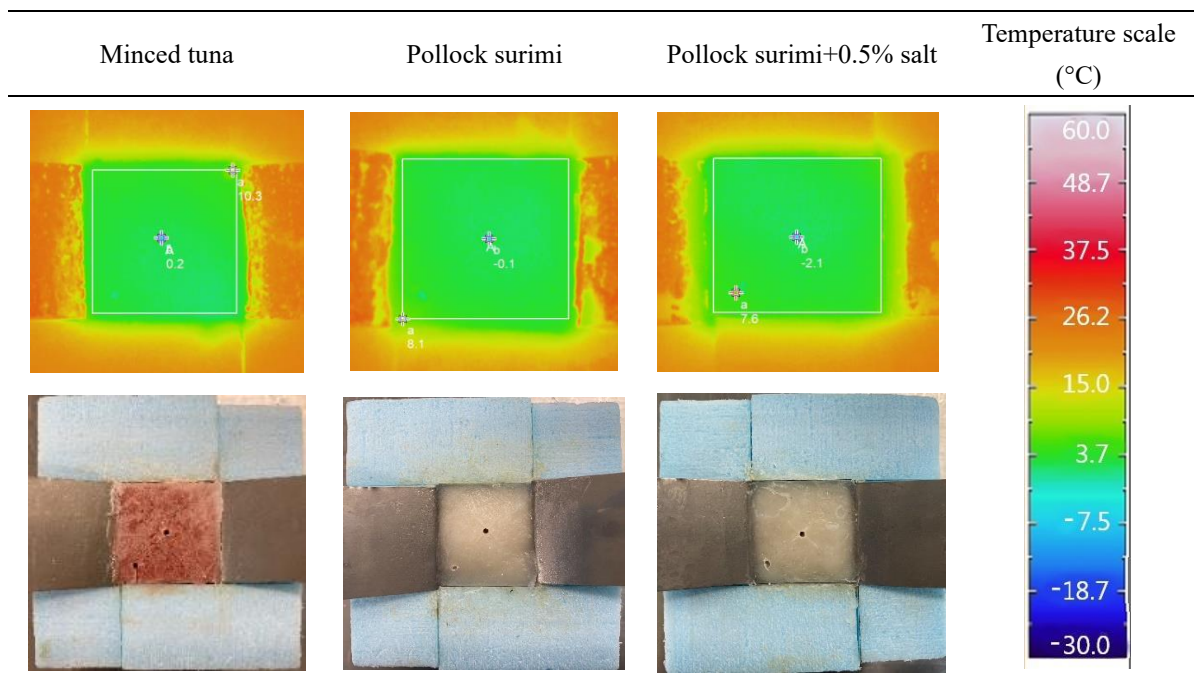


Fig. 4-13. Temperature distributions on the top surface of minced tuna and surimi-based model food without and with salt (0.5%) under the controlling voltage in three steps (400 V,  $-35 \sim -20$  °C; 200 V,  $-20 \sim -10$  °C; 100 V,  $-10 \sim -4$  °C) and their respective digital pictures.

#### 4.4 Conclusions

The EC values of lean minced tuna and Allaska pollock surimi at the temperature range of  $-40$  °C  $\sim$   $10$  °C and the frequency range of 50 Hz  $\sim$  20 kHz were studied with the target to evaluate the Allaska pollock surimi as a model food of minced tuna. For this purpose, salt was added to the surimi samples to fine-tuned their EC values to approximate the values of minced tuna. On the other hand, adjustment of voltage during OH process was also considered an important factor because it affects the OT performance. As the voltage applied increased, the heating rate of the evaluated samples increased. From the evaluated parameters, a more uniform temperature distribution result was obtained under the controlling voltage in three steps: 400 V from  $-35$  to  $-20$  °C, 200 V from  $-20$  to  $-10$  °C, and 100 V from  $-10$  to  $-4$  °C.

The evaluated EC values, temperature history and temperature distribution of pollock surimi with 0.5% added salt, resulted in the closest sample to the evaluated lean minced tuna during OT process at 20 kHz. This study provides a basis for the

development of model foods based on low-cost fish and its feasibility to replace high-value samples as minced tuna in OT development processes. It is thought that results obtained in this study can be useful in further studies on numerical simulations of OH of solid food samples.

## References

- Abudagga, Y., & Kolbe, E. (1997). Thermophysical properties of surimi paste at cooking temperature. *Journal of Food Engineering*, 32(3), p.325-337.
- Bozkurt, H., & İcier, F. (2012). Ohmic thawing of frozen beef cuts. *Journal of Food Process Engineering*, 35(1), 16-36.
- Çelebi, C., & İcier, F. (2014). Ohmic thawing of frozen ground meat. *Bulgarian Chemical Communications*, 46(B), 121-125.
- Cevik, M., & İcier, F. (2018). Effects of voltage gradient and fat content on changes of electrical conductivity of frozen minced beef meat during ohmic thawing. *Journal of Food Process Engineering*, 41(4).
- Chai, P. P., & Park, J. W. (2007). Physical properties of fish proteins cooked with starches or protein additives under ohmic heating. *Journal of Food Quality*, 30(5), 783-796.
- Cong, H., Liu, F., Tang, Z., & Xue, C. (2012). Dielectric properties of sea cucumbers (*Stichopus japonicus*) and model foods at 915MHz. *Journal of Food Engineering*, 109(3), 635-639.
- Darvishi, H. (2012). Ohmic heating behaviour and electrical conductivity of tomato paste. *Journal of Nutrition & Food Sciences*, 02(09).
- Döner, D., Çokgezme, Ö. F., Çevik, M., Engin, M., & İcier, F. (2020). Thermal image processing technique for determination of temperature distributions of minced beef thawed by ohmic and conventional methods. *Food and Bioprocess Technology*, 13(11), 1878-1892.
- Duguay, A.-J., Ramaswamy, H. S., Zareifard, R., Zhu, S., Grabowski, S., & Marcotte, M. (2015). Ohmic heating behaviour of cabbage and daikon radish. *Food and Bioprocess Technology*, 9(3), 430-440.
- Fattahi, S., & Zamindar, N. (2020). Effect of immersion ohmic heating on thawing rate and properties of frozen tuna fish. *Food Sci Technol Int*, 26(5), 453-461.
- Guo, W., Llave, Y., Jin, Y., Fukuoka, M., & Sakai, N. (2017). Mathematical modeling of ohmic heating of two-component foods with non-uniform electric properties at high frequencies. *Innovative Food Science & Emerging Technologies*, 39, 63-78.
- Hosain, D., Adel, H., Farzad, N., Hadi, K. M., & Hosain, T. (2011). Ohmic Processing: Temperature Dependent Electrical Conductivities of Lemon Juice. *Modern Applied Science*, 5(1), 209-216.
- İcier, F., & İlicali, C. (2005). The use of tylose as a food analog in ohmic heating studies. *Journal of Food Engineering*, 69(1), 67-77.
- İcier, F., İzzetoglu, G. T., Bozkurt, H., & Ober, A. (2010). Effects of ohmic thawing on histological and textural properties of beef cuts. *Journal of Food Engineering*, 99(3), 360-365.
- Jaczynski, J., & Park, J. W. (2010). Temperature prediction during thermal processing of surimi seafood. *Journal of Food Science*, 67(8), 3053-3057.
- Jiang, Q., Jia, R., Nakazawa, N., Hu, Y., Osako, K., & Okazaki, E. (2019). Changes in protein properties and tissue histology of tuna meat as affected by salting and subsequent freezing. *Food Chemistry*, 271, 550-560.

- Jin, Y., Cheng, Y.-d., Fukuoka, M., & Sakai, N. (2015). Electrical conductivity of yellowtail (*Seriola quinqueradiata*) fillets during ohmic heating. *Food and Bioprocess Technology*, 8(9), 1904-1913.
- Jin, Y., Jiang, C., Jiao, Y., Llave, Y., Fukuoka, M., & Sakai, N. (2020). Analysis of ohmic heating of yellowtail (*Seriola quinqueradiata*) fillets at high frequencies by 3D simulation—Effect of ohmic heating system (batch and pseudo-continuous), sample shape, and size. *Innovative Food Science & Emerging Technologies*, 66.
- Knirsch, M. C., Alves dos Santos, C., Martins de Oliveira Soares Vicent, A. A., & Vessoni Penna, T. C. (2010). Ohmic heating – a review. *Trends in Food Science & Technology*, 21(9), 436-441.
- Lee, S. Y., Ryu, S., & Kang, D. H. (2013). Effect of frequency and waveform on inactivation of *Escherichia coli* O157:H7 and *Salmonella enterica* Serovar Typhimurium in salsa by ohmic heating. *Applied and Environmental Microbiology*, 79(1), 10-17.
- Li, Y., Li, F., Tang, J., Zhang, R., Wang, Y., Koral, T., & Jiao, Y. (2018). Radio frequency tempering uniformity investigation of frozen beef with various shapes and sizes. *Innovative Food Science & Emerging Technologies*, 48, 42-55.
- Liu, L., Llave, Y., Jin, Y., Zheng, D.-y., Fukuoka, M., & Sakai, N. (2017). Electrical conductivity and ohmic thawing of frozen tuna at high frequencies. *Journal of Food Engineering*, 197, 68-77.
- Llave, Y., Mori, K., Kambayashi, D., Fukuoka, M., & Sakai, N. (2016). Dielectric properties and model food application of tylose water pastes during microwave thawing and heating. *Journal of Food Engineering*, 178, 20-30.
- Llave, Y., Terada, Y., Fukuoka, M., & Sakai, N. (2014). Dielectric properties of frozen tuna and analysis of defrosting using a radio-frequency system at low frequencies. *Journal of Food Engineering*, 139, 1-9.
- Llave, Y., Udo, T., Fukuoka, M., & Sakai, N. (2018). Ohmic heating of beef at 20 kHz and analysis of electrical conductivity at low and high frequencies. *Journal of Food Engineering*, 228, 91-101.
- Luan, D., Tang, J., Liu, F., Tang, Z., Li, F., Lin, H., & Stewart, B. (2015). Dielectric properties of bentonite water pastes used for stable loads in microwave thermal processing systems. *Journal of Food Engineering*, 161, 40-47.
- Miao, Y., Chen, J. Y., & Noguchi, A. (2007). Studies on the ohmic thawing of frozen surimi. *Food ence & Technology International Tokyo*, 13(4), 296-300.
- Muramatsu, Y., Sakaguchi, E., Kawakami, S., Orikasa, T., Koide, S., Imaizumi, T., & Tagawa, A. (2015). Simultaneous estimation and modeling of thermophysical properties of big-eyed tuna and pacific cod. *International Journal of Food Properties*, 18(10), 2213-2222.
- Nguyen, V.-T., Park, J. W., Liqiong, N., Nakazawa, N., Osako, K., & Okazaki, E. (2020). Textural properties of heat-induced gels prepared using different grades of Alaska pollock surimi under ohmic heating. *Food Science and Technology Research*, 26(2), 205-214.
- Nistor, O. V., Botez, E., Luca, E., Mocanu, G. D., & Timofti, M. (2013). Ohmic heating process characterizations during apple puree. *Journal of Agroalimentary*

- Processes and Technologies*, 19(2), 228-236.
- Rahman, M. S. (2010). Food stability determination by macro–micro region concept in the state diagram and by defining a critical temperature. *Journal of Food Engineering*, 99(4), 402-416.
- Seyhun, N., Ramaswamy, H. S., Zhu, S., Sumnu, G., & Sahin, S. (2012). Ohmic tempering of frozen potato puree. *Food and Bioprocess Technology*, 6(11), 3200-3205.
- Uemura, K., Noguchi, A., Park, S. J., & Kim, D. U. (1994). *Ohmic Heating of Food Materials Effects of Frequency on the Heating Rate of Fish Protein*: Springer US.
- Wang, J., Tang, J., Liu, F., & Bohnet, S. (2018). A new chemical marker-model food system for heating pattern determination of microwave-assisted pasteurization processes. *Food and Bioprocess Technology*, 11(7), 1274-1285.
- Wang, Y., Tang, J., Rasco, B., Wang, S., Alshami, A. A., & Kong, F. (2009). Using whey protein gel as a model food to study dielectric heating properties of salmon (*Oncorhynchus gorbuscha*) fillets. *LWT - Food Science and Technology*, 42(6), 1174-1178.
- Yildiz-Turp, G., Sengun, I. Y., Kendirci, P., & Icier, F. (2013). Effect of ohmic treatment on quality characteristic of meat: a review. *Meat Science*, 93(3), 441-448.

## **Chapter 5 Numerical simulation of ohmic tempering process of tuna**

### **5.1 Introduction**

OH has advantages such as high energy efficiency (more than 90 %) and environmental friendliness. Also, there are some disadvantages. Heterogeneous conductivity values of food materials, heterogeneous muscle tissues and the presence of connective tissues caused uneven temperature distribution during OH (Döner, Çokgezme, Çevik, Engin, & İçier, 2020; Duygu & Ümit, 2015; Jin, Jiang, Jiao, Llave, Fukuoka, & Sakai, 2020; Liu, Llave, Jin, Zheng, Fukuoka, & Sakai, 2017; Tang J, Schubert H, & M., 2005). Finite element modeling may serve as valuable tools to acquire deep insights on the heating uniformity of products and offer opportunity to clearly understand OH interactions with food samples without the necessity of extensive experiments.

Guo, Llave, Jin, Fukuoka, and Sakai (2017) compared experiments and numerical simulations and demonstrated that different components and different filling methods can lead to uneven distribution of conductivity, electric field strength and current density in the cavity during the process, thus increasing the heating inhomogeneity. For the thawing and tempering process, it is important to apply a suitable voltage gradient, ensure the homogeneity of the sample and guarantee complete contact between the frozen sample and the electrodes (Miao, Chen, & Noguchi, 2007). In experiments, inhomogeneity usually occurs due to the heat transfer between the sample and the environment or incomplete contact between the material and the electrodes, such as the volume change caused by the drip losses. This inhomogeneity can be reduced by voltage regulation. The OH rate is mainly related to the EC of the material and the applied voltage. During the actual experimental operation, the voltage can be adjusted according to the change of material conductivity to obtain the suitable tempering rate and ensure the quality of food materials. Numerical simulation can analyze the electromagnetic field and internal temperature distribution which cannot be seen in the experimental process during the OT process of tuna.

In this chapter, a numerical simulation model of the OT of tuna was established to specifically analyze the changes of electromagnetic field and temperature distributions during the tempering process. Thus, the tempering process was precisely optimized by computer simulation to improve the temperature uniformity of the sample during the process.

## 5.2 Materials and methods

### 5.2.1 Materials preparation

As in Section 4.2.1

### 5.2.2 Instruments and equipment

As in Section 4.2.2

### 5.2.3 Ohmic tempering of tuna

The tuna was tempered using a 20 kHz Joule heating equipment (FJB-5.5, Frontier Engineering Co., Ltd, Japan). The input voltage was set to 400 V for the OT process.

## 5.3 Computer simulation

### 5.3.1 Computer simulation of the tempering tuna process

It was considered that due to the short processing time, low final temperature and the high heating rate reached because of the use of a high frequency in this study (20 kHz), a significative evaporation in the structure of the sample do not occur (Jin et al., 2020; Llave, Morinaga, Fukuoka, & Sakai, 2018). During the energization process, a changing magnetic field is formed while an electric current is passed to both sides of the sample, so the ohmic tempering tuna process involves a multi-physical field coupled with electromagnetic and heat transfer.

Electromagnetic field:

The distribution of the electromagnetic field in time and space can be represented by Maxwell's equations:

$$\nabla \cdot B = \nabla \cdot \mu H = 0 \quad (5-1)$$

$$\nabla \cdot D = \nabla \cdot \varepsilon E = P_m \quad (5-2)$$

$$\nabla \times H = \frac{\partial D}{\partial t} + J = \frac{\partial \varepsilon E}{\partial t} + \sigma E \quad (5-3)$$

$$\nabla \times E = -\frac{\partial B}{\partial t} = -\frac{\partial \mu E}{\partial t} \quad (5-4)$$

$$\sigma = \omega \varepsilon_0 \varepsilon'' \quad (5-5)$$

where

$B$  is the magnetic flux density (Wb m<sup>-2</sup>)

$D$  is the electric displacement (C m<sup>-2</sup>)

$H$  is the magnetic field intensity (A m<sup>-1</sup>)

$E$  is the electric field intensity (V m<sup>-1</sup>)

$P_m$  is the electric volume charge density (C m<sup>-3</sup>)

$J$  is the current density (A m<sup>-2</sup>)

$$\mu = \mu_0 = 4\pi \times 10^{-7} H m^{-1}$$

$\omega$  is the angular acceleration (rad s<sup>-1</sup>)

$\varepsilon'$  is the dielectric constant,  $\varepsilon''$  is the dielectric loss factor,  $\varepsilon^* = \varepsilon' - j\varepsilon''$ ,  $j^2 = -1$ ,

$\varepsilon_0$  is the dielectric constant under vacuum, which is  $8.854 \times 10^{-12}$  (F m<sup>-1</sup>)

Temperature field:

The distribution of the temperature field in time and space can be represented by Fourier differential equations for thermal conductivity:

$$Q(x, y, z, t) = \omega \varepsilon_0 \varepsilon'' E^2 = \sigma |E|^2 \quad (5-6)$$

$$\rho Cp \frac{\partial T}{\partial t} = \nabla \cdot k \nabla T + Q \quad (5-7)$$

where

$\sigma$  is the electrical conductivity of the material

$\rho$  is the density of tuna (kg m<sup>-3</sup>)

$t$  is the time (s)

$T$  is the temperature (K)

$Q$  is the energy absorbed per unit volume of energized electricity, which can be expressed by the following Eq.:

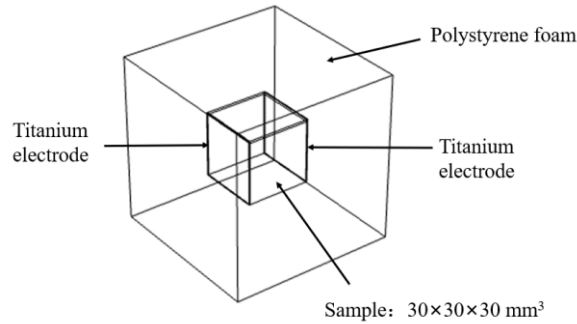
$$Q = JE = \frac{J^2}{\sigma} \quad (5-8)$$

where  $J$  is the current density (A m<sup>-2</sup>)

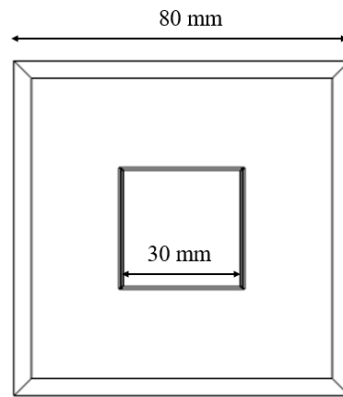
### 5.3.2 Modeling

As in Section 3.3.2, an electromagnetic field analysis and a temperature analysis were performed to simulate the OT process of tuna. The frequency-transient was

selected for the solution. All domains in the model were set using a free-dissecting tetrahedral mesh, and the meshing size for them were selected as “fine”. The model was solved with the default direct solver, and the time step used in this study was 1 s.



(a)



(b)

Fig. 5-1 Geometry model of ohmic tempering (a. Main view b. Top view)

The parameters of the OT process of tuna in simulation are shown in the table below:

Table 5-1 Parameters and boundary conditions used in the model.

Parameter	Value
Initial temperature	-35 [°C]
Surrounding temperature	20 [°C]
Thermal conductivity	Same as in 2.2.3 Table 2-5
Electrical conductivity	Same as in 4.2.1 Fig. 4-2(a) (b)
Sample specific heat	Same as in 2.3.3 Fig. 2-8
Frequency	20 [kHz]

Electrode voltage	Constant voltage 400V Segmented voltage 400V+200V
Convective heat transfer coefficient	15 [Wm <sup>-2</sup> ·K]
Titanium electrode distance	30 [mm]

The number of mesh for the whole system was 1979.

During the OT experiment, as shown in Figure 5-1, polystyrene foam wrapped around the material as an adiabatic layer to prevent the material from a heat exchange process with the ambient air. In the experiment, there were inevitably gaps due to the presence of titanium electrode, which can cause heat exchange between the material and the ambient air. This could make the EC of various parts of the material different during OT. Especially at higher voltages, a more pronounced phenomenon of uneven tempering temperature occurred. Taking this into account, a tiny air layer (1 mm) was added to the top surface of the material during the simulation to make the simulation process more consistent with the experimental condition.

### 5.3.3 Applying optimum voltage control

The OT rate of tuna under the control voltage of 400 V was obtained from the experiments in Chapter 4. According to the thawing rate, the temperature rise curve was fitted to the function in segments, and its intersection point was the time point suitable for reducing the thawing rate, which was 11.26 min (about 676 s). Therefore, in the computer simulation, the voltage of the ohmic thawing process was segmented. The voltage 400 V was applied from 0 to 676 s. The voltage was reduced to 200 V at 676 s until the central temperature of the material reached -4 °C, then the tempering process was completed.

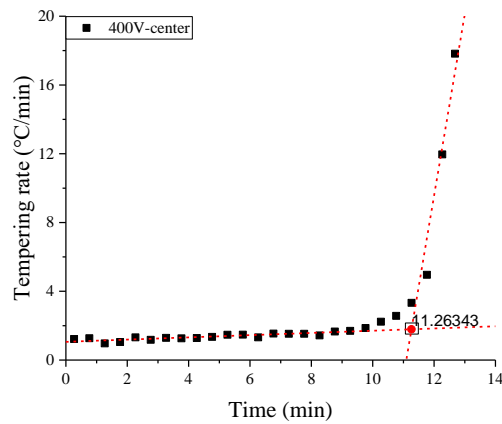


Fig.5-2 Tempering rate of minced tuna during ohmic tempering process under the controlling voltage

### 5.3.4 Temperature Uniformity Index (TUI)

Same as described in Section 3.3.5

## 5.4 Results and discussion

### 5.4.1 Temperature history of OT under constant voltage

The comparison between the experimental and simulated values of OT rate of tuna is shown in Fig. 5-3. In the simulation, the center temperature reached the target temperature  $-4\text{ }^{\circ}\text{C}$  and the corner temperature was  $-0.02\text{ }^{\circ}\text{C}$  at 12.35 min. In the experiment, the center temperature reached the target temperature  $-4\text{ }^{\circ}\text{C}$  and the corner temperature was  $-0.7\text{ }^{\circ}\text{C}$  at 12.85 min. In the experimental value, the initial temperature of the sample corner is higher than the initial temperature of the center, which is due to the fact that the measuring point of the corner was close to the surface. When the sample was taken from the refrigerator and placed in the Joule heating device, the surface of the sample was exposed to the environment and the temperature around the surface rose, which was inevitably caused by heat transfer with the environment. The simulated thawing rate was slightly faster than the experimental rate. Overall, the simulated values had the same trend as the experimental value.

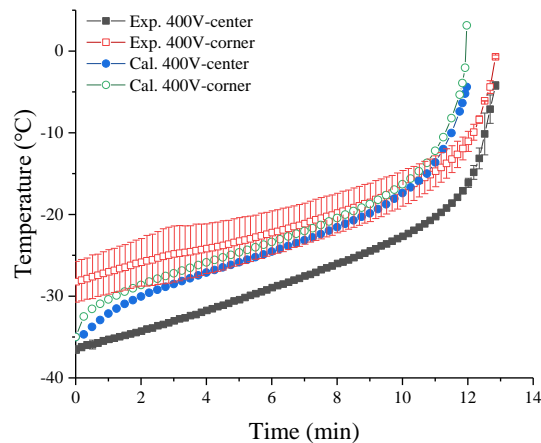


Fig.5-3 Comparison of experimental (exp.) and simulated (cal.) values of ohmic tempering rate of tuna

#### 5.4.2 Temperature history after OT under constant voltage

The comparison between the experimental and simulated temperature distribution of tuna after OT is shown in Fig. 5-4. When the center reached the target temperature, the cold and hot spot temperatures on the top surface of tuna samples were  $-1.6^{\circ}\text{C}$  and  $45.0^{\circ}\text{C}$ , respectively. According to the numerical simulation, the cold point temperature of the top surface was  $-0.58^{\circ}\text{C}$  and the hot spot temperature was  $35.6^{\circ}\text{C}$ . The simulated and experimental cold and hot spot temperatures on the top surface were similar, and the overall temperature distributions were not significantly different.

The internal temperature distribution of tuna after OT at 400 V is shown in Fig. 5-5. From the simulation results, when the center of tuna was tempered to the target temperature  $-4^{\circ}\text{C}$ , most of the material was close to the target temperature. The temperatures of the top surface and edges were higher than that of the center. This may be attributed to that the ion mobility in the sample increased with the increasing temperature, which accelerated the loss of moisture and fat as well as the protein denaturation in the sample. In the process, water molecules were transferred from the interior to the sample surface via drip channels formed by protein denaturation (Jin, et al., 2020; Van der Sman & M, 2017).

During the OT process, the temperature of the tuna increased because of the conversion of electrical energy into thermal energy when the electrical current passed

through the tuna. Fig. 5-6 shows the current density of tuna for constant voltage OT. The result showed that the current density was greater on the top surface. The main two factors affecting the temperature distribution of OT are the endothermic source generated by the current and the heat transfer between the masses. When the EC of the material was certain, the higher the current density of the region was, the higher the temperature distribution was. In the experimental, the heat exchange between the edge of the material and the surrounding environment accelerated the tempering rate of the edge part, and the increase of current density made the rate of hot spot heating faster, which in turn made the increase of EC values. The electric field was stronger at each edge of both electrodes because the edges of the electrodes were sharp and beginning points for the electric field to overshoot (Choi, Kim, & Jun, 2015; Nguyen, Choi, Lee, & Jun, 2013). So the nonuniform temperature distribution was more obvious in the case of 400 V.

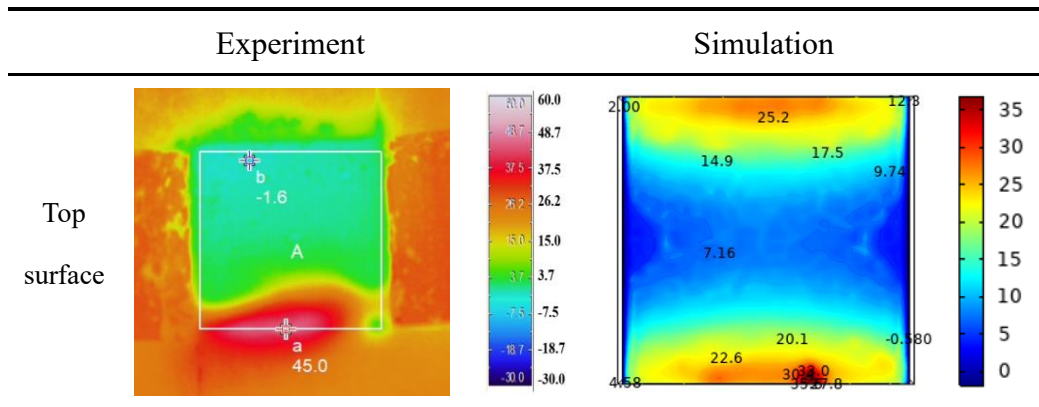


Fig.5-4 Comparison of experimental and simulated values of temperature distribution of tuna after OT (Unit: °C)

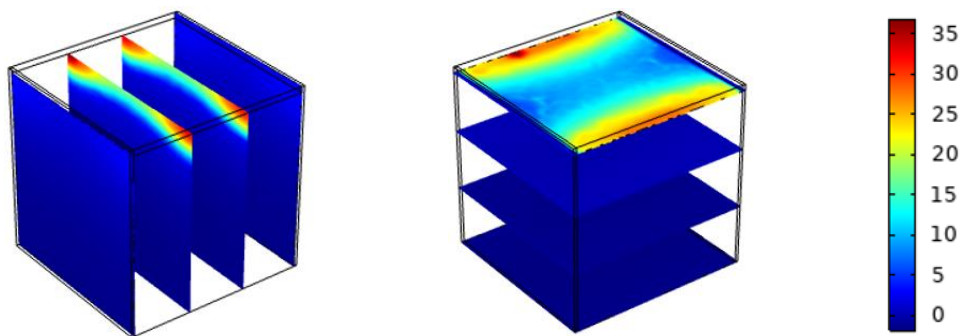


Fig. 5-5 Internal cross-section temperature distributions of tuna after OT in vertical (left) and horizontal directions (right) (Unit: °C)

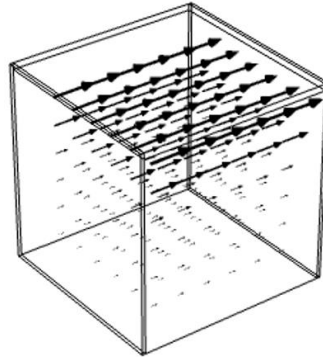


Fig. 5-6 Current density of tuna for constant voltage during OT (12.3 min)

#### 5.4.3 Computer simulation of OT under segmented voltage

Fig. 5-7 shows the tempering rate of numerical simulation values during OT process at the segmented voltages. A 15.2 min was necessary for the center to reach the target temperature of -4 °C. The application of segmented voltage significantly reduced the tempering rate. Fig. 5-8 and Fig. 5-9 show the top surface and internal temperature distribution of tuna after OT numerical simulation at the segmented voltages, respectively. The top surface temperatures of the numerical simulation were in the range of -3 to -1.3 °C, and the cold and hot temperatures were -3.04 °C and -1.25 °C, respectively. The overall internal temperature distribution of the numerical simulation was close to the target temperature, and the top surface temperature was also below 0 °C. The temperature difference between the top surface and interior positions was due to the natural convection heat transfer from the air to the top surface of the sample during the OT process, thus the edge was higher than the center. And the hot spot of the sample was more than 30 °C lower than that after thawing at a constant voltage of 400V. Fig. 5-10 shows the current density of tuna for segmented voltage OT. Due to the heat exchange between the top surface of the sample and surrounding air, the heating rate of the top surface was faster, which leads to the difference of electrical conductivity, and the current density of the top surface was greater. But the current distribution is more uniform than that at constant voltage, indicating that the segmented voltages obviously

improved the current density of the sample. The simulation results showed that the application of segmented voltages effectively reduced the hot spot temperature and made the material temperature distribution more uniform.

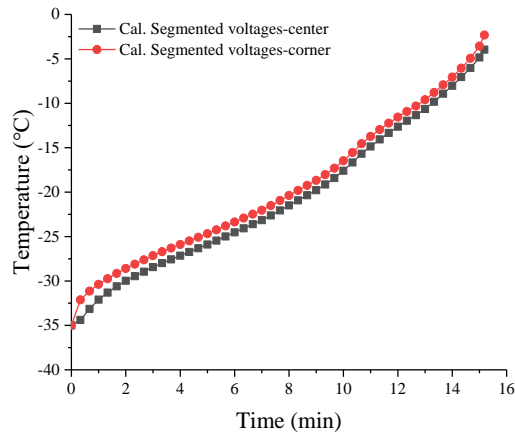


Fig. 5-7 Tempering rate of numerical simulation values during ohmic tempering process at the segmented voltages

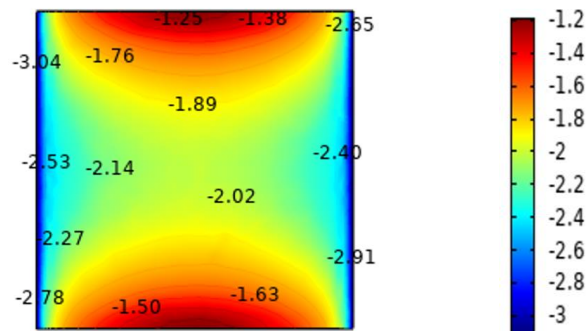


Fig. 5-8 Temperature distribution on the top surface of tuna after ohmic tempering numerical simulation at the segmented voltages (Unit: °C)

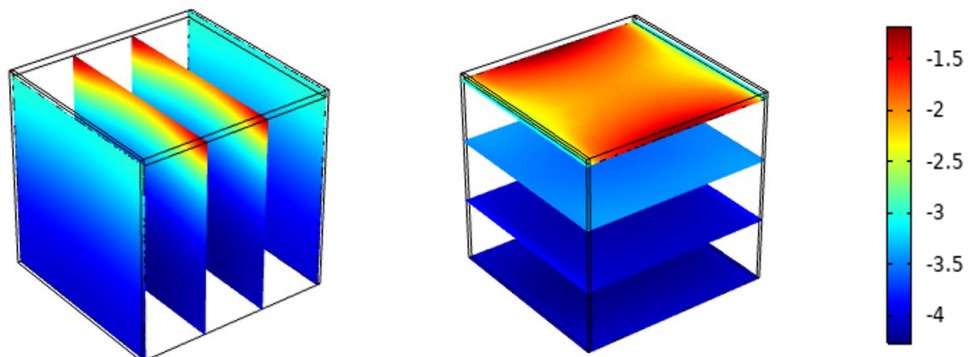


Fig. 5-9 Internal temperature distribution of tuna after ohmic tempering numerical simulation at the segmented voltages (Unit: °C)

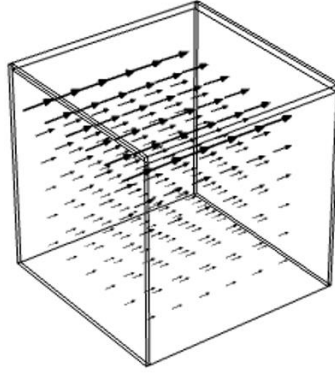


Fig. 5-10 Current density of tuna for segmented voltages ohmic tempering (at 15.2 min)

#### 5.4.4 Tempering uniformity evaluation under different voltages

The TUI values of materials after ohmic tempering calculated from the temperature uniformity equation ( $TUI = \frac{\int |T - T_{tg}| dV_{vol}}{(T_{tg} - T_{initial}) V_{vol}}$ ) were shown in Table 5-2. The lower value indicates the higher temperature uniformity after tempering. The simulation results show that when the target temperature (center temperature -4 °C) was reached, the volume uniformity and top surface uniformity of the tuna were 0.103 and 0.108 after tempering at constant voltage (400 V), while 0.007 and 0.017 after tempering at segmented voltages (400V and 200V). The temperature distribution uniformity obtained by tempering under segmented voltages was higher.

Table 5-2 TUI values of materials after OT

	Top surface	Volume
400 V	0.125	0.076
400 V+200 V	0.007	0.017

#### 5.5 Conclusions

In this chapter, the finite element model of OT was established by coupling electromagnetic field and solid heat transfer. The computer simulated values were close to the experimental values, indicating that the model could be used for the study of OT tuna process and could effectively predict the tempering process and temperature

distribution. Heat transfer occurred between some locations of the material and the environment, which aggravated the uneven temperature distribution, especially at 400 V. The higher temperature on the upper surface than the interior was mainly due to the heat exchange with the surrounding environment, and the heat transfer between the edge and the air was stronger than that between the middle and the air. The electric field was stronger at each edge of both electrodes and the temperature at the edges was higher. During OT process, the generation of heat and the resulting temperature distribution are related to the voltage. The uniformity of temperature distribution in the tempering process obtained by applying segmented voltages and reducing the thawing rate. Numerical simulation analyzed the OT process in more detail, accurately controlled the voltage and heating rate, and improved the material temperature distribution uniformity more effectively. In future work, a continuous voltage function can be fitted to the experimental thawing rate and then numerically simulated to control the thawing process more precisely, and an automatic control system can be designed to monitor and adjust the experimental voltage to improve its uniformity.

## References

- Choi, W., Kim, S. H. L. C.-T., & Jun, S. (2015). A finite element method based flow and heat transfer model of continuous flow microwave and ohmic combination heating for particulate foods. *Journal of Food Engineering*, *149*, 159-170.
- Döner, D., Çokgezme, Ö. F., Çevik, M., Engin, M., & İçier, F. (2020). Thermal image processing technique for determination of temperature distributions of minced beef thawed by ohmic and conventional methods. *Food and Bioprocess Technology*, *13*(11), 1878-1892.
- Duygu, B., & Ümit, G. (2015). Application of ohmic heating system in meat thawing. *Procedia - Social and Behavioral Sciences*, *195*, 2822-2828.
- Guo, W., Llave, Y., Jin, Y., Fukuoka, M., & Sakai, N. (2017). Mathematical modeling of ohmic heating of two-component foods with non-uniform electric properties at high frequencies. *Innovative Food Science & Emerging Technologies*, *39*, 63-78.
- Jin, Y., Jiang, C., Jiao, Y., Llave, Y., Fukuoka, M., & Sakai, N. (2020). Analysis of ohmic heating of yellowtail (*Seriola quinqueradiata*) fillets at high frequencies by 3D simulation—Effect of ohmic heating system (batch and pseudo-continuous), sample shape, and size. *Innovative Food Science & Emerging Technologies*, *66*.
- Liu, L., Llave, Y., Jin, Y., Zheng, D.-y., Fukuoka, M., & Sakai, N. (2017). Electrical conductivity and ohmic thawing of frozen tuna at high frequencies. *Journal of Food Engineering*, *197*, 68-77.
- Llave, Y., Morinaga, K., Fukuoka, M., & Sakai, N. (2018). Characterization of ohmic heating and sous-vide treatment of scallops: Analysis of electrical conductivity and the effect of thermal protein denaturation on quality attribute changes - ScienceDirect. *Innovative Food Science & Emerging Technologies*, *50*, 112-123.
- Miao, Y., Chen, J. Y., & Noguchi, A. (2007). Studies on the ohmic thawing of frozen surimi. *Food ence & Technology International Tokyo*, *13*(4), 296-300.
- Nguyen, L. T., Choi, W., Lee, S. H., & Jun, S. (2013). Exploring the heating patterns of multiphase foods in a continuous flow, simultaneous microwave and ohmic combination heater - ScienceDirect. *Journal of Food Engineering*, *116*(1), 65-71.
- Tang J, Schubert H, & M., R. (2005). *Dielectric properties of foods* (Vol. 3): Microwave Processing of Foods.
- Van der Sman, & M, R. G. (2017). Model for electrical conductivity of muscle meat during Ohmic heating. *Journal of Food Engineering*, *208*(SEP.), 37-47.

## **Chapter 6 General conclusions**

This study investigated the tempering process of tuna by two novel techniques of RF and OT, aiming to contribute to the development of tuna model food and the establishment of finite element simulation of tuna RF tempering and OT.

In Chapter 1, current research about novel thawing/tempering technology, model food and numerical simulation in food processing were reviewed.

In Chapter 2, based on the dielectric and thermal properties of tuna, grass carp was used as the raw material of model foods, and the model food effectively simulated the temperature rise and distribution of tuna RF tempering by adding vegetable oil, methylcellulose and salt. The dielectric properties of the model food were significantly changed by the addition of vegetable oil, methyl cellulose and salt. The dielectric properties of grass carp with 4.0% vegetable oil and 4.0% methylcellulose were more similar to those of tuna. The temperature distribution of grass carp with 4.0% vegetable oil, 4.0% methylcellulose and 1.0%NaCl was more similar to that of tuna during RF tempering.

In Chapter 3, the finite element model of tuna RF tempering was established by coupling electromagnetic field and heat transfer. The temperature change in the process of RF tempering tuna was analyzed, and its validity was verified by experiments. The effects of electrode plate shapes and material shapes on the RF tempering process were studied. The results showed that the electrode plate shapes and material shapes significantly improved the electromagnetic field distribution and temperature uniformity. The temperature distribution under the needle plate was more uniform, and the temperature distribution of the cylinder sample was more uniform than that of the rectangular sample.

In Chapter 4, based on the electrical conductivity of tuna, pollock surimi was used as the raw material of model foods, and the model food with 0.5%NaCl pollock surimi effectively simulates the temperature rise and distribution of tuna OT process. The electrical conductivity of model food increased with the increase of temperature, frequency and salt content. The electrical conductivity, temperature rise curve and

temperature distribution of pollock surimi with 0.5%NaCl were consistent with those of tuna.

In Chapter 5, the finite element model of OT tuna was established by coupling electromagnetic field and heat transfer. The temperature change in the tuna OT process was analyzed, and its validity was verified by experiments. The effect of voltage on ohmic thawing process was studied by computer numerical simulation. The results showed that the temperature uniformity of OT could be effectively improved by segmenting the voltage precisely and reducing the voltage at the right time which laid the foundation for further development of OT.

Compared with RF tempering and OT technology, RF is more suitable for the thawing of bulk materials. RF tempering can improve its uniformity by changing the shape of the electrode plate, while OT can improve its uniformity by segmented voltage.

## **Acknowledgement**

There are many people that have earned my gratitude for their contribution to my time in graduate school. More specifically, I would like to express my deepest appreciation and thanks to people, without whom this dissertation would not have been possible.

First, I am indebted to my Chinese supervisor, Associate Prof. Jiao Yang. I am deeply grateful for her continuous guidance and suggestion in my research process. I would also like to thank Japanese supervisor Prof. Mika Fukuoka and Prof. Noboru Sakai for their great help in my research. Under their supervision, I learned how to think and solve the problems during my experiment. My sincere thank also goes to Associate Prof. Yvan Llave for his patient guidance and precious support on paper writing.

Also, I am also grateful to all the members of Engineering Research Center of Food Thermal-processing Technology in Shanghai Ocean University and all the members of Laboratory of Food Thermal Processing in Tokyo University of Marine Science and Technology for their friendliness and general support. At the same time, I am also very grateful to the Asian Campus DDP project, which gives me the opportunity to go to Tokyo University of Marine Science and Technology for one-year exchange study.

Last but not the least, I would like to thank my family for everything they have done for me and for their support. And thanks for my own efforts during the period of studying for the master's degree.